Physics – Uspekhi **63** (5) 440 – 486 (2020)

PHYSICS OF OUR DAYS PACS numbers: 61.20.Gy, 61.30.Hn

Effects of action at a distance in water

L I Menshikov, P L Menshikov, P O Fedichev

DOI: https://doi.org/10.3367/UFNe.2020.01.038721

Contents

Abstract. **Dipole–dipole interaction between molecules of hydrogen-bonding polar liquids (HBPLs), which has a collective and long-range nature, determines the basic large-scale properties of such liquids. We present a two-scale phenomenological vector model of polar liquids (VMPLs), wherein the liquid is described by a polarization vector. The simplest version of this model satisfactorily reproduces the well-known properties of HBPLs and interaction between macroscopic objects in a liquid. The possible existence of a ferroelectric phase transition (FPT) in supercooled liquid water is discussed. Near the FPT, fluctuations of the polarization vector increase, which may be the cause of the so-called 'anomalous' properties of water. We propose a quantitative classification of body surfaces based on the properties of their wettability by polar liquids. The ordering of dipoles of molecules located in the near-surface layers of HBPLs and phase transitions in these layers are discussed. The proposed model enables a significant reduction in computer time in numerical simulations of systems that contain a large number of water molecules.**

Keywords: polar liquid, dipole–dipole interaction, phase transition, topological phase transition, ferroelectrics, paraelectrics, ferroelectric phase transition, interaction of bodies in a polar liquid, wetting, hydrophobic surfaces, hydrophilic surfaces, wetting phase transitions

L I Menshikov [1, 2, *], **P L Menshikov** [1], **P O Fedichev** [2, 3, **]
[1] National Research Center 'Kurchatov Institute', pl. Akademika Kurchatova 1, 123182 Moscow, Russian Federation
[2] Moscow Institute of Physics and Technology (State University), Institutskii per. 9, 141701 Dolgoprudnyi, Moscow region, Russian Federation
[3] Gero LLC, Nizhnii Susal'nyi per. 5/4, 105064 Moscow, Russian Federation
E-mail: [*] mleonid1954@mail.ru, [**] peter.fedichev@gmail.com

Received 8 April 2019, revised 19 August 2019
Uspekhi Fizicheskikh Nauk **190** (5) 475 – 524 (2020)
Translated by M Zh Shmatikov; edited by V L Derbov

1. Introduction

Coulomb long-range interaction between plasma particles, $\propto r^{-1}$, predetermines virtually all of the plasma's basic properties, which only weakly depend on the details of the interaction between particles at small distances r. Each particle moves then in a collective electric field created by a large number of other particles $\sim N_{\mathrm{D}} \gg 1$, where N_{D} is the number of particles inside a sphere with the Debye radius r_{D}. Unlike plasma particles, molecules of polar liquids, whose

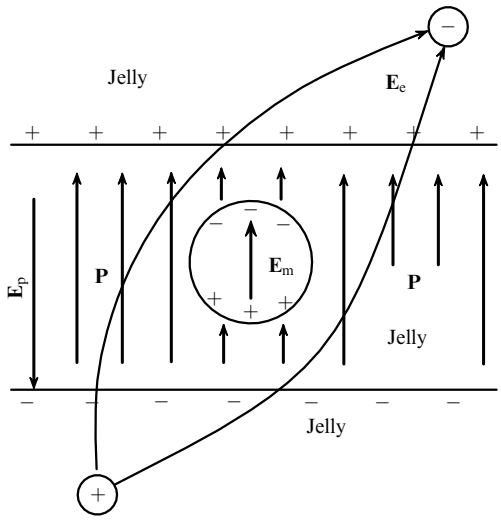

Figure 1. Charges and fields in a uniformly polarized liquid layer. Each molecule is located inside a cavity formed by other molecules. This entire system, including the foreign charges (indicated by the circles) that create the external field $\mathbf{E}_e$, is immersed in an electron 'jelly' (see Section 2.1.2). Foreign charges may be located both outside and inside the liquid.

main representative is water, are electrically neutral, but have a static electric dipole moment d_0. The interaction between molecules decreases in this case more rapidly as the distance r between particles increases, $\propto r^{-3}$. We show in this review that hydrogen-bonded polar liquids (HBPLs) possess a collective electric field generated by the dipole–dipole interaction, owing to which they exhibit a number of important and universal properties. Manifestations of this long-range action may be observed in experiments and the results of numerous calculations that are mainly based on the molecular dynamics (MD) method. In particular, the long-range dipole action is exhibited in MD via the strong dependence of calculation results on the conditions set at the computational domain boundaries. This should not be a surprise. If dipoles are oriented in the same direction, polarization charges arise at the domain boundaries that generate a depolarizing electric field $\mathbf{E}_p$ (Fig. 1). This field created by the entire ensemble of molecules affects, in turn, each of the particles. We show in Section 2.1.2 that the 'molecular' field $\mathbf{E}_m$ [1] shown in Fig. 1 is also generated by the long-range dipole interaction. This observation alone demonstrates that long-range effects play an important role in polar liquids, and that the latter are similar in this sense to plasma. We are not aware of studies wherein due attention has been paid to these features of polar liquids. The goal of this article is to fill the gap.

According to Earnshaw's theorem [2], a system of classical dipoles, which are a rather accurate approximation of HBPL molecules, is unstable; therefore, short-range interactions play a key role in polar liquids along with dipole–dipole forces. The complex phase diagram of water and the properties that distinguish it from many other liquids, which are referred to as 'anomalous', are due to the existence of short-range hydrogen bonds between molecules, whose energy is large compared to temperature, and a significant static dipole moment of the molecules [3–11].

The problem of interactions between macroscopic bodies immersed in water is of great interest for many applications in physics and chemistry, including computational physical chemistry, as well as biophysics and structural biology. This problem naturally arises, for example, in computer simulations of the interaction of molecules with biological objects in the development of new drugs [12]. The technique that is the most effective for such practical applications as calculating the free binding energy (inhibition constant) of protein–ligand complexes, predicting protonation states for biomolecules, studying membrane physics, etc. is the MD computer method based both on perturbation theory for free energy and on direct computer simulation of the microscopic dynamics of solvent molecules and dissolved substance. At present, MD makes it possible to determine thermodynamic parameters of biologically significant systems [11, 13] with an accuracy higher than that obtained from measurements. The technical difficulties arising in MD calculations are directly related to the advantages of this method: an accurate computer simulation of the interaction between macromolecules and a solvent requires coordinates and velocities to be computed for a very large number of atoms with a time step $\tau_s \sim 10^{-15}$ s. To have the solvent medium completely relaxed to the equilibrium state, effective averaging over time must span at least hydrogen bond lifetimes of $\sim 10^{-9}$ s (or even the much longer relaxation times of macroscopic solvent-substance clusters of $\sim 10^{-5}$ s). The capacities of state-of-the-art computers make it possible to numerically simulate the macromolecule dynamics in a solvent medium at time scales of up to 10^{-7} s, a value that may be insufficient for the complete relaxation of water molecules that surround the macromolecule. Although MD results are fairly accurate, specific practical applications require very large computing resources. They are especially needed in studying the properties of supercooled water, in which the relaxation times of structures $\gtrsim 1$ nm in size may be as long as several tenths of a second [14–17]. Thus, the main task is to make the results obtained reliable.

HBPLs and, in particular, water are characterized by large values of the static dielectric constant, $\varepsilon_0 \gg 1$. The theory of solvation (hydration) largely reduces for this reason to macroscopic electrostatics, where the solvent is described as a medium with large ε_0, and the macromolecule is assumed to be located in a spherical vacuum cavity. Such an approximation, which originates from the work of Born [18], enables obtaining quantitative predictions for the solvation energy of small molecules and estimating the binding energy of biomolecular complexes [19, 20]. On the other hand, the interactions between some small electrically neutral bodies immersed in an HBPL are known to be determined by the hydrophobic effect, associated with the short-range forces between molecules of liquid that arise due to the hydrogen bond network being deformed by the bodies immersed in that liquid. Models based on the analysis of the density functional are successful in explaining hydrophobic interactions at molecular scales (less than 1 nm) [21–23], but do not take into account effects characterized by large scales that are observed in MD calculations. These effects include electrostatic and long-range interactions due to the dipole moments of the molecules. As a result, techniques must be applied in many important cases that are more complex than the density functional method. A list of such effects includes the ordering of the dipole moments of solvent molecules parallel to the hydrophobic surface [24–27], the emergence of vortex structures in networks of molecular dipole moments, and the emergence of dipole bridges between macromolecules immersed in a solvent [28].

The long range nature of the interaction greatly complicates MD calculations, since, to analyze the motion of an

individual molecule, the collective field created by all molecules must be taken into account. However, a problem that is difficult for a computer might be solved by analytical methods. Application of first principles, i.e., a chain of Bogolyubov–Born–Green–Kirkwood–Yvon equations, fails to provide a significant advancement on this path [9]. To develop a unified picture of the hydration forces that are operative at mesometer distances, we employ a phenomenological description of the polar liquid [29–31]. We develop on its basis a theoretical scheme that provides an explanation of both hydrophilic and hydrophobic interactions in a unified approach.

We consider here a continuous vector model of a polar liquid (VMPL) that enables taking into account both long-range and short-range interactions in a polar liquid. The model is applicable to studying the interaction of mesoscopic charged or neutral bodies of various shapes both with solvent molecules and with each other. We use the VMPL to show that the combined effect of short-range hydrogen bonds and long-range dipole–dipole interactions in the HBPL leads to the emergence of strong long-range forces operating between macroscopic objects.

The mutual orientation of the liquid molecules (to be specific, we consider water) is correlated and ordered on a small scale, $\lesssim 1.5-2$ nm. This orientational correlation of molecules is destroyed on a large scale by thermal fluctuations. Thus, water is under normal conditions a liquid paraelectric substance that consists of separate domains, the presence of which is the cause of the high permittivity of water. As temperature decreases, a second-order ferroelectric phase transition (FPT) to an ordered ferroelectric state occurs in supercooled bulk liquid water at a temperature $T_c \sim -40\,^\circ$C. This phenomenon was theoretically predicted on the basis of the VMPL in [29, 30, 32] (the temperature of this transition is also referred to below as the λ-point). Indications of the possible existence of such a bulk-water state were seen as early as in experiments [33], while an assumption about this was made in [34]. However, the λ-point was not reached in [33] due to the accelerated bulk nucleation with a decrease in temperature and only a few degrees remained to be overcome before it. As the λ-point is approached from above on the temperature scale, the fluctuations of the order parameter, the $\mathbf{s}(\mathbf{r})$ polarization vector, are enhanced (see Section 2.1.1). It may be hypothesized that the enhancement of these fluctuations is a reason, if not the primary one, for the singularities to emerge in other physical properties of water that were observed in [35–40].

The FPT has been observed in experiments [16, 41, 42] at temperatures very close to that predicted. Lowering of the freezing temperature of water in porous materials was used to this end [43]. The VMPL phenomenological model considered here, which was proposed in [29–32, 41, 44–49], is a natural generalization of continuous models [50–59]. The VMPL was initially developed to calculate the solvation energies of small molecules and biomolecules and their mutual interaction in water. Although the mathematical form of this model is quite simple, it allows a number of important conclusions based on analytical solutions of its equations. Even the 'minimal' mathematical formulation of the VMPL presented here enables explaining numerous measurement data and making new predictions.

To avoid misunderstanding, we emphasize that the manifestations of long-range effects in water that are discussed in this publication and summarized in the Conclusions section do not imply at all that water, for example, remembers various kinds of effects to which it was subjected in the past (criticism of such a hypothesis may be found in [60]).

2. Phenomenology of polar liquid

In this section, advancing from simpler to more complex, we derive an expression for the free energy of HBPLs that describes their electrophysical properties under invariable external conditions. We consider four models based on the mean field approximation: the electronic 'jelly' model, the complete HBPL model with and without an external electric field $\mathbf{E}_e$ in the liquid, and a simplified model where the polarization of the electron shells of molecules is disregarded. To confirm the applicability of the mean field approximation and the conclusions obtained below on its basis, we calculate in Section 3 the equilibrium free energy in the ring-diagram approximation, the validity of which is based on the long-range nature of dipole interaction.

2.1 Internal energy and entropy of liquid

2.1.1 Starting expression for the internal energy of HBPL. Following [29, 30, 32], we derive an expression for the internal energy of a bulk liquid based on a microscopic description of interaction between molecules.

We specify the direction of the static electric dipole moment $\mathbf{d}_a$ of the molecule number a by the unit vector $\mathbf{S}_a = \mathbf{d}_a/d_0$, which we conventionally call the 'spin'. Here, $d_0 = |\mathbf{d}_a|$ is the absolute value of the static dipole moment. Polar liquids are similar to ferroelectrics. With this analogy in mind, it is now possible to develop a theory of the vector field, the VMPL, in which liquid is described by the local value of the molecular polarization vector

$$\mathbf{s}(\mathbf{r}) = \frac{\langle \mathbf{d} \rangle}{d_0}\,, \tag{1}$$

where averaging $\langle \ldots \rangle$ is carried out over a volume of liquid, which is small but nevertheless contains a large number of molecules. Thus, the proposed HBPL model belongs to the class of mean-field theories also referred to as the Rosing–Weiss approximation of the self-consistent molecular field [61]. Strictly speaking, the term 'static polarization vector' is used in publications for the average value of the sum of static dipole moments in the unit volume $\mathbf{P}_\mathrm{d}(\mathbf{r}) = n(\mathbf{r})\langle \mathbf{d} \rangle = n(\mathbf{r}) d_0 \mathbf{s}(\mathbf{r})$, where $n(\mathbf{r})$ is the local bulk particle number density of the liquid. We use the same name for $\mathbf{s}(\mathbf{r})$, which will not cause any confusion below.

The vector model is designed, in particular, to describe the properties of liquids on spatial scales that exceed the size of molecules (~ 0.3 nm). Variations of $n(\mathbf{r})$ may be ignored at such scales, at least in the phenomenological approach, to set

$$n(\mathbf{r}) = n_0 = \mathrm{const} \approx 3.3 \times 10^{22}\ \mathrm{cm}^{-3}\,. \tag{2}$$

Then, $\mathbf{P}_\mathrm{d}(\mathbf{r}) = n_0 \langle \mathbf{d} \rangle = P_0 \mathbf{s}(\mathbf{r})$, where $P_0 = n_0 d_0$.

In accordance with the nature of the interaction between the molecules, the internal HBPL energy U consists of three terms (it is shown in Section 2.2.2 that the most complete description needs one more term to be added):

$$U = U_\mathrm{sh} + U_\mathrm{dd} + U_\mathrm{e}\,. \tag{3}$$

Here, U_sh is due to the short-range part of the intermolecular interaction, i.e., the hydrogen bond, van der Waals attraction,

and repulsion of molecules at short distances caused by both the saturation of their covalent bonds and Coulomb repulsion between nuclei. The term $U_{\rm dd}$ describes the interaction of molecular dipole moments $\mathbf{D}_a = \mathbf{d}_a + \mathbf{d}_{{\rm e}a}$ with each other, where $\mathbf{D}_a$ is the total dipole moment of the ath molecule and $\mathbf{d}_{{\rm e}a}$ is the dipole moment induced in its electron shell. The term $U_{\rm e}$ includes the interaction between these dipoles and an external electric field,

$$\mathbf{E}_{\rm e}(\mathbf{r}) = -\nabla\varphi_{\rm e}\,, \tag{4}$$

which is created in a vacuum by foreign charges with density $\rho_{\rm e}(\mathbf{r})$, and the energy of this field itself. It should be noted that the foreign charges include both uncompensated charges and polar groups that have dipole moments, both of which can be located outside or inside the liquid, as well as on particles immersed in it.

2.1.2 Description of the dipole–dipole interaction between molecules in the electronic 'jelly' model. To describe the electron shell polarization at the circular frequencies of the external field $\omega \ll 10^{16}\ {\rm s}^{-1}$, we use the 'jelly' model, which naturally arises from the analysis of experimental data on the frequency dependence of the dielectric constant of water $\varepsilon(\omega)$ at, say, room temperature [62]. For example, the dielectric constant of water at $\omega \ll 10^{10}\ {\rm s}^{-1}$ is equal to the static value $\varepsilon_0 \approx 88$. However, at frequencies $10^{12} \ll \omega \ll 10^{16}\ {\rm s}^{-1}$, which are higher than the rotational frequencies of the molecules but lower than the characteristic electronic frequencies $\sim 10^{16}\ {\rm s}^{-1}$, $\varepsilon \approx \varepsilon_\infty \sim 5$. If the frequency increases further, $\varepsilon(\omega)$ tends to one. Thus, there is a wide transition region [63]

$$10^{10} \lesssim \omega \lesssim 10^{12}\ {\rm s}^{-1}\,, \tag{5}$$

the nature of which is associated with the presence of domains and superdomains (see Section 2.4). It should be noted that if the water molecule polarizability $\alpha = 1.455 \times 10^{-24}\ {\rm cm}^3$ is taken from reference books [64, 65], then, at the density n_0 we get $\varepsilon_\infty = 1 + 4\pi n_0\alpha = 1.61$, a value that greatly differs from that given above. This is explained by the mutual effect of the polarized shells of various molecules in the spirit of the Clausius–Mossotti relation. Thus, ε_∞ is a phenomenological parameter that corresponds to the description of the electronic subsystem in water within the jelly model, the essence of which is the formula for the electronic polarization vector

$$\mathbf{P}_{\rm e}(\mathbf{r}) = n(\mathbf{r})\langle\mathbf{d}_{\rm e}\rangle \approx n_0\langle\mathbf{d}_{\rm e}\rangle = \frac{\varepsilon_\infty - 1}{4\pi}\,\mathbf{E}(\mathbf{r})\,. \tag{6}$$

Equation (6) takes into account that the electron liquid responds to the total electric field created by all charges, which, according to the principle of superposition of electric fields, is expressed as

$$\mathbf{E}(\mathbf{r}) = \mathbf{E}_{\rm p}(\mathbf{r}) + \mathbf{E}_{\rm e}(\mathbf{r}) = -\nabla\varphi\,, \tag{7}$$

where $\mathbf{E}_{\rm p}$ is the 'depolarizing' electric field,

$$\mathbf{E}_{\rm p} = -\nabla\varphi_{\rm p}\,, \tag{8}$$

created at the molecule localization point by distant polarization charges whose density is

$$\rho_{\rm p} = -\nabla\,\mathbf{P}\,, \tag{9}$$

$\varphi_{\rm p}$ is the polarization potential, and $\varphi = \varphi_{\rm p} + \varphi_{\rm e}$ is the total potential. Here, $\mathbf{P}(\mathbf{r})$ is the total liquid polarization vector,

$$\mathbf{P}(\mathbf{r}) = n_0\langle\mathbf{D}\rangle = \mathbf{P}_{\rm d}(\mathbf{r}) + \mathbf{P}_{\rm e}(\mathbf{r})\,, \tag{10}$$

i.e., the total dipole moment of molecules per unit volume.

The depolarizing field is found from Eqns (8) and (9) and the formula

$$\nabla\,\mathbf{E}_{\rm p} = 4\pi\rho_{\rm p}\,. \tag{11}$$

The field $\mathbf{E}_{\rm p}$ depends on the liquid sample geometry. Some calculations of this field for specific samples are presented, e.g., in [66]. The meaning of the field $\mathbf{E}_{\rm p}$ and charges of various types that exist in a polar liquid is illustrated in Fig. 1, using as an example a dielectric layer with uniform polarization $\mathbf{P} = {\rm const}$. The surface density of polarization charges on the upper surface of the layer is positive, $P = |\mathbf{P}|$. The upper surface together with the lower one forms two capacitor plates, yielding $\mathbf{E}_{\rm p} = -4\pi\mathbf{P}$. Thus, the field $\mathbf{E}_{\rm p}$ is directed opposite to the polarization vector. Given Eqn (6), we bring the last expression to the form $\mathbf{E}_{\rm p} = -4\pi\mathbf{P}_{\rm d} - (\varepsilon_\infty - 1)\mathbf{E}$. This formula, combined with Eqn (7), implies a relation that is natural for the jelly model:

$$\mathbf{E} = -\frac{4\pi\mathbf{P}_{\rm d}}{\varepsilon_\infty} + \frac{\mathbf{E}_{\rm e}}{\varepsilon_\infty}\,. \tag{12}$$

In the absence of electrons and at $\mathbf{E}_{\rm e} = 0$, the field in the capacitor would be equal to $-4\pi\mathbf{P}_{\rm d}$. As it should be, the electron liquid contained in the capacitor reduces the field in its interior by a factor of ε_∞ and reduces the energy of interaction between the static dipoles of any pair of molecules by the same amount.

So in the jelly model the static dipoles of molecules $\mathbf{d}_a$ are immersed in a homogeneous electron liquid with dielectric constant ε_∞. We assume that both the entire liquid sample and the foreign charges are immersed in this jelly. We also assume that the size of the jelly is much larger than that of the sample. We can avoid in this way discussing effects of no significance for further analysis, which are associated with the field of polarization charges located at the jelly boundaries. The problem of finding $U_{\rm dd}$ is then simplified: this energy should be found in a vacuum, taking into account only static dipoles, and then divided by ε_∞ (the same should be done with the vacuum field $\mathbf{E}_{\rm e}(\mathbf{r})$). Thus, the energy of the dipole–dipole interaction between molecules in the jelly model has the form

$$\begin{aligned} U_{\rm dd} &= \frac{1}{\varepsilon_\infty}\sum_{a,\,b\,(a>b)} \frac{\mathbf{d}_a\mathbf{d}_b - 3(\mathbf{n}_{ab}\mathbf{d}_a)(\mathbf{n}_{ab}\mathbf{d}_b)}{r_{ab}^3} \\ &= -\frac{1}{2}\sum_a \mathbf{d}_a\mathbf{E}_{\rm act}(\mathbf{r}_a)\,, \end{aligned} \tag{13}$$

where $r_{ab} = |\mathbf{r}_{ab}|$, $\mathbf{r}_{ab} = \mathbf{r}_a - \mathbf{r}_b$, $\mathbf{n}_{ab} = \mathbf{r}_{ab}/r_{ab}$, and

$$\mathbf{E}_{\rm act}(\mathbf{r}_a) = \frac{1}{\varepsilon_\infty}\sum_{b\,(b\neq a)} \frac{3\mathbf{n}_{ab}(\mathbf{n}_{ab}\mathbf{d}_b) - \mathbf{d}_b}{r_{ab}^3}\,.$$

Attention should be paid to the factor 1/2 on the right-hand side of Eqn (13), without which the interaction between each pair of dipoles would be taken into account twice.

As Fig. 1 clearly shows, there are also polarization charges on the surface of the spherical cavity that surrounds the

molecule; therefore, the field inside the cavity, which acts on the molecule, has the form [1]

$$\mathbf{E}_{\rm act} = \mathbf{E}_{\rm p} + \mathbf{E}_{\rm m}\,, \tag{14}$$

where $\mathbf{E}_{\rm m}$ is the additional, molecular field created by these charges. The field $\mathbf{E}_{\rm act}$ is referred to as the 'acting' field. Thus, according to Eqn (14), each polar molecule 'feels' two fields; therefore, the energy being sought consists of two terms:

$$U_{\rm dd} = U_{\rm p} + U_{\rm m}\,. \tag{15}$$

The term $U_{\rm p}$ describes the interaction between molecules and polarization charges located far from the molecules. For example, in the case of uniform polarization (see Fig. 1), these charges are located on the surface of the layer. This clearly shows that the term $U_{\rm p}$ describes the long-range interaction between molecules generated by their dipole–dipole interaction. It is for this reason that the main contribution to $U_{\rm p}$ comes from spatial scales far exceeding the molecule size. Therefore, to calculate this contribution, it is sufficient to perform in Eqn (13) integration rather than summation:

$$U_{\rm p} = -\frac{1}{2}\int {\rm d}^3 r\, \mathbf{P}_{\rm d}\mathbf{E}_{\rm p}\,, \tag{16}$$

where

$$\mathbf{E}_{\rm p}(\mathbf{r}) = \frac{1}{\varepsilon_\infty}\,\mathbf{E}_{\rm d}\,, \qquad \mathbf{E}_{\rm d} = \int {\rm d}^3 r'\,\frac{3\mathbf{n}(\mathbf{n}\mathbf{P}_{\rm d}) - \mathbf{P}_{\rm d}}{R^3}\,, \tag{17}$$

$\mathbf{R} = \mathbf{r} - \mathbf{r}'$, $\mathbf{n} = \mathbf{R}/R$. We introduced here the vacuum field of static dipoles $\mathbf{E}_{\rm d}$ that satisfies the equation $\nabla\,\mathbf{E}_{\rm d} = 4\pi\rho_{\rm d}$. Comparing (17) with (9) and (11), we conclude that in the jelly model

$$\rho_{\rm p} = \frac{1}{\varepsilon_\infty}\,\rho_{\rm d}\,, \tag{18}$$

where $\rho_{\rm d} = -\nabla\,\mathbf{P}_{\rm d}$ is the density of only static charges.

Formula (16) is also valid for an infinite sample of liquid; therefore, upon integrating by parts with consideration for Eqns (8), (9), and (11) and assuming that both polarization $\mathbf{P}$ and field $\mathbf{E}_{\rm p}$ vanish at infinity, we obtain

$$U_{\rm p} = -\frac{1}{2}\int {\rm d}^3 r\, \mathbf{P}_{\rm d}\mathbf{E}_{\rm p} = \int {\rm d}V\,\frac{\mathbf{E}_{\rm d}^2}{8\pi\varepsilon_\infty}\,. \tag{19}$$

The jelly uniformly fills the liquid, including the cavity. Therefore, the polarization charges on the cavity surface are only created by static dipoles. In the absence of the jelly [1],

$$\mathbf{E}_{\rm m} = \frac{4\pi}{3}\,\mathbf{P}_{\rm d}\,. \tag{20}$$

Given the additional factors 1/2 and $1/\varepsilon_\infty$ discussed above, we arrive at the expression for the contribution $U_{\rm m}$:

$$U_{\rm m} = -\frac{2\pi}{3\varepsilon_\infty}\int {\rm d}^3 r\,\mathbf{P}_{\rm d}^2 = -\frac{2\pi}{3\varepsilon_\infty}\,P_0^2\int {\rm d}^3 r\,\mathbf{s}^2(\mathbf{r})\,. \tag{21}$$

2.1.3 Orientational entropy. We consider first the case of a weakly polarized liquid,

$$s(\mathbf{r}) = \left|\mathbf{s}(\mathbf{r})\right| \ll 1\,, \tag{22}$$

which arises if the electric field is weak, $E \ll P_0$. The single-particle distribution function over the molecular-dipole orientations has in this case the form

$$f(\theta) \approx \frac{1}{4\pi}(1 + 3s\cos\theta)\,, \tag{23}$$

where θ is the angle between the 'spin' $\mathbf{S}$ and the polarization vector $\mathbf{s}(\mathbf{r})$. Indeed, let the coordinate origin be placed at the point $\mathbf{r}$ and the z axis be directed along the vector $\mathbf{s}(\mathbf{r})$. Then, as required, we have for the average value of $\langle s_z\rangle$: $\langle s_z\rangle = \int {\rm d}\Omega_{\mathbf{S}}\, f(\theta) s\cos\theta = s$, where ${\rm d}\Omega_{\mathbf{S}}$ is the solid angle element into which the spin $\mathbf{S}$ is directed. Using the basic formula of statistical physics, we obtain the following expression for the configurational entropy of liquid:

$$S = -\int n_0\,{\rm d}^3 r\,{\rm d}\Omega_{\mathbf{S}}\, f\ln f \approx \int n_0\,{\rm d}V\left(-\frac{3}{2}\,s^2(\mathbf{r}) - \frac{1}{15}\,s^4(\mathbf{r})\right). \tag{24}$$

2.1.4 Term $U_{\rm sh}$ due to the short-range part of the intermolecular interaction. Due to approximation (2), it is sufficient to take into account in energy $U_{\rm sh}$ only the contribution from the distortion of the hydrogen bond network caused, e.g., by immersed bodies. Thus, the contribution of $U_{\rm sh}$ to free energy is quite similar to that considered in Refs [67, 68], which is called 'hydrophobic interaction.' If this network is deformed, a nonzero polarization of liquid $\mathbf{s}(\mathbf{r})$ inevitably emerges. Since $\mathbf{s}(\mathbf{r}) = 0$ in the absence of bodies and an external field (or at least $\mathbf{s}(\mathbf{r}) = {\rm const}$), such a distortion is described by the derivatives of the polarization vector with respect to the coordinates $\partial s_\alpha/\partial x_\beta$, where $\alpha, \beta = x, y, z$ are spatial indices. The energy $U_{\rm sh}$ should not change if the sign of the polarization vector is reversed; therefore, the 'minimal', simplest expression for this energy is given by the Oseen formula quadratic in those derivatives [69]:

$$U_{\rm sh} = \frac{1}{2}\,P_0^2\int {\rm d}^3 r\left[C\sum_{\alpha,\beta}\frac{\partial s_\alpha}{\partial x_\beta}\,\frac{\partial s_\alpha}{\partial x_\beta} + C'(\nabla\,\mathbf{s})^2\right]. \tag{25}$$

Integration is carried out here over the volume of liquid; C and C' are positive constants (energy should be the smallest at $\mathbf{s}(\mathbf{r}) = {\rm const}$!) expressed in cm^2.

In all the applications of the vector model considered here, the constant C' only affects quantitative rather than qualitative conclusions regarding the properties of the liquid. The point is that if $\nabla\,\mathbf{s} \neq 0$, when a polarizing charge is present in the volume, the terms containing both C' and C are simultaneously nonzero. We have no confidence that both parameters can be reliably found in this case from a comparison of the VMPL- and MD-based calculations. However, in considering many important cases, e.g., phase transitions in bulk and surface water, the main role is played, as is shown below, by the 'force-free' polarization configurations, $\nabla\,\mathbf{s} = 0$, wherein there is no polarization charge. For these reasons, below, we set $C' = 0$. Of course, here, as elsewhere in this article, we choose the simplest of all possible ways to describe HBPL. Otherwise, no useful information about these properties could be extracted.

In deriving Eqn (25), simpler arguments may be used as is done, e.g., in the theory of ferromagnetism. The terms in the formula for internal energy that depend on the vector $\mathbf{s}$ and this vector squared $\mathbf{s}^2$ and reflect the major large-scale properties of the polar liquid are presented in Sections 2.1.1–

2.1.3. It is now only required to take into account large-scale deviations from inhomogeneities that, given Eqn (2), depend on derivatives $\partial s_\alpha/\partial x_\beta$ and, for the reasons described above, have the most general Oseen form (25).

2.2 Free energy of polar liquid in the absence of foreign charges

2.2.1 Jelly model. If $\mathbf{E}_e = 0$, taking into account Eqns (3), (15), (19), (21), and (25), we obtain the following expression for the nonequilibrium Gibbs free energy, which is a functional of the polarization $\mathbf{s}(\mathbf{r})$:

$$G\big[\mathbf{s}(\mathbf{r})\big] = U - TS + pV_l = P_0^2 \int \mathrm{d}^3 r \left[\frac{C}{2}\sum_{\alpha,\beta}\frac{\partial s_\alpha}{\partial x_\beta}\frac{\partial s_\alpha}{\partial x_\beta} + V(s^2)\right] + \int \mathrm{d}V\,\frac{\mathbf{E}_d^2}{8\pi\varepsilon_\infty} + pV_l\,. \tag{26}$$

Here, p is the pressure and V_l is the volume of the liquid. Formula (26) is presented in a form applicable for arbitrary values of the polarization vector modulus $0 \leqslant s < 1$, for which the 'equation-of-state' function $V(s^2)$ was introduced. The temperature T is given here and below in units of energy, i.e., $T = k_B T$, where k_B is the Boltzmann constant, while the temperature T is measured in degrees Kelvin. We assume in all applications of the model that the pressure p has a fixed constant value, and the variation in the density of a liquid is small (see Eqn (2)), so we ignore the constant pV_l below.

Free energy (26) with a potential of the general form $V(s^2)$ may be considered a phenomenological expression in the mean field approximation. If $s \sim 1$, the short-range part of the intermolecular interaction potential is essential, and so $V(s^2)$ depends in this region on the details of the interaction between individual molecules.

The equilibrium polarization $\mathbf{s}(\mathbf{r})$ should be found from the condition of minimum free energy (26). We obtain for δG under an arbitrary small variation in the static polarization vector $\delta\mathbf{P}_d(\mathbf{r})$ after several integrations by parts with Eqns (11) and (18) taken into account

$$\delta G = \int \mathrm{d}^3 r \left[-C\Delta\mathbf{P}_d + 2\,\frac{\mathrm{d}V(s^2)}{\mathrm{d}s^2}\,\mathbf{P}_d - \mathbf{E}_p\right]\delta\mathbf{P}_d\,,$$

which yields the Euler equation

$$-C\Delta\mathbf{P}_d + 2\,\frac{\mathrm{d}V(s^2)}{\mathrm{d}s^2}\,\mathbf{P}_d = \mathbf{E}_p\,. \tag{27}$$

We used here the formula $\delta\int \mathrm{d}^3 r\,\mathbf{P}_d\mathbf{E}_p = -2\int \mathrm{d}V\,\mathbf{E}_p\,\delta\mathbf{P}_d$.

We now discuss properties of the function $V(s^2)$. The exact form of $V(s^2)$ can only be found by comparing the VMPL predictions with experimental results or MD calculations. However, some properties of $V(s^2)$ may be determined using a number of simple arguments. For example, polarization should be saturated in the limit of a strong electric field. According to (27), this observation implies that $\mathrm{d}V(s^2)/\mathrm{d}s^2 \to \infty$ if $s \to 1$. If the polarization of the liquid is small, $s \ll 1$, then, according to Eqns (21) and (24), we have, with an accuracy of up to $\sim s^2$,

$$V(\mathbf{s}^2) \approx \frac{2\pi}{3\varepsilon_\infty}\left(-1 + \frac{T}{T_c}\right)s^2\,, \tag{28}$$

where

$$T_c = \frac{4\pi n_0 d_0^2}{9\varepsilon_\infty}\,. \tag{29}$$

The physical meaning of temperature T_c is discussed in Section 3. We also retain for further applications the term $\sim s^4$:

$$V(\mathbf{s}^2) \approx \frac{1}{2}\,As^2 + Bs^4\,, \quad s \ll 1\,. \tag{30}$$

Here, A and B are dimensionless positive constants that depend on the type of liquid:

$$A = \frac{4\pi\tau}{3\varepsilon_\infty}\,, \qquad B = \frac{4\pi}{135\varepsilon_\infty}\,, \tag{31}$$

$$\tau = \frac{T - T_c}{T_c}\,. \tag{32}$$

The formula for B in (31) takes into account that the temperatures considered in this article are close to T_c (see Section 3), as a result of which the condition

$$|\tau| \ll 1 \tag{33}$$

is fulfilled.

2.2.2 Account for the deformation of the electron shells of HBPL molecules. The free energy of a liquid was previously believed to be a functional of the polarization vector $\mathbf{s}(\mathbf{r})$ (or, equivalently, of the vector $\mathbf{P}_d(\mathbf{r})$) associated with the static dipole moments of molecules. Equation (6) in this case 'hangs in the air'. In the most comprehensive approach, $\mathbf{P}_e(\mathbf{r})$ should be another independent parameter on which the free energy $G[\mathbf{P}_d(\mathbf{r}),\,\mathbf{P}_e(\mathbf{r})]$ depends, and Eqns (6) and (27) should follow from the condition of minimum energy

$$\frac{\delta G\big[\mathbf{P}_d(\mathbf{r}),\,\mathbf{P}_e(\mathbf{r})\big]}{\delta\mathbf{P}_d(\mathbf{r})} = 0\,, \quad \frac{\delta G\big[\mathbf{P}_d(\mathbf{r}),\,\mathbf{P}_e(\mathbf{r})\big]}{\delta\mathbf{P}_e(\mathbf{r})} = 0\,. \tag{34}$$

The form of correction required may be determined using a simple model of two classical charges: q and $-q$ connected by a spring with stiffness coefficient k. Their energy U in an electric field E is $U = kx^2/2 - qEx$, where x is the spring length. We use the minimum condition for this energy to derive the formula $d_e = qx = q^2E/k$, which is similar to (6). We arrive in this case at the expression $U_{\min} = -q^2E^2/(2k)$, similar to the well-known expression $-\alpha E^2/2$ for the energy of an unexcited atom in an external field, where α is atom polarizability. A term similar to $kx^2/2$, which describes the electron shell 'elasticity', should be added for these reasons to the right-hand side of Eqn (3):

$$U_{el} = \int \mathrm{d}^3 r\,\frac{2\pi}{\varepsilon_\infty - 1}\,\mathbf{P}_e^2(\mathbf{r})\,. \tag{35}$$

Given Eqns (8)–(11), (34), and (35), we arrive at the formula (cf. (26))

$$G\big[\mathbf{P}_d(\mathbf{r}),\,\mathbf{P}_e(\mathbf{r})\big] = P_0^2 \int \mathrm{d}^3 r\left[\frac{C}{2}\sum_{\alpha,\beta}\frac{\partial s_\alpha}{\partial x_\beta}\frac{\partial s_\alpha}{\partial x_\beta} + V(s^2)\right] + \int \mathrm{d}V\,\frac{\mathbf{E}_p^2}{8\pi} + \int \mathrm{d}^3 r\,\frac{2\pi}{\varepsilon_\infty - 1}\,\mathbf{P}_e^2(\mathbf{r})\,. \tag{36}$$

2.3 General expression for the free energy of polar liquid with hydrogen bonds in the presence of foreign charges

To derive the expression for U_e included in Eqn (3), we turn to study [66, §10]. We consider a conductive body with a charge q_e, which creates a field $\mathbf{E}_e(\mathbf{r})$ in a vacuum, immersed in a liquid. Since the body is conductive, the potential φ_Γ on its

surface Γ is constant. The vectors of electric induction in the liquid and $\mathbf{E}_e$ satisfy the same equations: $\nabla\mathbf{D} = 4\pi\rho_e$ and

$$\nabla\mathbf{E}_e = 4\pi\rho_e\,, \tag{37}$$

from which we have

$$q_e = -\frac{1}{4\pi}\int_\Gamma \mathbf{D}\,\mathrm{d}\mathbf{f} = -\frac{1}{4\pi}\int_\Gamma \mathbf{E}_e\,\mathrm{d}\mathbf{f}\,.$$

Here, $\mathrm{d}\mathbf{f}$ is the vector of the surface area element Γ of the body directed at its interior, i.e., outward with respect to the liquid. It should be noted that, generally speaking, $\mathbf{D}(\mathbf{r}) \neq \mathbf{E}_e(\mathbf{r})$: due to the presence in the general case of polarization charges, these vectors are only equal in some particular geometric arrangements of the liquid sample and external charges. To establish the dependence of U_e on $\mathbf{E}_e(\mathbf{r})$, we fix the molecular dipoles,

$$\delta\mathbf{P}_d = 0, \quad \delta\mathbf{P}_e = 0\,. \tag{38}$$

We now consider an infinitesimal charge δq_e transported to the conductor from infinity. Due to Eqn (38), the work needed to transport the charge increases the term U_e in the free energy of the liquid: $\delta G = \delta U_e$. Given that outside the conductor $\nabla\mathbf{E}_e = 0$, we obtain

$$\begin{aligned}
\delta U_e &= \varphi_\Gamma \delta q_e = -\frac{1}{4\pi}\int_\Gamma \varphi\delta\mathbf{E}_e\,\mathrm{d}\mathbf{f} = -\frac{1}{4\pi}\int \nabla(\varphi\delta\mathbf{E}_e)\,\mathrm{d}^3r \\
&= -\frac{1}{4\pi}\int \delta\mathbf{E}_e\nabla\varphi\,\mathrm{d}^3r = \frac{1}{4\pi}\int \delta\mathbf{E}_e\big(\mathbf{D}(\mathbf{r}) - 4\pi\mathbf{P}(\mathbf{r})\big)\,\mathrm{d}^3r \\
&= \delta U_e^{(1)} + \delta U_e^{(2)}\,, \\
\delta U_e^{(1)} &= -\int \mathrm{d}^3r\,\mathbf{P}(\mathbf{r})\delta\mathbf{E}_e(\mathbf{r})\,, \\
\delta U_e^{(2)} &= \frac{1}{4\pi}\int \delta\mathbf{E}_e(\mathbf{r})\mathbf{D}(\mathbf{r})\,\mathrm{d}^3r\,.
\end{aligned}$$

Thus, $U_e = U_e^{(1)} + U_e^{(2)}$. Since molecular dipoles are fixed (see Eqn (38)), the first of the terms that emerges upon completion of charge transport makes the contribution $U_e^{(1)} = -\int \mathrm{d}^3r\,\mathbf{P}(\mathbf{r})\mathbf{E}_e(\mathbf{r})$. Using Eqn (4) and the relation $\nabla\mathbf{D} = 0$, which is valid in the volume of the liquid, we transform the second term:

$$\begin{aligned}
\delta U_e^{(2)} &= -\frac{1}{4\pi}\int \nabla\big(\delta\varphi_e(\mathbf{r})\mathbf{D}(\mathbf{r})\big)\,\mathrm{d}^3r \\
&= -\frac{1}{4\pi}\int_\Gamma \delta\varphi_e(\mathbf{r})\mathbf{D}(\mathbf{r})\,\mathrm{d}\mathbf{f} \\
&= -\frac{1}{4\pi}\,\delta\varphi_e^\Gamma\int_\Gamma \mathbf{D}(\mathbf{r})\,\mathrm{d}\mathbf{f} = \delta\varphi_e^\Gamma q_e\,.
\end{aligned}$$

Since $\delta\varphi_e^\Gamma \propto q_e$, upon completion of charge transport we obtain

$$U_e^{(2)} = \frac{1}{2}\,\varphi_e^\Gamma q_e = -\frac{1}{8\pi}\int_\Gamma \varphi_e\mathbf{E}_e\,\mathrm{d}\mathbf{f} = \int \frac{\mathbf{E}_e^2}{8\pi}\,\mathrm{d}^3r\,.$$

The final full expression for free energy has the form

$$\begin{aligned}
G\big[\mathbf{P}_d(\mathbf{r}),\,\mathbf{P}_e(\mathbf{r})\big] &= P_0^2\int \mathrm{d}^3r\left[\frac{C}{2}\sum_{\alpha,\beta}\frac{\partial s_\alpha}{\partial x_\beta}\frac{\partial s_\alpha}{\partial x_\beta} + V(s^2)\right] \\
&+ \int \mathrm{d}^3r\left(\frac{\mathbf{E}_p^2}{8\pi} - \mathbf{P}(\mathbf{r})\mathbf{E}_e(\mathbf{r}) + \frac{\mathbf{E}_e^2}{8\pi} + \frac{2\pi\mathbf{P}_e^2}{\varepsilon_\infty - 1}\right).
\end{aligned} \tag{39}$$

We obtain from this the formula for the variation of free energy

$$\begin{aligned}
\delta G\big[\mathbf{P}_d(\mathbf{r}),\,\mathbf{P}_e(\mathbf{r})\big] &= \int \mathrm{d}^3r\left[-C\Delta\mathbf{P}_d + 2\,\frac{\mathrm{d}V(s^2)}{\mathrm{d}s^2}\,\mathbf{P}_d - \mathbf{E}\right]\delta\mathbf{P}_d \\
&+ \int \mathrm{d}^3r\left(\frac{4\pi}{\varepsilon_\infty - 1}\,\mathbf{P}_e(\mathbf{r}) - \mathbf{E}\right)\delta\mathbf{P}_e\,,
\end{aligned}$$

which yields Eqn (6) and

$$-C\Delta\mathbf{P}_d + 2\,\frac{\mathrm{d}V(s^2)}{\mathrm{d}s^2}\,\mathbf{P}_d = \mathbf{E}\,. \tag{40}$$

Equations (6) and (40) combined with Eqns (7), (8), (10), (11), and (37) form a closed system, which we call below the VMPL equations. These equations are nonlocal and nonlinear. We only consider below, whenever possible, approximation (22) that enables determining in an analytical form the asymptotic behavior of long-range interactions between large objects in bulk water and investigating physical phenomena both in the volume of water and in its layers adjacent to the surfaces of bodies of various natures.

2.4 Dielectric constant of polar liquid with hydrogen bonds. The two-scale nature of the vector model

We consider the case of a weakly polarized liquid (22), where, according to (30), $V(s^2) \approx As^2/2$. The VMPL equations for an unbounded liquid are analytically solved in this case using the transition to Fourier components. Here and below, the following definition of the Fourier transform of an arbitrary function $f(\mathbf{r})$ is adopted: $f_\mathbf{k} = \int \mathrm{d}^3r f(\mathbf{r})\exp(-\mathrm{i}\mathbf{k}\mathbf{r})/\sqrt{V_1}$. The inverse Fourier transform is given in this case by the formula $f(\mathbf{r}) = \sum_\mathbf{k} f_\mathbf{k}\exp(\mathrm{i}\mathbf{k}\mathbf{r})/\sqrt{V_1}$. The sample of liquid is assumed to have the form of a cube with the side $l = V_1^{1/3}$ and the physical quantities to be periodic in all three coordinates (x, y, z) with the period l. Thus, the wave vector $\mathbf{k}$ takes the discrete values

$$\mathbf{k} = \frac{2\pi}{l}\,(n_x,\,n_y,\,n_z)\,,$$

where n_x, n_y, and n_z are integers. The procedure for replacing the sum over wave vectors with the integral has in this case the following form:

$$\sum_\mathbf{k} \equiv \sum_{n_x,n_y,n_z} \to V_1\int \frac{\mathrm{d}^3k}{(2\pi)^3}\,.$$

A solution of linearized VMPL equations (6) and (40) has the form

$$\mathbf{P}_\mathbf{k} = \frac{\varepsilon(k) - 1}{4\pi}\,\mathbf{E}_\mathbf{k}\,, \qquad \mathbf{E}_\mathbf{k} = \frac{\mathbf{E}_{e\mathbf{k}}}{\varepsilon(k)}\,, \qquad \varphi_\mathbf{k} = \frac{\varphi_{e\mathbf{k}}}{\varepsilon(k)}\,. \tag{41}$$

Here,

$$\varepsilon(k) = \varepsilon_\infty + \frac{4\pi}{Ck^2 + A} = \varepsilon_0\,\frac{R_d^2k^2 + 1}{L_T^2k^2 + 1}\,, \tag{42}$$

$$L_T = \sqrt{\frac{C}{A}}, \quad R_d = \sqrt{\frac{\varepsilon_\infty C}{4\pi + \varepsilon_\infty A}} = L_T\sqrt{\frac{\varepsilon_\infty}{\varepsilon_0}} \approx L_T\sqrt{\frac{\tau}{3}}, \tag{43}$$

$$\varepsilon_0 = \varepsilon_\infty + \frac{4\pi}{A} = \varepsilon_\infty\left(1 + \frac{3}{\tau}\right). \tag{44}$$

The following formula follows for the electric displacement vector from Eqn (41): $\mathbf{D}_\mathbf{k} = \mathbf{E}_\mathbf{k} + 4\pi\mathbf{P}_\mathbf{k} = \varepsilon(k)\mathbf{E}_\mathbf{k}$. Therefore, $\varepsilon(k)$ is the effective dielectric constant for the wave vector $\mathbf{k}$

and zero frequency $\omega = 0$ (since the foreign charges are immobile), and ε_0 is the dielectric constant for $\mathbf{k} = 0$ that corresponds to a uniform field $\mathbf{E}(\mathbf{r}) = \text{const}$, for which we obtain the standard formula $\mathbf{P} = \mathbf{E}(\varepsilon_0 - 1)/(4\pi)$. An estimate $A \approx 0.15$ follows from Eqn (44) for water at room temperature. We use this estimate and Eqn (43) to conclude that at this temperature $R_\mathrm{d} \approx 0.25 L_T$.

Equation (42) shows that water acquires the property of spatial dispersion owing to hydrogen bonds. It is also seen that two characteristic scales, R_d and L_T, arise naturally. Their origin is associated with the existence of domains and superdomains in water, i.e., molecule clusters in which the directions of 'spins' $\mathbf{S}$ are strongly and weakly correlated. The existence of such structures was hypothesized in [70]. Indeed, the directions of the molecule dipole moments should correlate due to the combined effect of hydrogen bonds and the dipole–dipole interaction on a certain characteristic scale R_0, comparable to the molecule size. The dipoles of neighboring molecules act on each other within this region of space, which we call the domain, by means of rather large electric fields: $\sim P_0 \sim 10^7\ \mathrm{V\,cm^{-1}}$. The energy of interaction between neighboring dipoles inside such a domain is of the order of the hydrogen bond energy, $U_\mathrm{dd} \sim U_\mathrm{H}$. Since in the vector model $U_\mathrm{H} \sim U_\mathrm{sh} \sim C P_0^2 R_0$ and $U_\mathrm{dd} \sim P_0^2 R_0^3$, we obtain the following estimated size of the domain: $R_\mathrm{d} \sim R_0 \sim \sqrt{C}$. The second scale, L_T (the 'superdomain' size), describes correlations between the domains. It follows from the estimate L_T obtained in Section 2.8 that the superdomain contains $N_T \sim 100$ molecules. Correlations between domains are destroyed at scales larger than L_T by thermal fluctuations. At the same time, L_T is nothing but an analog of the Debye screening radius in plasma physics, i.e., the characteristic size at which the dipoles screen each other (see Section 3.3). Superdomains determine the response of the polar liquid to a weak uniform and static electric field applied to the liquid, i.e., static dielectric constant ε_0. They do not have sufficient time to adjust to the high-frequency electromagnetic field, to which smaller and more rigid domains manage to respond. As the frequency of the electric field applied to water increases, a gradual transition occurs from the excitation of domain vibrations in superdomains to oscillations of the dipole moments of individual molecules in the domains. It is for this reason that a transition frequency range (5) exists.

The qualitative arguments set forth above are confirmed by calculations of the correlation function of polarization vectors at various points of the infinite liquid $Q_{\alpha\beta}(\mathbf{R}) = \langle s_\alpha(\mathbf{r}) s_\beta(\mathbf{r}')\rangle$, where $\mathbf{R} = \mathbf{r} - \mathbf{r}'$, and averaging is carried out over thermal fluctuations of polarization with the Gibbs weight $\exp(-G/T)$. In approximation (22), retaining in $V(s^2)$ the s^2 term alone and expanding functional (47) in a Fourier series, we find

$$G\big[\mathbf{P}(\mathbf{r})\big] = \sum_{\mathbf{k}} (G_\mathbf{k} - \mathbf{E}_{\mathrm{e}\mathbf{k}} \mathbf{P}_{-\mathbf{k}}) = \sum_{\mathbf{k}\,(k_z>0)} (2G_\mathbf{k} - \mathbf{E}_{\mathrm{e}\mathbf{k}} \mathbf{P}_{-\mathbf{k}} - \mathbf{E}^*_{\mathrm{e}\mathbf{k}} \mathbf{P}^*_{-\mathbf{k}}) , \tag{45}$$

$$G_\mathbf{k} = \frac{1}{2} \sum_{\alpha,\beta} F_{\alpha\beta}(\mathbf{k}) P_{\mathbf{k}\alpha} P_{-\mathbf{k}\beta} = \frac{1}{2}\left[(Ck^2 + A)|\mathbf{P}_\mathbf{k}|^2 + \frac{4\pi}{\varepsilon_\infty} |\hat{\mathbf{k}}\mathbf{P}_\mathbf{k}|^2\right] ,$$

$$F_{\alpha\beta}(\mathbf{k}) = (Ck^2 + A)\delta_{\alpha\beta} + \frac{4\pi}{\varepsilon_\infty} \hat{k}_\alpha \hat{k}_\beta .$$

The terms that do not contain polarization $\mathbf{s}$ and are therefore inessential for this calculation are omitted here. In addition, the unit vector $\hat{\mathbf{k}} = \mathbf{k}/k$ is introduced, and it is taken into account that

$$\mathbf{P}(\mathbf{r}) = \sum_\mathbf{k} \frac{\mathbf{P}_\mathbf{k} \exp(\mathrm{i}\mathbf{k}\mathbf{r})}{\sqrt{V_1}} ,$$

$$\mathbf{P}_\mathbf{k} = \int \mathrm{d}^3 r\, \frac{\mathbf{P}(\mathbf{r}) \exp(-\mathrm{i}\mathbf{k}\mathbf{r})}{\sqrt{V_1}} = \mathbf{P}'_\mathbf{k} + \mathrm{i}\mathbf{P}''_\mathbf{k} .$$

The Fourier components have the property $\mathbf{P}_\mathbf{k} = \mathbf{P}^*_{-\mathbf{k}}$; therefore, the real ($\mathbf{P}'_\mathbf{k}$) and imaginary ($\mathbf{P}''_\mathbf{k}$) parts of the vectors $\mathbf{P}_\mathbf{k}$ in the semi-space of the wave vectors $k_z > 0$ may be chosen as a complete set of independent variables. Taking into account the procedure for replacing the sum over the wave vectors with the integral $\sum_\mathbf{k} \to V_1 \int \mathrm{d}^3 k/(2\pi)^3$, we arrive at the expression

$$Q_{\alpha\beta}(\mathbf{R}) = \frac{T}{4\pi P_0^2 C} L_{\alpha\beta} ,$$

$$L_{\alpha\beta} = \frac{\exp(-R/L_T)}{R} \delta_{\alpha\beta} - \nabla_\alpha \nabla_\beta \frac{L_T^2\big[1 - \exp(-R/L_T)\big] - R_\mathrm{d}^2\big[1 - \exp(-R/R_\mathrm{d})\big]}{R} . \tag{46}$$

The limiting cases are instructive:

$$L_{\alpha\beta}(\mathbf{R}) = \begin{cases} \dfrac{1}{R}\, \delta_{\alpha\beta} , & R_\mathrm{d} \ll R \ll L_T , \\ \dfrac{L_T^2}{R^3} (\delta_{\alpha\beta} - 3\hat{R}_\alpha \hat{R}_\beta) , & R \gg L_T , \end{cases}$$

where $\hat{\mathbf{R}} = \mathbf{R}/R$. The polarization correlations decrease according to a power law, since they are due to the dipole–dipole interaction between molecules, which, as has been shown, has a long range. They are characterized by the scale L_T. The reason is that at $|\tau| \ll 1$ the fluctuations in model (26) are basically 'force-free': $\nabla \mathbf{s} = 0$, $\rho_\mathrm{p} = 0$, $\mathbf{E}_\mathrm{p} = 0$ [29]. No energy is required in this case to create an electric field, and the correlations span a distance $\sim L_T$ that is larger than the molecule size.

2.5 Simplified form of the free energy of polar liquid with hydrogen bonds

The electronic contribution ε_∞ to permittivity (~ 5) is at normal temperatures much less than that provided by static molecular dipoles ($\sim \varepsilon_0 \sim 80$); therefore, to simplify the calculations, whenever possible, we disregard the electron shell polarization. In other words, we put $\mathbf{P}_\mathrm{e} = 0$ and $\varepsilon_\infty = 1$ in all the formulas above, where ε_∞ can be ignored due to its smallness compared to ε_0. For example, we now have $\varepsilon_0 = 1 + 4\pi/A$ instead of Eqn (44). It is of importance at the same time to preserve the electrophysical properties of the liquid at temperatures close to normal, in particular, the previous value of the dielectric constant. We use to this end $A \approx 0.144$ instead of $A \approx 0.15$. Formula (39) is simplified in this approximation:

$$G_\mathrm{b}\big[\mathbf{P}(\mathbf{r})\big] = \frac{C}{2} \sum_{\alpha,\beta=x,y,z} \int \mathrm{d}^3 r\, \frac{\partial P_\alpha}{\partial x_\beta} \frac{\partial P_\alpha}{\partial x_\beta} + \int \mathrm{d}^3 r\, P_0^2 V(\mathbf{s}^2) + \int \mathrm{d}^3 r \left(-\frac{1}{2}\, \mathbf{P}(\mathbf{r})\mathbf{E}_\mathrm{p}(\mathbf{r}) - \mathbf{P}(\mathbf{r})\mathbf{E}_\mathrm{e}(\mathbf{r}) + \frac{\mathbf{E}_\mathrm{e}^2(\mathbf{r})}{8\pi}\right) . \tag{47}$$

All properties of $V(\mathbf{s}^2)$ are preserved, in particular (30) with $B \sim 1$. The polarization of the liquid in this approximation, $\mathbf{P} = P_0\mathbf{s}$, determines the polarization charge density $\rho_\mathrm{p} = -\mathrm{div}\,\mathbf{P}$. The polarization electric field $\mathbf{E}_\mathrm{p} = -\nabla\varphi_\mathrm{p}$ is a solution to the Poisson equation $\mathrm{div}\,\mathbf{E}_\mathrm{p} = 4\pi\rho_\mathrm{p}$. The total field in the liquid is $\mathbf{E} = \mathbf{E}_\mathrm{e} + \mathbf{E}_\mathrm{p}$. The Euler equation $\delta G_\mathrm{b}[\mathbf{P}(\mathbf{r})]/\delta\mathbf{P}(\mathbf{r}) = 0$ preserves its previous form (40) in the notations introduced here.

2.6 Equilibrium free energy

If the VMPL equations are solved, then, by substituting (6) and (40) into (39), we obtain the following formula for the free energy of the liquid at the minimum:

$$G_\mathrm{min} = \int \mathrm{d}^3r\, P_0^2\left(V - s^2\frac{\mathrm{d}V}{\mathrm{d}s^2}\right) - \int \mathrm{d}^3r\left(\frac{1}{2}\,\mathbf{P}_\mathrm{d}(\mathbf{E}_\mathrm{p} - \mathbf{E}_\mathrm{e}) + \frac{2-\varepsilon_\infty}{8\pi}\,\mathbf{E}_\mathrm{e}^2 + \frac{\varepsilon_\infty}{8\pi}\,\mathbf{E}_\mathrm{p}^2\right). \quad (48)$$

Equations (40) and (48) in case (22) take the following form:

$$-C\Delta\mathbf{P}_\mathrm{d} + A\mathbf{P}_\mathrm{d} = \mathbf{E}\,, \quad (49)$$

$$G_\mathrm{min} = \sum_\mathbf{k}\frac{1}{8\pi\varepsilon(k)}\,\mathbf{E}_\mathbf{ek}^2\,. \quad (50)$$

2.7 Solvation energy of foreign charges immersed in liquid

Solvation energy is a change in Gibbs equilibrium energy in the process of moving a system of charges from a vacuum, wherein their energy is

$$G_\mathrm{vac} = \int \mathrm{d}^3r\,\frac{\mathbf{E}_\mathrm{e}^2}{8\pi} = \int\frac{V_1\,\mathrm{d}^3k}{(2\pi)^3}\,\frac{|\mathbf{E}_\mathbf{ek}|^2}{8\pi}\,,$$

into a liquid: $G_\mathrm{solv} = G_\mathrm{min} - G_\mathrm{vac}$. We have in the linear approximation (50)

$$G_\mathrm{solv} = \int\frac{V_1\,\mathrm{d}^3k}{(2\pi)^3}\,\frac{|\mathbf{E}_\mathbf{ek}|^2}{8\pi}\left(\frac{1}{\varepsilon(k)} - 1\right) = \frac{1}{2}\int\frac{V_1\,\mathrm{d}^3k}{(2\pi)^3}\,\frac{4\pi|\rho_\mathbf{ek}|^2}{k^2}\left(\frac{1}{\varepsilon(k)} - 1\right), \quad (51)$$

or in coordinate representation

$$G_\mathrm{solv} = -\frac{1}{2\varepsilon_0\varepsilon_\infty}\int \mathrm{d}^3r\,\mathrm{d}^3r'\,\frac{\rho_\mathrm{e}(\mathbf{r})\rho_\mathrm{e}(\mathbf{r}')}{|\mathbf{r}-\mathbf{r}'|}\,L\,, \quad (52)$$

$$L = \varepsilon_\infty(\varepsilon_0 - 1) - (\varepsilon_0 - \varepsilon_\infty)\exp\left(-\frac{|\mathbf{r}-\mathbf{r}'|}{R_\mathrm{d}}\right).$$

Equation (52) shows that in the presence of external charges the polarization of a liquid is characterized by the scale R_d. In this case, $\nabla\mathbf{P} \neq 0$, $\mathbf{E}_\mathrm{p} \neq 0$, and a solvation shell $\sim R_\mathrm{d}$ in size is formed around the external charges.

We consider the charge q concentrated on a sphere of radius R (for practical applications, the case $R \sim R_\mathrm{d}$ is most interesting). Then,

$$G_\mathrm{solv} = -\frac{q^2}{2\varepsilon_0\varepsilon_\infty R}\,\bar{G}\,,$$

$$\bar{G} = \varepsilon_\infty(\varepsilon_0 - 1) - \frac{R_\mathrm{d}(\varepsilon_0 - \varepsilon_\infty)\left[1 - \exp(-2R/R_\mathrm{d})\right]}{2R}\,.$$

The point charge limit $R \to 0$ does not exist in this case, since formula (42) is only valid for the wave vector region that corresponds to the frequencies $\omega \lesssim 10^{16}$ s^{-1}; therefore, Eqn (42) does not satisfy the physical requirement $\varepsilon(k) \to 1$ for $k \to \infty$ that is equivalent to $\omega \to \infty$. This requirement may be satisfied if, e.g., ε_∞ in (42) is replaced with $1 + a/(k^2 + \gamma^2)$, where $a = (\varepsilon_\infty - 1)\gamma^2$, $\gamma = 1/R$. Then, omitting the terms $\sim \varepsilon_\infty/\varepsilon_0 \ll 1$, we obtain

$$G_\mathrm{solv} = -q^2\,\frac{a + (\gamma + \sqrt{b})\sqrt{b}}{2\sqrt{(\gamma + \sqrt{b})^2 + a}}\,, \quad (53)$$

$$b = \frac{4\pi}{C} \sim \gamma^2\varepsilon_\infty \sim a\,.$$

An alternative approach may be used: since $\varepsilon_0 \gg \varepsilon_\infty$, we put $\varepsilon_\infty = 1$, and then obtain for a point charge $G_\mathrm{solv} = -(1 - 1/\varepsilon_0)q^2/(2R_\mathrm{d})$. This formula is analogous to the standard result of the classical Born solvation theory [18]. The solvation energy is almost completely concentrated inside the $\sim 2R_\mathrm{d}$ domain that surrounds the electric charge. The size of this domain rarely exceeds that of the ion itself (or the charged molecule); for this reason, the exact value of the Born radius of the ion depends on the specific features of the ion interaction with ambient water molecules.

The obtained expressions for the solvation energy are derived in linearized model (22) and (45); therefore, they are only applicable for charges $q \lesssim P_0R^2$. It should be noted that they exhibit a strong dependence of G_solv on the behavior of the function $\varepsilon(k)$ at $k \gtrsim 1/R_\mathrm{d}$, which corresponds to small distances to the charge $r \lesssim R_\mathrm{d}$. Formula (53), which contains several adjustable parameters, may turn out to be preferable in this sense for the ion solvation energy.

2.8 Surface tension. Estimation of two model scales

Hydrophobic substances do not form hydrogen bonds with water molecules; therefore, the molecules that border a hydrophobic surface lose at least one of the four hydrogen bonds that they have when located in the bulk of the liquid. For this reason, the dipole moments of the molecules close to the hydrophobic surface are parallel to it, which is confirmed by MD calculations [24–27].

Molecules located at the interface with a vacuum or a gaseous medium also lose one hydrogen bond, i.e., such an interface is also hydrophobic. Thus, the solution of the VMPL equations should be sought in the case of a free water surface in the form

$$\mathbf{s} = \big(s(z),\,0,\,0\big)\,, \quad (54)$$

where the z axis is perpendicular to the surface. The solution of Eqn (49) has the form $s(z) = s_0\exp(-z/L_T)$, i.e., the characteristic thickness of the near-surface polarized layer is $\sim L_T$. Free energy per unit area, i.e., surface tension, is expressed in this case as

$$\sigma = \frac{1}{2}\,P_0^2 s_0^2\sqrt{AC}\,. \quad (55)$$

We obtain from this the estimates for water at $s_0 \sim 1$: $C \sim 0.9$ nm^2, $L_T \sim 2$ nm, and $R_\mathrm{d} \sim 0.5$ nm. These estimates are obtained in the mean-field approximation, i.e., ignoring thermal fluctuations. In addition, when searching for a solution in the form of (54), it is assumed that there is a long-range order in the directions of the 'spins' of the molecules located in the near-surface layer of the liquid. Section 4 shows that, indeed, such ordering sometimes

occurs. In the general case (see Section 2.4), the 'spin' correlation extends along the surface to a distance of $\sim L_T$. Both Eqn (55) and the estimates obtained on its basis are for these reasons approximate. The values of Refs [29–32]:

$$C \approx 0.25\ \mathrm{nm}^2,\ \ R_\mathrm{d} \sim 0.2-0.3\ \mathrm{nm}\,,\ \ L_T \sim 1.2-1.5\ \mathrm{nm} \quad (56)$$

are in better agreement with experiment (see Section 5.3).

The solution obtained belongs to the force-free class, $\nabla \mathbf{s} = 0$, of which the scale L_T is characteristic. Such types of polarization are energetically advantageous over 'force-based' ones, for which $\nabla \mathbf{s} \neq 0$, because $\mathbf{E}_\mathrm{p} = 0$ for these solutions.

An important role in the physics of the near-surface HBPL layers is played by the solution of Eqn (27) in the form of a vortex: $\mathbf{s} = s(r, z)\hat{\boldsymbol{\varphi}}$, belonging to the same class. A cylindrical coordinate system (r, φ, z) with the corresponding basis unit vectors $(\hat{\mathbf{r}}, \hat{\boldsymbol{\varphi}}, \hat{\mathbf{z}})$ is introduced here. The z axis coincides with the vortex axis, r is the distance to this axis, and φ is the azimuthal angle. It follows from (27) that $s(r, z) \approx g(r) \exp(-z/L_T)$, $g(0) = 0$, and $g(r \gg L_T) \to s_0$, i.e., the vortex has a core of radius $\sim L_T$.

We show next that thermal fluctuations that emerge in the form of vortex-antivortex pairs play a key role in the physics of surface water layers.

3. Ferroelectric phase transition in liquid supercooled water

We show in this section that the long-range nature of dipole interactions between molecules leads at sufficiently low temperatures to instability of the paraelectric state of the liquid and to a second-order ferroelectric phase transition. The FPT temperature T_c is calculated both in the mean field approximation and using a more rigorous ring diagram method. We discuss experimental data on the observation of the FPT in the supercooled water contained in pores whose size far exceeds the molecule size. It is argued that the properties of water in the pores and those of bulk water are essentially the same. It may be asserted on this basis that experiments [33] testify in favor of the existence of the ferroelectric phase of supercooled liquid bulk water.

3.1 Prediction of the ferroelectric phase transition in the vector model of polar liquids

We show following primarily studies [29, 30, 32] that, according to the results of the VMPL calculations, the FPT is possible in supercooled liquid bulk water.

Consider a strongly elongated water sample and assume that the polarization $\mathbf{s}$ is directed along its largest dimension. The depolarizing field can then be disregarded: $\mathbf{E}_\mathrm{p} = 0$. If $\mathbf{E}_\mathrm{e} = 0$, we obtain both from (26) and from (39) and (47) in weak polarization limit (22), which is valid near the phase transition (33), the formula

$$G = V_1 P_0^2 \left(\frac{A}{2}\, s^2 + B s^4 \right). \quad (57)$$

Equations (31) and (32) clearly show that free energy (57) has the form characteristic of the Landau theory of second-order phase transitions. Thus, if the temperature is lowered in bulk water, a second-order phase transition, the FPT, occurs. At temperature $T > T_\mathrm{c}$, the equilibrium state corresponds to the disordered paraelectric phase with $\mathbf{s} = 0$ and $G_\mathrm{min} = 0$, while at low temperatures $T < T_\mathrm{c}$, a transition occurs to the long-range ferroelectric state where $\mathbf{s}(\mathbf{r}) = \mathrm{const} \neq 0$, $s = \sqrt{|A|/(4B)} \equiv s_0$, as a result of which the free energy decreases to $G_\mathrm{min} = -V_1 P_0^2 A^2/(16B)$.

The long-range order that exists at $T < T_\mathrm{c}$ originates from the dipole long-range interaction between molecules. Indeed, the first term on the right-hand side of (28) is generated by molecular field (20), i.e., the polarization vector $\mathbf{P}_\mathrm{d}$ that emerges in the liquid due to the correlation between the 'spins' of the molecules generated by their dipole interaction. Both the vector $\mathbf{P}_\mathrm{d}$ and the molecular field $\mathbf{E}_\mathrm{m}$ are by their very nature collective and mesoscopic characteristics of the state of the liquid formed by a large number of molecules. It is owing to this property that the first term in (28) generates a long-range order. The second term, entropy, is responsible for the opposite effect: it describes polarization fluctuations that destroy the long-range order, which occurs if $T > T_\mathrm{c}$.

We now suppose that the polarization vector is directed along the small dimension of the elongated water sample, e.g., in the case of a disk, perpendicular to its plane. We then have $\mathbf{E}_\mathrm{p} = -4\pi \mathbf{P}_\mathrm{d}$ and

$$G = V_1 P_0^2 \left(\frac{A}{2}\, s^2 + \frac{2\pi}{\varepsilon_\infty}\, s^2 + B s^4 \right) \approx V_1 P_0^2 \left(\frac{2\pi}{\varepsilon_\infty}\, s^2 + B s^4 \right).$$

The value of G reaches a minimum at $\mathbf{s} = 0$.

We conclude from these two examples that the resulting liquid ferroelectric most likely consists of elongated domains. However, as is the case of ferromagnets, domain structures with $\nabla \mathbf{P} = 0$ considered in [66, § 44] may emerge that have no polarization charges.

The critical temperature T_c for water can be obtained from the measured asymptotic values $\varepsilon_\infty \approx 4.9$ [71], $\varepsilon_\infty = 5.1$ [72], or $\varepsilon_\infty = 5.5$ [73]. Consequently, we have, according to Eqn (29), $T_\mathrm{c} = 236$ K ($-37\,^\circ$C), $T_\mathrm{c} = 226$ K ($-47\,^\circ$C), or $T_\mathrm{c} = 210$ K ($-63\,^\circ$C). The obtained values of the transition temperature are close to the assumed position of the singularity for bulk supercooled water — the λ point obtained in both the early ($T_\lambda \approx 228$ K) [33, 35, 36] and subsequent ($T_\lambda \approx 231$ K) [37] experiments.

The FPT is manifested in the singular behavior of the dielectric constant of the liquid ε_0 near the transition point T_c. To analyze the dielectric response, a weak uniform electric field is applied along the sample. As follows from Section 2, $\mathbf{E}_\mathrm{p} = 0$ and $\mathbf{E} = \mathbf{E}_\mathrm{e}/\varepsilon_\infty$; therefore, ignoring the term quadratic in the field, we conclude that an additional field-dependent term emerges in (57): $-V_1 \varepsilon_\infty P_0 E s$. We obtain from the minimum condition $\mathrm{d}G/\mathrm{d}s = 0$ the equation for s:

$$As + 4Bs^3 - \frac{\varepsilon_\infty}{P_0}\, E = 0\,.$$

If $\tau > 0$ and condition (33) is fulfilled, the term with B may be ignored, which leads to Eqn (44). We find at $T = 0\,^\circ$C that $\varepsilon_0 = 61-99$, depending on the choice of ε_∞. Both values are fairly close to that observed in experiments $\varepsilon_0 = 88$ (see, e.g., [71]).

If $\tau < 0$, we look for a solution in the form $s = s_0 + \delta s$, which gives $\delta s = \varepsilon_\infty E/(2P_0|A|)$. We obtain in this case

$$\frac{\mathrm{d}P}{\mathrm{d}E} = P_0 \frac{\mathrm{d}s}{\mathrm{d}E} + \frac{\varepsilon_\infty - 1}{4\pi}\,,$$

$$\varepsilon_0 = 1 + 4\pi \frac{\mathrm{d}P}{\mathrm{d}E} = \varepsilon_\infty \left(1 + \frac{3}{2|\tau|} \right).$$

This formula and Eqn (44) show that the behavior characteristic of the λ point and the divergence at $T = T_c$ may be expected in the temperature dependence $\varepsilon_0(T)$ measured in supercooled water:

$$\varepsilon_0(T) = \varepsilon_\infty\big(1 + f(T)\big)\,, \tag{58}$$

where

$$f(T) = \frac{3T_c}{T - T_c} \qquad \text{if} \quad T > T_c\,,$$

$$f(T) = \frac{3T_c}{2(T_c - T)} \qquad \text{if} \quad T < T_c\,.$$

In concluding this section, we add that the model of a polar liquid that consists of freely rotating molecules with static dipole moments [74] predicts the existence of the FPT at an unreachably high temperature of ~ 1200 K. Thus, account of the electron shell polarization plays a key role and yields a lower FPT temperature (29).

3.2 Equilibrium free energy of polar liquid with hydrogen bonds taking account of polarization fluctuations in the mean-field approximation

3.2.1 Calculation scheme. Taking account of fluctuations becomes important near the phase transition, at $|\tau| \ll 1$. The equilibrium free energy of the liquid G, which is obtained from the nonequilibrium value obtained in Section 2 by averaging over these fluctuations, is given by an expression that contains functional integration over HBPL polarizations (see, e.g., [69]).

We first calculate G using a simplified formula for the nonequilibrium free energy (47):

$$G = -T \ln Z\,. \tag{59}$$

The argument of the logarithm is the statistical sum

$$Z = \int D\mathbf{P}(\mathbf{r}) \exp\left\{-\frac{G\big[\mathbf{P}(\mathbf{r})\big]}{T}\right\}, \tag{60}$$

which is due to long-wave collective degrees of freedom of the liquid, such as its various polarization states. Integration is carried out over a complete set of independent variables that characterize the polarization $\mathbf{P}(\mathbf{r})$; therefore,

$$D\mathbf{P}(\mathbf{r}) = \prod_{\mathbf{k}\,(k_z>0)} \mathrm{d}P'_{\mathbf{k}x}\,\mathrm{d}P'_{\mathbf{k}y}\,\mathrm{d}P'_{\mathbf{k}z}\,\mathrm{d}P''_{\mathbf{k}x}\,\mathrm{d}P''_{\mathbf{k}y}\,\mathrm{d}P''_{\mathbf{k}z}\,.$$

If condition (33) is fulfilled, approximation (45) is valid, wherein, in addition, one should set $\mathbf{E}_e = 0$. After calculating Gaussian integrals in (59), we obtain the following expression for the equilibrium free energy:

$$G \approx T \sum_{\mathbf{k}\,(k_z>0)} \ln\left(1 - \frac{T_c}{T} + \frac{3\varepsilon_\infty C}{4\pi}\,k^2\right) + \text{const}$$

$$\approx V_1 T \int \frac{\mathrm{d}^3k}{(2\pi)^3} \ln\left(1 - \frac{T_c}{T} + 3R_d^2k^2\right) + \text{const}\,, \tag{61}$$

where only the term which is singular at $T = T_c$ is retained, while the terms that are not singular and, therefore, insignificant for determining the FPT temperature are included in the constant. The singular term comes from 'force-free' fluctuations $\nabla\,\mathbf{s} = 0$, whose amplitude grows infinitely as the liquid is cooled and its temperature approaches T_c.

The same calculation can be easily carried out for the general expression for nonequilibrium free energy (39). We have now, instead of (60),

$$Z = \int D\mathbf{P}_d(\mathbf{r}) D\mathbf{P}_e(\mathbf{r}) \exp\left\{-\frac{G\big[\mathbf{P}_d(\mathbf{r}),\,\mathbf{P}_e(\mathbf{r})\big]}{T}\right\}.$$

Integration again yields result (61) but with another constant, which, as mentioned above, is not significant.

3.2.2 Criterion for applicability of Eqn (61). The importance of fluctuations may be estimated in quantitative terms as follows. The fluctuations in the polarization of a liquid are significant when the additional contribution to the specific heat C_{fl}, which is associated with them, becomes comparable with a jump in heat capacity ΔC at the FPT [75, 76]: $C_{\text{fl}} \gtrsim \Delta C$, where, according to (61),

$$C_{\text{fl}} = -T\,\frac{\partial^2 G}{\partial T^2} \approx V_1 \int \frac{\mathrm{d}^3k}{(2\pi)^3}\,\frac{1}{(\tau + 3R_d^2k^2)^2} = \frac{V_1}{24\pi\sqrt{3\tau}R_d^3}\,. \tag{62}$$

Estimating ΔC by means of (57), we find as in [69] that $C_{\text{fl}}/\Delta C \sim 1/(z\sqrt{|\tau|})$, where $z = 4\pi n_0 R_d^3/3$ is the number of particles in a volume with radius R_d. For water, $z \sim 4$. Therefore, fluctuations are significant if

$$|\tau| \lesssim \frac{1}{z^2}\,. \tag{63}$$

This implies that the phenomenological formulas for free energies (26), (39), (47), and (61), which are based on the mean field approximation, are applicable to water at $T \gtrsim -20\,^\circ$C, while in region (63) this approximation is not applicable, and more sophisticated approaches should be used (see, e.g., [77]).

3.2.3 Possible explanation of the anomalous temperature dependence of the density of water. The density of water reaches its maximum at $T = 4\,^\circ$C [78–80], which is often associated with the anomalous behavior of supercooled water [81]. It may be hypothesized that it is precisely the 'force-free' fluctuations of polarization near the FPT that cause the anomalous behavior of the water density.

We consider the HBPL at $\tau \ll 1$, $T > T_c$. The expression for the total free energy in the region where the fluctuations are small takes at $s \ll 1$ the form

$$G = \int \mathrm{d}^3r\, d_0^2 n^2(\mathbf{r}) \left[\frac{C}{2}(\nabla_\alpha s_\beta)^2 + \frac{A}{2}\,s^2\right] + \int \mathrm{d}V\,\frac{\beta}{2}(n')^2\,. \tag{64}$$

Here, the difference $n'(\mathbf{r}) = n(\mathbf{r}) - n_0$ describes density fluctuations, $\beta = mc_s^2/n_0$ is an approximate expression for the adiabatic compressibility of liquid, m is the mass of its molecule, and c_s is the adiabatic speed of sound in the liquid. Since fluctuations of G with a large wavelength make the main contribution to $\mathbf{s}$, the vector field $\mathbf{s}$ can be considered a slow variable. Owing to this, we can apply the approximation similar to the Born–Oppenheimer one, well known in the quantum mechanics of molecules, i.e., separate fast and slow variables to find the density for a given polarization $\mathbf{s}(\mathbf{r})$ by minimizing the free energy with respect to $n'(\mathbf{r})$ and obtain

$$n'(\mathbf{r}) = -\frac{P_0^2}{n_0\beta}\left[C(\nabla_\alpha s_\beta)^2 + As^2 + 2Bs^4\right]. \tag{65}$$

Averaging this quantity over polarization field fluctuations with a weight $\exp[-G(\mathbf{s}(\mathbf{r}))/T]$, as in (59), we find [29]

$$\langle n' \rangle = \text{const} + n_0 D\sqrt{\tau}\,. \tag{66}$$

Here, $D = \xi Q$, $Q = BT^2 k_{\max}\varepsilon_\infty^2/(mc_s^2 P_0^2 R_d^5) \sim 1$, and $k_{\max} \sim 1/R_d$. As mentioned earlier, the parameter R_d is of the order of the size of a domain of strongly correlated molecular dipoles. The factor $\xi = 5(2\pi)^{-5}/\sqrt{3} \ll 1$, so the quantity D seems at first glance small. The smallness of ξ is actually a consequence of the incompleteness of the mean field theory. In the complete theory that takes into account scale-invariant fluctuations of the order parameter, $\xi \sim 1$ [75, 82] (for the same reason it should be assumed that $B \sim 1$ in formula (30)). We conclude from Eqn (66) that the density of the liquid initially increases as the temperature grows and deviates from the FPT point. This increase in density is subsequently suppressed by thermal expansion of the liquid. It is seen that the density should have a maximum at a certain temperature.

3.3 Calculation of the equilibrium free energy of polar liquid with hydrogen bonds in the ring-diagram approximation

The analysis carried out in Section 3.2 is not perfect, because it is based on the mean-field approximation that does not explicitly take into account the requirement that 'spins' must be equal to one, $|\mathbf{S}_a| = 1$. We now calculate the free energy accurately taking this requirement into account and show that, nevertheless, the mean field approximation reliably predicts both the very existence of the FPT and the value of T_c.

We consider the potential energy (13) of a system of dipoles (molecules) with numbers $a, b, \ldots = 1, 2, \ldots, N$ located at points $\mathbf{r}_a$:

$$U = \frac{1}{2}\sum_{a,\,b(a\neq b)} u_{ab}\,. \tag{67}$$

Pair interactions u_{ab} between molecules a and b may be approximately represented as

$$u_{ab} = \frac{f(r_{ab})d_0^2}{\varepsilon_\infty}\sum_{\alpha,\,\beta=x,\,y,\,z}(\mathbf{S}_a)_\alpha(\mathbf{S}_b)_\beta\left[\delta_{\alpha\beta} - 3(\mathbf{n}_{ab})_\alpha(\mathbf{n}_{ab})_\beta\right], \tag{68}$$

where it is taken into account that $\mathbf{d}_a = d_0\mathbf{S}_a$. The $f(r_{ab})$ function describes the spatial dependence of the strength of the interaction between the molecules. We have at large distances $f(r_{ab}) \approx 1/r_{ab}^3$, which corresponds to the dipole–dipole interaction. This approximation fails at short distances. To take into account at these distances hydrogen bonds and other short-range forces, we use the following approximation:

$$f(r_{ab}) = \begin{cases} \dfrac{1}{r_{ab}^3}\,, & r_{ab} > r_0\,, \\ 0\,, & r_{ab} \leqslant r_0\,. \end{cases} \tag{69}$$

Here, $r_0 \sim R_d$ is a microscopic scale that characterizes the short-range part of interaction between molecules. This approximation is sometimes used in MD (see, e.g., [54]).

Similar to plasma physics, we calculate the equilibrium free energy of HBPL by means of thermodynamic integration. We gradually 'turn on' interaction (67) between molecules, $U \to \lambda U$, by increasing the scale factor λ from 0 to 1. The free energy then becomes a function of λ: $G(\lambda) = -T\ln Z$, where

$$Z = \int \mathrm{d}\Gamma \exp\left(-\frac{\lambda U}{T}\right), \tag{70}$$

$$\mathrm{d}\Gamma = \prod_a \mathrm{d}\gamma_a\,, \qquad \mathrm{d}\gamma_a = \frac{\mathrm{d}^3 r_a}{V_1}\,\frac{\mathrm{d}\Omega_{\mathbf{S}_a}}{4\pi}\,.$$

The sought equilibrium free energy has the form

$$G = \int_0^1 \mathrm{d}\lambda\,\frac{\partial G(\lambda)}{\partial\lambda} = \int_0^1 \mathrm{d}\lambda\,\langle U(\lambda)\rangle\,. \tag{71}$$

The symbol $\langle\ldots\rangle$ denotes here and below the thermodynamic averaging over the Gibbs distribution:

$$\langle U(\lambda)\rangle = Z^{-1}\int \mathrm{d}\Gamma\, U \exp\left(-\frac{\lambda U}{T}\right). \tag{72}$$

Integration over the directions of the molecule 'spin' vectors $\mathrm{d}\Omega_{\mathbf{S}_a}$ is carried out in (70) and (72) keeping all the time $|\mathbf{S}_a| = 1$. Such a calculation is in this sense exact, with the exception of approximation (69) regarding intermolecular interaction at small distances. However, we show below that the properties of the liquid on a large scale, which determine the FPT nature and origin, do not depend on the choice of r_0.

Expanding the exponential function in (72) in a Taylor series, we obtain

$$\frac{\partial G}{\partial\lambda} = \sum_{n=0}^{\infty}\frac{\partial G^{(n)}}{\partial\lambda}\,. \tag{73}$$

The term $\partial G^{(n)}/\partial\lambda$ in the summand consists of the integral over the product of $n+1$ pairwise interactions u_{ab} between the molecules with numbers a and b; summation is performed in accordance with (67) over all the numbers. We consider an interaction term u_{ab} included in this product. In plasma physics, $u_{ab} = q_a q_b/r_{ab}$. Due to quasineutrality, $\sum_a q_a = 0$ and $\sum_b q_b = 0$; therefore, a contribution to $\partial G^{(n)}/\partial\lambda$ is nonzero only if the number a in the interaction u_{ab} under consideration coincides with the number in some other interaction in the specified product of pairwise interactions. The same applies to the number b in u_{ab}. Such coincidences, 'pairings,' are shown in Fig. 2 by dashed closed loops. Suchlike pairings in the case of the dipole–dipole interaction of interest to us occur because integrals like

$$\int \mathrm{d}\Omega_{\mathbf{S}_a} u_{ab} u_{cd}$$

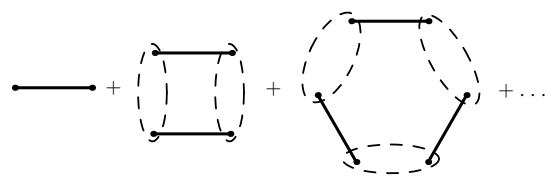

Figure 2. Ring-diagram approximation for free energy of a system with interaction (67): bold straight lines correspond to the energy of dipole–dipole interaction u_{ab} from (68), where $a \neq b = 1, 2, \ldots, N$ are the numbers of molecules. The dashed closed loops indicate the same numbers, i.e., coincident molecules. Summation is carried out over the molecule numbers, and integration over $\mathrm{d}\gamma_a$ for the variables that pertain to these molecules (see text).

are equal to zero if $a \neq c$ or $a \neq d$. The terms in which the numbers of more than two molecules coincide make a negligible contribution to the free energy ($\sim 1/N$). The factor Z^{-1} in (72) eliminates the contributions of disconnected diagrams, i.e., those that consist of separate 'islands'. Connected diagrams alone make a nonzero contribution, as can be seen in Fig. 2.

In an ideal plasma, the number of particles in a sphere with a Debye radius r_{D} is large ($N_{\mathrm{D}} \sim n r_{\mathrm{D}}^3 \gg 1$); therefore, due to Coulomb long-range action, the free energy may be calculated with an accuracy of $\sim 1/N_{\mathrm{D}}$ in the ring-diagram approximation [83, 84]. This is also true for HBPL, but a dipole–dipole interaction between molecules operates there instead of the Coulomb interaction (see Fig. 2). The corresponding error in calculating the energy is in this approximation $\sim 1/N_T$, where $N_T \sim n_0 L_T^3$ is the number of molecules in a superdomain. It should be recalled that for water at room temperature $N_T \sim 100$.

In accordance with the rule of constructing ring diagrams shown in Fig. 2,

$$\frac{\partial G^{(n)}}{\partial \lambda} = \frac{1}{2}\left(-\frac{\lambda}{T}\right)^n \sum_{a_1 \ldots a_{n+1}} \int \mathrm{d}\gamma_{a_1}\, \mathrm{d}\gamma_{a_2} \ldots \mathrm{d}\gamma_{a_{n+1}} \times u_{a_1 a_2} u_{a_2 a_3} \ldots u_{a_n a_{n+1}} u_{a_{n+1} a_1} \left[1 + O\left(\frac{1}{N_T}\right)\right]. \qquad (74)$$

The contribution from nonring connected diagrams in plasma is less than that from ring diagrams by a factor of $\sim N_{\mathrm{D}}$. Similarly, the contribution to the polarization part of free energy from nonring connected diagrams in water is less than that from ring diagrams by a factor of $\sim N_{\mathrm{T}}$.

Formula (74) refers to the class of convolutions that are calculated using Fourier transform. We need for subsequent analysis the following relation:

$$f(r)(\delta_{\alpha\beta} - 3\hat{r}_\alpha \hat{r}_\beta) = \int \frac{\mathrm{d}^3 k}{(2\pi)^3} F(k) M_{\alpha\beta}(\hat{k}) \exp(\mathrm{i}\mathbf{kr}), \qquad (75)$$

where

$$M_{\alpha\beta}(\hat{k}) = \delta_{\alpha\beta} - 3\hat{k}_\alpha \hat{k}_\beta,$$

$$F(k) = \frac{4\pi(z\cos z - \sin z)}{z^3}, \qquad z = k r_0.$$

Upon integration over the directions $\mathrm{d}\Omega_{\mathrm{S}}$ of molecule dipole moments using Eqn (75), we obtain

$$\frac{\partial G^{(n)}}{\partial \lambda} = \frac{V_1}{2}\left(-\frac{\lambda}{T}\right)^n \left(\frac{d_0^2 N}{3\varepsilon_\infty V_1}\right)^{n+1} \int \frac{\mathrm{d}^3 k}{(2\pi)^3} \left[F(k)\right]^{n+1} Q_n,$$

where $Q_n = 2[1 - 2^n(-1)^n]$ and the relation $n_0 V_1 = N$ is taken into account. Using this formula and taking into account (71) and (73), we finally arrive at

$$G = T \int \frac{V_1\, \mathrm{d}^3 k}{(2\pi)^3} \left[\ln\left(1 + \frac{n_0 d_0^2 F(k)}{3\varepsilon_\infty T}\right) + \frac{1}{2}\ln\left(1 - \frac{2 n_0 d_0^2 F(k)}{3\varepsilon_\infty T}\right)\right]. \qquad (76)$$

If $k r_0 \ll 1$, the quantity $F(k) \approx -4\pi/3 + 2\pi(k r_0)^2/15$ and the first term of interest to us on the right-hand side of (76), which contains a singularity at the FPT point, given Eqn (33), takes the form

$$G^{(1)} = V_1 T \int \frac{\mathrm{d}^3 k}{(2\pi)^3} \ln\left[1 - \frac{T_{\mathrm{c}}}{T} + \gamma (k r_0)^2\right], \qquad (77)$$

where $\gamma = 1/10$. The parameter γ depends on the choice of the model and the structure of short-range forces acting between the molecules. Although the values of γ for specific liquids are not known, it can be expected from comparison with (61) that $\gamma \sim 1$.

Coulomb-interacting particles cause Debye screening of each other's electric fields. As a result, the free energy of an ideal plasma, in addition to the principal term arising in the approximation of a mixture of two ideal gases, electronic and ionic, has an additional term — the correlation free energy G_{corr} that generates an addition to the heat capacity:

$$C_{\mathrm{corr}} = \frac{1}{2} V_1 \int \frac{\mathrm{d}^3 k}{(2\pi)^3} \frac{1}{(1 + r_{\mathrm{D}}^2 k^2)^2}. \qquad (78)$$

The correlation contribution to energy originates from the motion of particles separated by the distance $\lesssim r_{\mathrm{D}}$ being correlated rather than independent. A comparison of Eqns (62) and (78) shows that a role similar to that of the Debye radius is played in HBPL by size $L_{\mathrm{corr}} = R_{\mathrm{d}}\sqrt{3/\tau} \approx L_T$ (definition (43) is taken into account here).

Since (61) and (77) have the same form, it can be assumed that the ring-diagram approximation is equivalent to averaging over fluctuations in the mean-field approximation. We conclude from here that the ring-diagram approximation is applicable to water at $T \gtrsim -20\,^\circ$C.

3.4 Observation of the ferroelectric phase transition in water contained in mesopores

The freezing temperature may be significantly decreased if water is contained in mesopores (see [6, 10, 43, 85]). Water may stay liquid in pores with radius $R \lesssim 2$ nm if temperatures decrease to $\sim -100\,^\circ$C [85]; therefore, the phase transition at $T = T_{\mathrm{c}}$ predicted above may be observed and explored in the liquid water filling such pores.

To observe the FPT in supercooled water, the behavior of dielectric response was studied in [41, 42] in samples of water in pores of polymerized silicate MCM-41 with pore diameter $D \sim 3-10$ nm [85] (following the conventional terminology [87, 88], we call them mesopores). The dielectric spectroscopy method was used in the low-frequency range, 25 Hz – 1 MHz. The measured permittivity of water is displayed in Fig. 3. A well-pronounced behavior is seen that is characteristic of the λ transition at the temperature $T_{\mathrm{c}}^{\mathrm{exp}} \approx -38\,^\circ$C, in complete agreement with the physical picture of the second-order transition presented in Section 3.3. The permittivity of liquid water contained in pores was found to exhibit a steep jump from a typical value of $\varepsilon_0 \sim 10^2$ to $\varepsilon_0 \sim 2 \times 10^4$ in the narrow temperature range $\Delta T \sim 5$ K. The jump in permittivity is unambiguous evidence of the FPT [89]. The recent observation in [16] of the Barkhausen effect in liquid water contained in pores is also a confirmation of this conclusion.

The increase in ε_0 with temperature growth at $T > T_{\mathrm{c}}$, which may be detected in Fig. 3, disagrees with both the results of earlier experiments [33, 71] and the prediction of theory (44). This increase should be attributed to rather large errors inherent in the dielectric spectroscopy method.

The pore size in MCM-41 is large in comparison with that of the molecules; therefore, as shown in Section 3.5, the

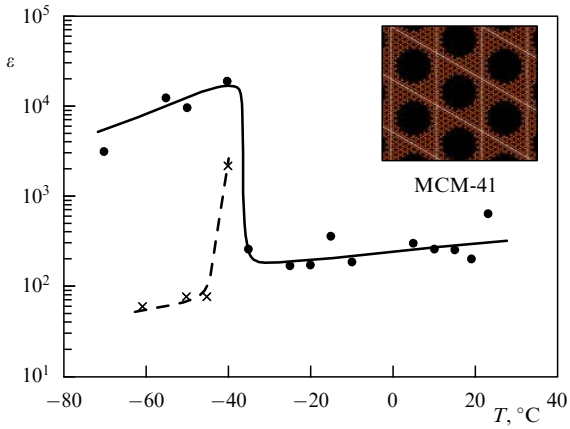

Figure 3. Measured temperature dependence of the low-frequency real part of the dielectric constant of liquid water (solid curve) and ice (dashed curve) for porous material MCM-41 with a pore diameter of 3.5 nm.

microscopic properties of water in mesopores are almost the same as in large volumes. The equilibrium freezing point of water in MCM-41 with $D = 3.5$ nm is $-49\,^{\circ}$C [10]; therefore, the water was in a liquid state in the experiments under consideration at $T \sim T_{\rm c}^{\rm exp}$. The liquid and solid states of water were distinguished by means of the hysteresis effect [10, 90, 91]: the solid curve in Fig. 3 corresponds to the supercooled liquid state obtained upon gradual cooling of the sample. The dashed curve corresponds to superheated ice that is obtained by the reverse process, i.e., the process of subsequent heating of the sample until it melts. A weak dependence of the shape of the curves on the rate of heating and cooling was observed; this behavior is not surprising for hysteresis phenomena that depend on the kinetics of the processes. The singularity of the dashed curve shows that the ferroelectric state inherited from the liquid persists in a substantial part of the ice.

Hard evidence that the singular behavior of the dielectric constant is associated with a phase transition precisely in liquid water was obtained in [16], where water was studied in pores of SBA-15 material. The pore diameter in this material (~ 10 nm) is much larger than that in MCM-41; therefore, the water at $T \sim T_{\rm c}^{\rm exp}$ was obviously in a solid state. No specific behavior has been observed at $T \sim T_{\rm c}^{\rm exp}$. Consequently, the FPT either does not occur in ice at such temperatures or is extremely slowed down due to the long relaxation time. This implies at the same time that the pores in the above experiments with MCM-41 contained at $T \sim T_{\rm c}^{\rm exp}$ liquid water rather than ice.

We add in conclusion that some signs of the FPT may be found in experimental data [6]. The existence of the ferroelectric state of water in beryl nanochannels has been confirmed recently in [92, 93].

3.5 Identity of the microscopic properties of bulk water and water contained in the mesopores of MCM-41 material

This section presents an analysis of the thermodynamics of water contained in small volumes such as mesopores. We prove that, although the freezing temperature in mesopores can be significantly below zero degrees Celsius, the suppression of nucleation that leads to a decrease in the freezing temperature is a macroscopic and collective effect rather than a consequence of the difference between the microscopic structures of water contained in pores and bulk water. The thermodynamic properties of the liquid in pores and bulk liquids are described by macroscopic thermodynamics with the same physical parameters. The freezing temperature of water in pores is shown to be determined by a simple balance of free energy that takes into account the contribution of surface tension of the solid/liquid phase interface. This implies that the microscopic properties of water in pores, at least in pores whose diameter is sufficiently large, as is the case in experiments [16, 41, 42], are virtually the same as those of bulk water.

The generalization of the conclusions made in Section 3.4 for the case of bulk water may cause natural criticism, since there is no clear answer to the question: in what way are the microscopic properties of water in pores related to those of bulk liquid? In particular, how similar or different are the phase transitions and thermodynamic properties of liquid in pores and bulk liquid?

The history of the question is rather long. A detailed discussion of existing opinions can be found in [94]. On the one hand, the water contained in a mesoscale pore features several differences from bulk water:

(1) the freezing temperature of such water is much lower (the so-called freezing suppression phenomenon) and can decrease to a value of the order of $-100\,^{\circ}$C;

(2) a hysteresis appears in the cooling/freezing cycle of water in pores, i.e., there is a difference between the melting point and the freezing point in the same experiment, as described, e.g., in [6, 10, 42, 43, 85, 95];

(3) the results of neutron scattering experiments processed using molecular dynamics calculations [96–105] indicate that water inside mesoscale volumes can be rather heterogeneous;

(4) experiments using infrared (IR) spectroscopy indicate a slight difference between the vibrational frequencies of the OH groups of some molecules in the pores and those in bulk water.

On the other hand, as emphasized in the same review [94], according to calculations [106, 107], hydrophilic surfaces, such as those in the used MCM-41 silicate material [41, 42], do not significantly affect the microscopic properties of water except for a significant reduction in freezing temperature. The same conclusions may be drawn from studies [43, 85, 108], in which only a slight hysteresis was observed in calorimetric measurements and X-ray scattering experiments in the MCM-41 system. For example, it was found in [43] that the difference between the melting and freezing temperatures in MCM-41 with a pore diameter of 3.5 nm was only $(\Delta T)_{\rm h} \sim 1$ K.

Thus, we have an enigmatic phenomenon: the microscopic properties of water in pores and bulk water are very similar, but their freezing temperatures differ significantly.

To get closer to the solution, it should be recalled that there is a so-called nonfreezing water layer with a thickness of $t \approx 0.4$ nm [6, 43, 85] near a surface of any kind. It was shown in [17, 109, 110] that the microstructure of water at distances $\gtrsim t \approx 0.4$ nm from the wall barely differs from that for bulk water, and, according to [106, 107, 111], for hydrophilic surfaces, which are walls of MCM-41, this is also true for water in the nonfreezing layer.

It is also helpful to look at the well-known calculations of lowered freezing temperature $\Delta T_{\rm f}$ (see, e.g., [43, 112]) from a new perspective. We derive below an expression for $\Delta T_{\rm f}$ only using macroscopic arguments. It should be noted that the pores in MSM-41 are almost identical and parallel to each

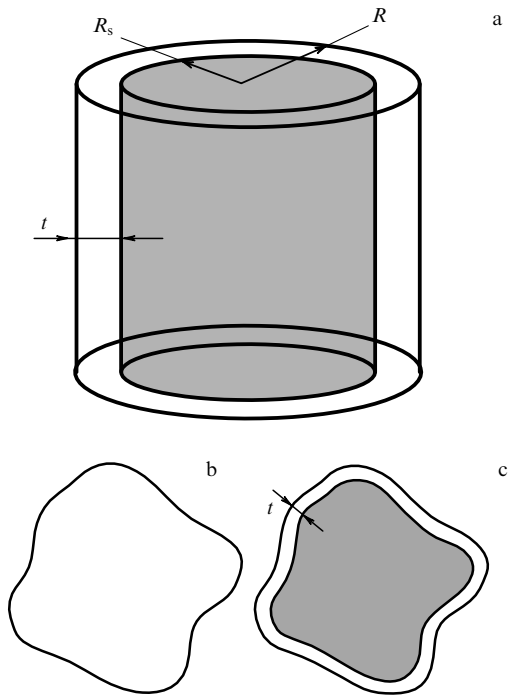

Figure 4. (a) Idealized model of a cylindrical pore. Schematic representation of the cross section of a water sample enclosed in a pore at two temperatures: (b) above and (c) below the freezing point. The ice phase area is shadowed. The nonfreezing layer is located next to the pore wall.

other, so it is sufficient to consider only one of the pores. To simplify the analysis, we consider, following [43, 112], a simple cylindrical pore of length L and radius R filled with liquid water at a temperature above the freezing point (Fig. 4a). A generalization for the case of pores with an arbitrary cross-sectional shape shown in Fig. 4b, c is presented at the end of this section.

As temperature decreases, ice emerges in the pore. To describe in this model the existence of a nonfreezing layer adjacent to the pore walls, we assume that ice fills a coaxial cylinder with height L and radius $R_s = R - t$, where $t \approx 0.4$ nm is the thickness of this liquid layer. Without loss of generality, we can disregard the difference between the particle number densities of molecules in the liquid (l) and solid (s) phases and assume that $n_s = n_l$. Each of the liquid phases can be characterized for any given pressure p by the corresponding chemical potentials (i.e., Gibbs energy per molecule) $\mu_l(p, T)$ and $\mu_s(p, T)$. The Gibbs energies of the solid and liquid phases with the number of molecules N_s and N_l they contain are equal then to $G_s = N_s\mu_s(p, T)$ and $G_l = N_l\mu_l(p, T)$, respectively. The Gibbs energy of the entire system consists for a certain intermediate value of the ice radius R_s of three terms [69]:

$$G(R_s) = G_s + G_l + G_{s-l}\,. \tag{79}$$

Here, $G_{s-l} = f\sigma_{s-l}$ is the surface contribution to the energy due to the ice/liquid interface, $f = 2\pi R_s L$ is the area of this interface, and $\sigma_{s-l} = 32$ erg cm^{-2} is the surface tension coefficient [113]. The Gibbs energy of ice formation is given accordingly by the formula

$$\Delta G(R_s) = G(R_s) - G(0) = \Delta\mu n_s \pi R_s^2 L + f\sigma_{s-l}\,, \tag{80}$$

where $\Delta\mu = \mu_s - \mu_l$. Using the equilibrium condition $\Delta G = 0$ for $R_s = R - t$, we can find the equilibrium freezing temperature, $T_f = T_\infty + \Delta T_f$, where T_∞ is the freezing temperature of bulk liquid (273 K for water at normal pressure) that satisfies the equation $\Delta\mu_\infty = \mu_s(p, T_\infty) - \mu_l(p, T_\infty) = 0$. Using the Gibbs–Duhem equation,

$$\mathrm{d}\mu_s = -s_s\,\mathrm{d}T + \frac{\mathrm{d}p}{n_s}\,, \qquad \mathrm{d}\mu_l = -s_l\,\mathrm{d}T + \frac{\mathrm{d}p}{n_l}\,,$$

where $\mathrm{d}p = 0$ (note that freezing occurs under a constant pressure, $p = \mathrm{const}$), and s_s and s_l are the entropy per molecule values in the solid and liquid states, we conclude that $\Delta\mu \approx \Delta\mu_\infty + \Delta T_f(s_l - s_s) = \Delta T_f \Delta h / T_\infty$, where Δh is the specific melting heat per molecule; therefore,

$$\Delta T_f = -\frac{C_0}{R - t}\,, \tag{81}$$

where $C_0 = 2\sigma_{s-l}T_\infty/\Delta H_m = 52.4$ nm K and $\Delta H_m = n_s\Delta h = 3.3 \times 10^9$ erg cm^{-3}. This result agrees well with most published values, e.g., $C_0 = 52.4 \pm 0.6$ nm K [10] or $C_0 = 52 \pm 2$ nm K [85]. It should be noted that Eqn (81), which is well known, is used, for instance, in cryoporometry [43].

The fact that formula (81) for lowering the freezing temperature, which was reliably substantiated by experiments, can be derived on the basis of macroscopic thermodynamics alone is an indication of the macroscopic nature of the freezing of water in sufficiently wide pores ($R \gg t$).

Further analysis of the above calculations enables a number of conclusions to be drawn. First, the hysteresis phenomenon noted in review [94] to emphasize the difference between the liquid retained in pores and macroscopic liquid is fully explained in terms of the macroscopic thermodynamics presented here as a consequence of the metastability of the liquid and solid phases in the process of supercooling and/or overheating of the liquid [6, 43, 114]. Similar to the hysteresis phenomena known in ferromagnets, the observed difference between the freezing and melting temperatures $(\Delta T)_h$ (a measure of hysteresis) is determined by the value of the Gibbs free energy barrier ΔG_b that separates the molten and frozen states of water in pores, and as such depends on the heat removal rate and a specific way to overcome this barrier. It follows from Eqn (80) that the barrier height

$$\Delta G_b = \frac{\pi}{2}\,\sigma_{s-l}L(R - t) \tag{82}$$

corresponds to the Gibbs energy of a half-frozen pore with the ice-particle radius $R_s = (R - t)/2$. It should be noted that, due to the linear dependence of the barrier height on the pore length L, ice begins emerging in experiments in the form of short segments $\sim R$ in length that gradually occupy the entire pore.

Thus, the freezing temperature of the entire sample is only determined by the balance of the total Gibbs energy of the system:

$$\Delta G = 0\,. \tag{83}$$

Based on the meaning of Eqn (83), we can conclude that the phase transition occurs in the system as a whole, including the ice/liquid interface, rather than just in the water contained in the pore volume. Therefore, suppression of ice crystallization in mesopores is not a microscopic, but rather a macroscopic and collective phenomenon: liquid in the pore volume 'feels' the molecules at the interface. This conclusion is a rigorous

consequence of thermodynamics. It is worth quoting in this regard the famous statement by A S Eddington [115]: "But if your theory is found to be against the Second Law of Thermodynamics, I can give you no hope; there is nothing for it but to collapse in deepest humiliation." The task for a more detailed theory is to derive the effect of suppression of ice formation in mesopores in a microscopic approach. There are two promising avenues here.

(1) A possible explanation for the effect, which does not require a change in the microscopic properties of the liquid, is given in [116].

(2) Another reason for lowering the freezing point in microscopic samples of liquids may be the enhancement of the role of fluctuations in such systems, namely, in the ice premelting phenomenon [117, 118]. It is owing to the fluctuations that barrier (82) is overcome more easily if the system size decreases. This issue is worth a dedicated exploration.

For the sake of completeness, we present an alternative derivation of Eqn (79). In contrast to (79), the Gibbs energy in this approach (see, e.g., [69]) only consists of two terms: G_s and G_l. To be more general, we consider the case of an arbitrary shape of the formed piece of ice, as shown in Fig. 4b, c. An additional Laplace pressure emerges in the ice particle, which is associated with the interface curvature $\Delta p = 2\sigma_{s-l} h_{curv}$, where h_{curv} is the average curvature of the solid/liquid phase interface. Thus, the pressure in the ice particle is equal to $p + \Delta p$, where p is the pressure in the liquid. We conclude from the mechanical equilibrium condition $p + \Delta p = \text{const}$ that $h_{curv} = \text{const}$ at all interface points. If the ice particle volume increases by $\mathrm{d}V_s$, the number of molecules in the solid phase increases by $\mathrm{d}N = n_s \,\mathrm{d}V_s$. Its surface area increases at the same time by $\mathrm{d}f$. Consequently, the change in the Gibbs energy of the system is $\mathrm{d}G = \mathrm{d}G_s + \mathrm{d}G_l$. Here, $\mathrm{d}G_s = \mu_s(p + \Delta p, T)\,\mathrm{d}N$, $\mathrm{d}G_l = -\,\mathrm{d}N\mu_l(p, T)$ are the changes in the Gibbs energy in each of the phases. Using the Gibbs–Duhem equation and the mathematical relation $\mathrm{d}V_s h_{curv} = \mathrm{d}f/2$, we find that

$$\mu_s(p + \Delta p, T) \approx \mu_s(p, T) + \delta\mu_s\,,$$

$$\mathrm{d}G_s \approx \left[\mu_s(p, T) + \delta\mu_s\right]\mathrm{d}N = \mu_s\,\mathrm{d}N + \sigma_{s-l}\,\mathrm{d}f\,,$$

where $\delta\mu_s = \Delta p/n_s$. The Gibbs energy of the pore G is found by integrating $\mathrm{d}G$. The result obtained coincides with Eqn (79).

A useful conclusion also follows from the analysis above: Eqn (81) is valid for pores with an arbitrary cross-sectional shape if the value $l/(2\pi)$, where l is the perimeter of this cross section, is substituted into this equation instead of R.

Thus, in this section we presented arguments in favor of the collective nature of the liquid-solid phase transition in the pores filled with water and a deep relationship between the properties of bulk water and water inside pores with a sufficiently large radius $R \gg t \approx 0.4$ nm.

3.6 Two-liquid model of supercooled water in mesopores

3.6.1 Key assumptions. It should be recalled that the specific heat, compressibility, coefficient of thermal expansion, and dielectric constant of strongly supercooled bulk water have been measured in [33, 35, 36]. Based on the extrapolation of the measurement data to lower temperatures, the authors of these studies hypothesized that these quantities have a singularity at a temperature of $T_\lambda = 228$ K. This singularity looks rather weak, and it was assumed, therefore, in [119, 120] that different states of water continuously replace each other in the vicinity of the λ point as temperature changes. The observed λ anomaly is explained in this approach by a first-order phase transition between two liquid-water phases that differ in their spatial packing of molecules: a low-density (LD) and a high-density (HD) phase. The LD/HD phase at mesoscopic scales is characterized by a cubic/hexagonal lattice, respectively. The possible existence of such structures was noted in [121, 122]. The two-phase liquid-water model proposed in [119, 120] predicts the existence of a second critical point at a temperature of $T_{cr} \sim 200$ K and a pressure of ~ 1 kbar [9, 123–127]. The known anomalous properties of water, including the λ anomaly observed in the vicinity of T_λ, are widely thought to be related to the existence of the Widom line originating from this critical point in the pressure–temperature diagram [128], near which density and entropy fluctuations are large [129]. The enhancement of fluctuations is due to a sharp increase in the derivatives of thermodynamic quantities (coefficient of thermal expansion, heat capacity at constant pressure, etc.) with respect to temperature near the Widom line.

The hypothesized important role of these fluctuations is confirmed by a number of MD calculations made in realistic water models [103, 123, 130–139], simplified analytical models [140–144], and a number of experiments [125, 145–148]. It was found in [128, 149, 150] that, when the Widom line is crossed, the Arrhenius temperature dependence of the molecule self-diffusion coefficient is replaced with a power law, i.e., enhanced fluctuations near the Widom line affect not only the thermodynamic but also the kinetic characteristics of the liquid.

MD calculations [149, 151] indicate that the Einstein relation between diffusion and mobility coefficients is violated, which brings us back to the issue of whether the equilibrium state of strongly supercooled water may be attained in the MD calculations. As indicated in reviews [7, 94, 125, 152–156], the metastability of the bulk liquid phase at temperatures significantly lower than the freezing point greatly complicates the experimental study and MD simulation of the properties of a strongly supercooled liquid. Other approaches to the explanation of the anomalous properties of water are described in [157–162]. Thus, this area of research is far from fully explored.

In our opinion, each of the above assumptions regarding the nature of the λ anomaly encounters an obvious difficulty in explaining the observed singularity of the dielectric constant $\varepsilon_0(T)$. The collection of these facts and observations indicates the existence of a richer physical picture that, in our opinion, far from being limited by the first-order liquid-liquid phase transition alone, gives a second wind to the old idea [33] that relates the weak singular behavior of the dielectric constant in bulk water to the FPT.

The FPT temperature (29) is surprisingly close to T_λ. Nevertheless, the HBPL vector model fails to reproduce in detail the behavior $\varepsilon_0(T)$ observed in [15, 41, 42], which is not surprising, since the model is extremely simplified. It overlooks, for example, the fact that the tetrahedral geometry of the electronic orbitals in the water molecule leads to the aforementioned polymorphism, i.e., to the coexistence of two or more liquid phases with molecule packing patterns that differ on mesometer scales — phases of the liquid with cubic and hexagonal lattices [125, 153, 165].

A theoretical description is developed in this section wherein the FPT is combined with a first-order phase transition between two liquid phases: LD and HD. The

VMPL is combined to this end with the analytical model of the liquid–liquid phase transition proposed in [164–166].

We assume that the equilibrium state of supercooled water is a mixture of macroscopic clusters of two types: a liquid with low and high densities, which corresponds to the well-known model [103, 125] and is confirmed by experiments [146, 147, 167]. We also assume that the FPT only occurs in the LD liquid, while a ferroelectric state cannot exist in the HD phase. There are two reasons for this assumption. First, the LD liquid is locally 'softer' than the HD liquid, since the density of the latter is approximately 20% higher [125, 168–172]. It seems natural for this reason to assume that the molecules can rotate in the LD phase more or less freely, while the molecule rotation in the HD phase is hindered. Thus, the nature of the LD phase is closer to that of the liquid with pairwise and isotropic interactions, for which Eqn (29) is derived. The feasibility of the FPT in the LD phase is also indicated by the similarity between the local structure of the latter and the crystal lattice of the stable (paraelectric) phase of Ih ice [173, 174]. According to [3, 5, 175, 176], Ih ice transforms under normal pressure and at temperatures below $T \sim 70$ K to the ferroelectric state, which is referred to as XI ice. Since the LD liquid density is lower than that of the Ih ice, the assumption that the FPT exists in the liquid LD phase does not seem to be surprising. It should be noted, however, that the existence of the FPT in the Ih ice is not a firmly established fact. The possibility of such a transition is confirmed by MD calculations (see, e.g., [177, 178]), but the results are sensitive to the choice of a specific water model [178]. Arguments pro and con regarding the existence of such a transition in ice are presented in review [179]. Recent MD calculations also lend support to the existence of the FPT in the Ih ice [8, 180]. The main reason that hinders detecting this transition is the long time of ice transition to the ferroelectric state [181]: this time is so long that it was suggested in [182] that bulk samples of ferroelectric ice are only available on planets located far away from stars. However, we note that, according to [183], the FPT in ice was probably observed in experiments with neutrons.

The assumption of freely rotating molecules of the LD phase seems at first glance doubtful, since it is usually believed that the properties of water are primarily determined by a rigid network of hydrogen bonds [184] that hinder the rotation of molecules. We now compare the values of three parameters: the enthalpy of water dimer formation $\Delta H = 12-15$ kJ mol^{-1} [185, 186], the dipole–dipole interaction energy $u_{\rm dd} = 2d_0^2/\bar{r}^3 \sim 20$ kJ mol^{-1} for neighboring molecules with parallel dipoles, and the energy of a single hydrogen bond breaking of ~ 20 kJ mol^{-1}. Thus, in reality, at a typical distance between the nearest molecules in water $\bar{r} \sim 0.3$ nm, it is not possible to clearly distinguish in the total intermolecular interaction, which is mainly of an electrostatic nature, between the effect of hydrogen bonds and dipole–dipole interactions, $u_{\rm dd}$. The magnitudes of these energies are comparable.

As a result of the combined action of the hydrogen bonds and the dipole–dipole interaction, a short-range order is realized in water, such that, at small distances, the molecules are assembled into lattice-like structures [126, 184]. The Gibbs free energy of LD clusters $G_{\rm LDL}$ at a given pressure p is a sum of the contributions of the polar (rotational), $G_{\rm LDL}^{\rm pol}$, and lattice, $G_{\rm LDL}^{\rm lat}$, degrees of freedom:

$$G_{\rm LDL} = G_{\rm LDL}^{\rm pol} + G_{\rm LDL}^{\rm lat} \approx -D\tau^2\theta(-\tau) + G_{\rm LDL}^{\rm lat}(p,T)\,. \qquad (84)$$

Here, $D \sim V_0 n_0^2 d_0^2 \sim 150$ cal mol^{-1}, $V_0 = N_{\rm A}/n_0 \approx 22$ cm^3 is the molar volume of the LD cluster, and $N_{\rm A}$ is the Avogadro number. The equilibrium state of the LD cluster corresponds at high temperatures, $T > T_{\rm c}$, to a disordered paraelectric phase, while at low temperatures, $T < T_{\rm c}$, the LD cluster is in a long-range order ferroelectric state. Therefore, the term $G_{\rm LDL}^{\rm pol}$ in (84) is presented in the form characteristic of the Landau theory [69] (see Section 3.1).

The question arises as to which density n_0 should be substituted into (29): either total density n_0 or density of the LD phase alone $n_{\rm LDL} = cn_0$. Here and below, $c \equiv c_{\rm LDL}$ is the molar fraction of the LD phase, i.e., the proportion of molecules contained in LD clusters. According to estimates made in the analysis below, the difference in the FPT temperature $T_{\rm c}$ is in this case ~ 5 K, which is less than the spread due to inaccurate determination of ε_∞. We use for this reason definition (29) with full density n_0.

Model [164–166] enables an analytical description of the first-order phase transition between two liquid phases and the second critical point. According to this model, the non-equilibrium Gibbs energy of water has the form

$$G(c,p,T) = G_{\rm HDL}(p,T) + \Delta G(c,p,T)\,. \qquad (85)$$

Here,

$$\Delta G(c,p,T) = c\Delta G(p,T) + f(c), \qquad (86)$$

$$f(c) = \varphi c(1-c) + N_{\rm A}T\left[c\ln c + (1-c)\ln(1-c)\right],$$

$$\Delta G(p,T) = G_{\rm LDL}(p,T) - G_{\rm HDL}(p,T) = \Delta U^0 - T\Delta S^0 + p\Delta V^0\,, \qquad (87)$$

where $G_{\rm HDL}(p,T)$ is the free energy of the HD component, $G_{\rm LDL}(p,T)$ is the free energy of the LD component, φ is the energy of mixing of the LD and HD phases, and $\Delta U^0(p,T) = U_{\rm LDL} - U_{\rm HDL}$, $\Delta S^0(p,T) = S_{\rm LDL} - S_{\rm HDL}$, $\Delta V^0(p,T) = V_{\rm LDL} - V_{\rm HDL}$ are the differences between the molar internal energies, entropies, and volumes of the LD and HD phases, respectively. Similar to [164–166], we focus on the singular behavior of thermodynamic quantities and, for this reason, we further omit the smoothly varying term $G_{\rm HDL}(p,T)$ in (85), and simply refer to quantity (86) as the Gibbs energy.

The LD phase fraction $c(p,T)$ in equilibrium and the free energy of the equilibrium state $\Delta G[c(p,T),p,T]$ are found from the condition of the minimum $G(c,p,T)$ with respect to c: $G'(c) \equiv [\partial\Delta G(c,p,T)/\partial c]_{p,T} = 0$, i.e., from the equation

$$\Delta G(p,T) + \varphi(1-2c) + N_{\rm A}T\ln\left(\frac{c}{1-c}\right) = 0\,. \qquad (88)$$

Following [164, 166, 187], we assume that the expansion coefficients do not depend on temperature or pressure:

$$\Delta E^0(p,T),\ \Delta S^0(p,T),\ \Delta V^0(p,T) \approx \text{const}\,. \qquad (89)$$

This assumption, which works well in the theory of binary alloys [187], enables a description of the properties of water near the second critical point [164, 166]. It is indicated by the letter K in Fig. 5 that displays the phase diagram of water described by formulas (85) and (88) in the model under consideration.

The Gibbs potential (86) has a single minimum in the region above the AKB spinodal (see Fig. 5) and two minima

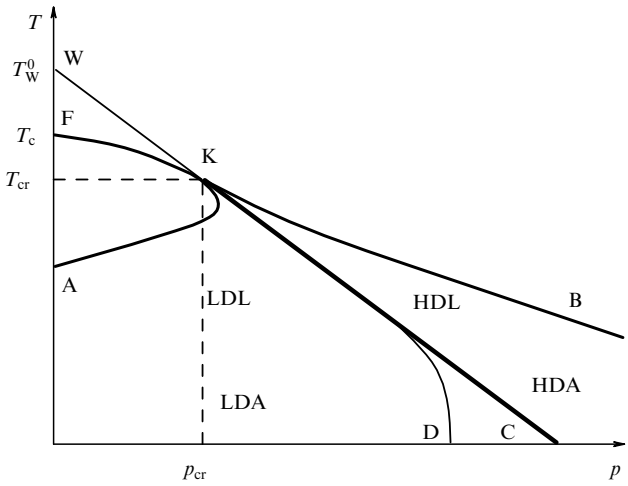

Figure 5. Phase diagram of bulk water in our model (see details in the text). LDA (Low Density Amorphous ice) and HDA (High Density Amorphous ice) are the amorphous ice phases with low and high density, respectively. HDL and LDL are the liquid phases with high and low density, respectively.

in the region below this curve. The LD phase concentrations at these minima $c = c_{1,2}$, which are found from the condition $G'(c_{1,2}) = 0$, are the roots of implicit equation (88). Stable equilibrium corresponds to the root with the smaller Gibbs energy (86). The KC line is the curve of a first-order liquid-liquid phase transition that corresponds to the equilibrium of the LD and HD phases:

$$\Delta G(c_1, p, T) = \Delta G(c_2, p, T)\,. \tag{90}$$

The function $f(c)$ in (86) is even with respect to the middle point of the interval, i.e., $f(0.5 + x) = f(0.5 - x)$. The first term on the right-hand side of Eqn (86) violates this symmetry; therefore, if $\Delta G(p, T) \neq 0$, phase equilibrium condition (90) cannot be satisfied: one of the energy minima (86) is necessarily deeper than the other. Therefore, the equilibrium condition (90) has the form

$$\Delta G(p, T) = 0\,. \tag{91}$$

According to (87) and (91), KC, the equilibrium phase curve in the model [164–166], is a straight line, and the LD phase concentration is found from the equation

$$T = -\frac{\varphi(1 - 2c)}{N_A T \ln\left[c/(1 - c)\right]}\,. \tag{92}$$

The joint solution of Eqns (91) and (92) enables the determination of the LD phase temperature and concentration on the equilibrium curve for the given pressure.

The local minimum of the function $\Delta G(c, p, T)$ that corresponds to the LD phase disappears on the KB segment of the AKB spinodal, so that the LD phase loses its thermodynamic stability on it. Consequently, the KA curve is a spinodal curve of the HD phase. We conclude from this observation that the spinodal curve AKB is found from the simultaneous fulfillment of the conditions $G'(c) = 0$ and $G''(c) \equiv [\partial^2 \Delta G(c, p, T)/\partial c^2]_{p,T} = 0$.

The difference between the LD and HD phases disappears at the critical point K; therefore, here, $c_{LDL} = c_{HDL} = 1/2$ [188, 189]. We obtain then from Eqn (92) the temperature at this point: $T_{cr} = \varphi/(2N_A)$.

Amorphous phases of ice with low and high density are labeled in Fig. 5, similar to Ref. [7], as LDA and HDA, respectively. Approximation (89) is violated at low temperatures, and the liquid–liquid equilibrium curve should bend downward here, like KD, which corresponds according to the third law of thermodynamics to the limit $\Delta S \to 0$ at $T \to 0$.

The molar entropy of water $S(p, T)$ and the heat capacity C_p under a constant water pressure are expressed as

$$\begin{aligned} S(p, T) &= -\left\{\frac{\partial \Delta G\left[c(p, T), p, T\right]}{\partial T}\right\}_p \\ &= c\Delta S^0 - N_A\left[c \ln c + (1 - c)\ln(1 - c)\right], \\ C_p &= T\left[\frac{\partial S(p, T)}{\partial T}\right]_p = C_p^{pol} + C_p^{lat}\,. \end{aligned} \tag{93}$$

Here, C_p^{lat} is the Debye heat capacity of the lattice,

$$C_p^{lat} = C_p^{\infty}\frac{(T/\Theta)^3}{1 + (T/\Theta)^3}\,,$$

$C_p^{\infty} = 18$ cal mol^{-1} K^{-1} [35], and $\Theta \approx 150$ K is the Debye temperature for the water lattice. The contribution C_p^{pol} of the polar degree of freedom to the heat capacity of the liquid has the form

$$C_p^{pol} \approx T\frac{\left\{\Delta S^0 - N_A \ln\left[c/(1 - c)\right]\right\}^2}{G''(c)}\,,$$

where $G''(c) = -2\varphi + N_A T/[c(1 - c)]$.

The contribution C_p^{pol} is by definition maximal on the Widom line, i.e., $G''(c) = \min$; therefore, the relations $G'(c) = 0$ and $G'''(c) = 0$ hold on this line, which are equivalent in our model to $c = 1/2$. Using this result and taking into account (88), we arrive at Eqn (91). Thus, the WK Widom line (see Fig. 5), which is a continuation of the straight line CK, is determined by the equation $T = (\Delta U^0 + p\Delta V^0)/\Delta S^0 \equiv T_W$. Given that near the Widom curve $c \approx 1/2$, we obtain

$$C_p^{pol} \approx \frac{N_A \Delta T^2}{(T - T_W)^2 + \delta^2}\,, \tag{94}$$

where $\Delta T = T_W - T_{cr}$ and $\delta = 2N_A\Delta T\sqrt{\Delta T/T_W}/|\Delta S^0|$. The value of C_p^{pol} exhibits a pronounced peak at $T = T_W$ in accordance with the results of experiment [7, 152], qualitative analysis [128], and MD calculations [139].

Equation (94) may be compared with the formula for the specific heat calculated, for example, in [139] using the MD method. It is possible to ignore pressure in this case and set $T_W = \Delta U^0/\Delta S^0 \equiv T_W^0$. We obtain from here the following estimates for the parameters of our model:

$$\begin{aligned} &\Delta U^0 = -860 \text{ cal mol}^{-1}, \\ &\Delta S^0 = -3.5 \text{ cal mol}^{-1}\text{ K}^{-1}, \\ &\varphi = 880 \text{ cal mol}^{-1}. \end{aligned} \tag{95}$$

This set of parameters corresponds to $T_W^0 = 245$ K, $T_{cr} = 220$ K, and $p_{cr} = 1$ kbar, where the value $\Delta V^0 \approx 3.8$ cm^3 mol^{-1} taken from [164, 166] was used to find p_{cr}. According to [164, 166], values similar to (95) are as

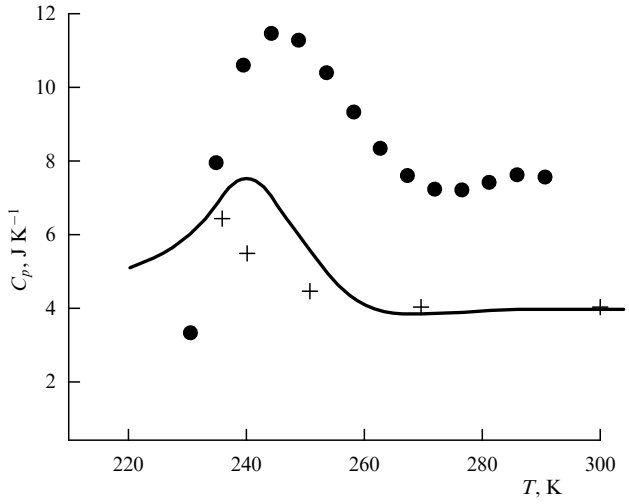

Figure 6. Heat capacity of water according to Eqns (93)–(95) (solid curve), results of MD calculations [139] (dots), and measurement data [35] (crosses).

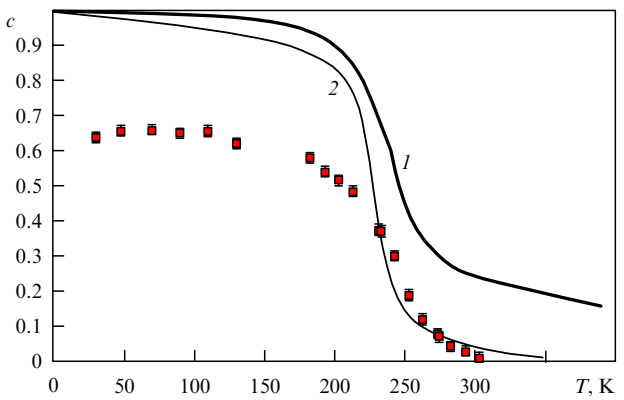

Figure 7. Theoretical dependence of the LD phase fraction on temperature. Curve *1* corresponds to the theory with parameters (95), while curve *2* corresponds to the theory with parameters (96) found by the least squares method from comparison with experimental data [147] that are shown by squares.

follows: $U \approx 900$ cal mol^{-1}, $\Delta E^0 = -250$ cal mol^{-1}, and $\Delta S^0 = -1$ cal mol^{-1} K^{-1}. The temperature dependence of the specific heat C_p calculated using Eqns (93)–(95) is displayed in Fig. 6, where experimental data [35] and results of MD calculations [139] are also shown. Both our and MD-based calculations correctly reproduce on a qualitative level the characteristic features of these dependences and, thus, describe the same physics.

According to [152], the LD phase entropy turns out to be less than that of the HD phase, $\Delta S^0 < 0$. This is another argument in favor of the conclusion that the LD phase is more ordered than the HD phase [139]; it also implies that the FPT is present and implicitly taken into account in the MD calculations.

The consistency of the model can be checked after determining parameters (95) using the results for the LD phase fraction $c(T)$ found from Eqn (88), which are represented by curve *1* in Fig. 7. The figure shows that there is a quantitative agreement between the predictions of the model and experimental data [147] (squares) at temperatures above 200 K. It should be noted that $\Delta G(p, T = 0) < 0$; therefore, at low temperatures the entire liquid must inevitably consist of the LD phase, i.e., the property $c \to 1$ should be satisfied at $T \to 0$. This implies that the equilibrium state of water at low temperatures has not been achieved in experiments [147]. It can be asserted with certainty that the reason is the increased relaxation time [162, 190].

We now compare the model predictions for the molar fraction of the LD phase with the experimental data at temperatures of 220–300 K, at which the agreement between theory and observations may be considered satisfactory. We find here that the agreement with the experiment is better for a slightly modified set of parameters:

$$\Delta E^0 = -920 \text{ cal mol}^{-1}, \qquad \Delta S^0 = -4 \text{ cal mol}^{-1} \text{ K}^{-1}, \tag{96}$$

to which curve *2* in Fig. 7 corresponds.

It should be noted that, according to the model presented in this section, the LD phase fraction tends at high temperatures to a nonvanishing constant, which does not agree with measurements. This is due to the linear approximation used in (89). Nevertheless, the LD phase fraction remains small, even at high temperatures, for the set of parameters (96).

Based on the arguments above, we can conclude that the presented model is in reasonable agreement with the measurements.

3.6.2 Permittivity of water in the two-liquid model. The permittivity of water considered as a mixture of LD and HD clusters is approximately expressed as

$$\varepsilon(T) = c(T)\varepsilon_{\text{LDL}}(T) + \left[1 - c(T)\right]\varepsilon_{\text{HDL}}(T)\,,$$

where ε_{LDL} and ε_{HDL} are the permittivity of the LD phase (see (58)) and HD phase, respectively,

$$\varepsilon_{\text{LDL}}(T) = \varepsilon_0(T)\,, \qquad \varepsilon_{\text{HDL}} = \varepsilon_\infty + \frac{2\pi n_0 d_0^2}{9T}\,(\varepsilon_\infty + 2)^2\,.$$

It is taken into account here that the HD phase is a paraelectric substance; therefore, the expression for ε_{HDL} can be found from the Debye–Onsager model [191]:

$$\varepsilon(T) = \varepsilon_\infty + \varepsilon_\infty c(T) f(\tau) + \left[1 - c(T)\right]\frac{2\pi n_0 d_0^2}{9T}\,(\varepsilon_\infty + 2)^2. \tag{97}$$

The measurement results and predictions of the theory that correspond to the set of model parameters (95), $\varepsilon_\infty = 4.7$ and $T_c = T_c^{\text{exp}} = 236$ K, are displayed in Fig. 8. The value of T_c^{exp} is taken from [16, 41, 42]. Our model is in good agreement with experiments at temperatures above the transition point, $T > T_c$, T_W^0, [16, 41, 42]. Due to the rapid decrease in the LD phase proportion with an increase in temperature (see Fig. 7), the temperature dependence of the dielectric constant for $T > T_c$ exhibits a more pronounced singular behavior than that predicted by the simple single-component liquid model (58) of Ref. [30]. Thus, the two-liquid nature of water being taken into account significantly improves the agreement between the theory and measurements.

The reason for the difference at $T < T_c$ between the experimental data for MSM-41 and the predictions of the

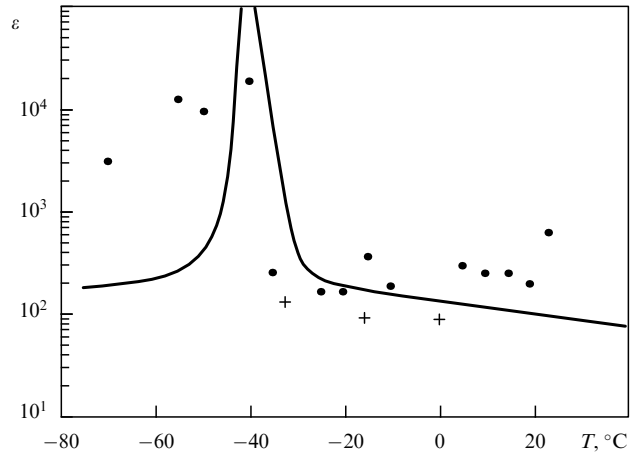

Figure 8. Dielectric constant of 3D water as a function of temperature. The solid curve shows the values of ε obtained in the two-liquid model using Eqn (97) with parameters (95); the dots correspond to the results of the experiment with porous material MCM-41 [15, 41], and the crosses represent the measurement results [33].

two-liquid model presented here can be traced to the following circumstance. As described in Sections 3.1–3.5 and above in this section, the temperature T_c depends on the size and shape of ferroelectric clusters in the LD phase. For this reason, as temperature decreases, a 'continuous sequence' of FPTs may occur in LD clusters. This leads to large observable values of $\varepsilon(T)$ for $T < T_c$.

So, according to the predictions of the model presented here, the FPT in the LD component leads to a strong increase in the dielectric constant in the vicinity of T_c. Equation (84) shows at the same time that at low pressures in the vicinity of the FPT, i.e., at $|\tau| \ll 1$, the contribution of the dipole–dipole interaction to the Gibbs energy of the liquid is small, $|\Delta G_{\text{pol}}| \ll |\Delta G_{\text{lat}}|$. Thus, the FPT at $T \approx T_c$ occurs as if against the background of a 'stronger' liquid–liquid transition caused by rearrangements in the lattice. Consequently, the FPT effect on the properties of water at temperatures near and above the Widom curve seems at first glance negligible. The FPT curve may in this case look like the KF line in Fig. 5. Another point of view seems more natural. As shown in Section 3.2, the polarization degree of freedom of the liquid is 'weakened' near the FPT. Polarization fluctuations increase as a result, which in turn gives rise to density fluctuations. Enhanced fluctuations are precisely the main characteristic feature of the region in the (p, T) plane adjacent to the Widom line. Thus, it can be assumed that the FPT is one of the reasons, and perhaps the primary one, for the emergence of the Widom line in water. The lines KF and KW (see Fig. 5) should in this case coincide.

3.7 Discussion of the results

Water is an example of a polar liquid which is of most importance and interest for practice. The high density of water, the significant magnitude of the dipole moments of its molecules, and the tetrahedral geometry of electronic orbitals are the main reasons for the complexity of the phase diagram and the 'anomalous' properties of water [3–8, 10]. A clear understanding of how a liquid behaves under the effect of an external electric field is of utmost importance for many applications of computational chemistry and biophysics, in the development of new drugs [12, 192], etc. The problem of the temperature dependence of the dielectric constant, the role of fluctuations, and the feasibility of the FPT in a bulk polar liquid is rather old [193], but interest in it has been rekindled after the thermodynamic characteristics of supercooled water as it approaches temperature $T_\lambda \approx 228$ K from above was discovered [33, 35, 36] (according to [37], $T_\lambda = 231$ K). The behavior of isothermal compressibility, density, diffusion coefficient, viscosity, static dielectric constant ε_0, and some other quantities when approaching T_λ appears as singular.

The phase diagram of metastable supercooled water has been studied in detail, and a large number of seemingly different but apparently related theories have been proposed to explain this λ anomaly. According to one rather popular approach, the anomalous behavior of thermodynamic quantities is associated with the limit of mechanical stability (spinodal curve) that emerges in the vicinity of the critical gas–liquid transition point [36, 161]. Another approach based on MD calculations involves an assumption that λ anomalies can be associated with a new critical point, such that, if the critical-point temperature is exceeded, two phases of the liquid, hexagonal and cubic, are no longer distinguishable [123]. The λ anomalies are explained in Ref. [194] by the properties of a network of hydrogen bonds.

On the other hand, the singularity in the behavior of ε_0 is known to be a characteristic FPT feature [89, 193, 194]. The ferroelectric nature of λ anomalies is also supported by MD calculations performed for various model polar liquids (see, e.g., [195–197]). A ferroelectric liquid phase was observed in the model of so-called soft spheres with static finite-size dipoles located inside the spheres [195, 197–200], in models with hard spheres [198, 201], and in a Stockmayer liquid [202, 203]. The existence of a ferroelectric liquid phase apparently does not depend on the choice of a specific model, since this phase was also observed in the calculations based on the models of rigid spheres with point dipoles [198, 201] or soft spheres with finite-size dipoles [200]. There are unfortunately a number of reasons due to which it is difficult to confirm with certainty the relationship between the FPT and the λ point in water in MD models with a finite number of particles. First of all, due to the long-range nature of dipole–dipole interactions between molecules, the simulated liquid tends to form strongly correlated domains, and its calculated properties heavily depend on the boundary conditions in any system of a reasonable size [197]. Due to low temperatures, relaxation processes take a very long time [204]. These circumstances necessitate calculating large and strongly interacting molecular systems for a very long time, which may cast doubt on the reliability of the findings.

The mean-field approximation underlying the VMPL provides an explanation for some of the features observed in supercooled water [33, 35–37]. The 'gas parameter' z introduced in Section 3.2 is not too large for water, i.e., our approach, which is based on the mean-field theory, is not able to explain in detail the results of measurements or MD calculations. However, the main conclusion regarding the existence of the FPT made in the mean-field approximation is confirmed by a more rigorous calculation of the free energy of HBPL using the ring-diagram method. Estimates (29) for T_c and (44) for the dielectric constant are in reasonable agreement with experiments. Nevertheless, the calculation of quantities such as critical indices near the FPT point requires the use of a complete theory that describes the formation of a network of short-range hydrogen bonds [34, 194, 205], as well

as scale-invariant fluctuations of the order parameter $\mathbf{s}(\mathbf{r})$ near the phase transition [69]. One way or another, the dipole–dipole interaction between molecules and the long-range effects it causes play a key role in explaining the anomalous behavior of supercooled water and interactions between bodies in liquid media [29, 58].

The divergence of the observed value of $\varepsilon_0(T)$ in bulk supercooled water directly indicates the FPT [89, 193], so it is surprising that this circumstance has not been fully understood and recognized by the authors of [33]. In our opinion, this is due to two reasons. First, the FPT temperature T_c in the quoted experiments could not be reached because of the fast volume nucleation. Bulk water was cooled in experiments [33] to a temperature of $-35\,^\circ$C; only a few degrees remained to reach the transition point. Second, the weakness of the observed singular behavior $\varepsilon_0 \propto |\tau|^{-\alpha}$, where $\alpha = 0.13$, made the authors of [33] abandon the assumption of FPT at the λ point since, according to [89, 193] and Eqn (44), in the mean-field approximation $\alpha = 1$.

Deeper water cooling and direct observation of the FPT at $T_c^{\text{exp}} \approx -38\,^\circ$C became possible owing to the use of mesoporous materials [15, 16, 41, 42]. Arguments are given in Sections 3.1–3.6 in favor of the small difference between the microscopic structure of water contained in the mesopores of the MCM-41 material used for measurements and large volumes of liquids. With this circumstance taken into account, it may be asserted that the measurements in [15, 16, 41, 42] indicate the real existence of the FPT in bulk liquid water, which confirms theoretical arguments [29–31].

Order parameter fluctuations should be taken into account in close proximity to the phase transition point. Polarization fluctuations $\mathbf{s}(\mathbf{r})$ are 'force-free' at $|\tau| \ll 1$, and, as a result, are scale-invariant, because the correlation radius of the molecule dipole moments L_T becomes infinite at the FPT point. A corresponding analysis based on the theory [77] gives for the critical index considered above $\alpha \approx 1 + (4-d)/6 = 7/6 \approx 1.2$, where $d = 3$ is the number of spatial dimensions. This implies that, in accordance with Fig. 3, the singularity is stronger than that predicted by the mean field theory. It should be noted, however, that although the number of experimental points is rather small, the divergence ε_0 in experiments [15, 16, 41, 42] looks even stronger. This should not be a surprise, since the VMPL is an oversimplified model.

The description can be improved if we take into account various microscopic states of liquid water, such as hexagonal and cubic structures. If we associate the FPT with a single structure, cubic, the critical behavior of the dielectric constant becomes much sharper due to the strong temperature dependence of the fraction of this water component [147].

A natural question arises: why is the singularity in $\varepsilon_0(T)$ weak in [33], while it is strong in [15, 16, 41, 42] (a jump by a factor of about 200 was observed)? Several hypotheses may be set forth in this regard.

(1) It is likely that it was the third term in Eqn (97) that was mainly measured in [33], while to observe the FPT described by the second term, the temperature should have been reduced by a few more degrees, as was done in [15, 16, 41, 42]. It is sometimes argued (see, e.g., [92]) that the ferroelectric state of water observed in capillaries is due to the orientation of water molecules being imposed by the forces that act on the molecules from the side of the walls. This issue is far from resolved because, as noted in Section 3.1, a number of fairly realistic MD calculations predict the existence of the FPT even in bulk water. In addition, as shown in Section 3.1, the role of the depolarizing field $\mathbf{E}_p$ in the pores is much less significant than in bulk water, which makes the FPT possible in water in pores.

(2) Finally, and this explanation seems more plausible, the reason for the existing discrepancy between the data of experiments with pores and [33] may be due to the difference between the kinetics of the ferroelectric phase formation in the pores and that in the volume; namely, within a short time interval when bulk liquid freezes, a domain structure in which there is no depolarizing field (see [66, § 44]) does not have time to form. The ferroelectric state in liquid bulk water may turn out in this case to be fundamentally unreachable. The issue may be resolved by experiments with microsamples of water, e.g., in a setup similar to that used in [40].

4. Manifestations of long-range dipole action on the interfaces between polar liquid with hydrogen bonds and immersed bodies

We now discuss the HBPL properties in a layer adjacent to the surface of a body immersed in a liquid. The phenomena under discussion occur provided $A > 0$. According to (31) and (32), this implies that the bulk liquid is in the paraelectric state. We assume that $\varepsilon_0 \gg \varepsilon_\infty$; therefore, a simplified description of the properties of a bulk solid-liquid structure presented in Section 2.5 is applicable.

4.1 Classification of surfaces by wettability type

4.1.1 Phenomenology of interaction of a liquid with the surface of immersed bodies. Taking into account the interaction with the surface of the body, the free HBPL energy may be represented as

$$G\big[\mathbf{s}(\mathbf{r})\big] = G_{\text{bulk}} + G_{\text{s}}, \tag{98}$$

where G_{bulk} is the contribution to the energy of the system from the bulk liquid (47) and G_{s} is the free energy of the surface layer of the liquid contacting the bodies or vacuum or air.

We consider a layer of water molecules immediately adjacent to the surface Γ of an immersed body. The term of interest in the energy G_{s}, which depends on the polarization of the liquid, is expressed in the most general form as follows:

$$G_{\text{s}} = \frac{1}{2}\sqrt{C}P_0^2 \int_\Gamma \mathrm{d}f\, Q(s^2, \cos\varphi)\,. \tag{99}$$

Here and below, $\mathrm{d}f$ is the area element on the surface Γ and φ is the angle between the vector $\mathbf{s}$ and the unit normal $\mathbf{n}$ to the surface directed into the water. It was taken into account in Eqn (99) that, as per the definition of the polarization vector (1), mesoscopic-scale surface inhomogeneities are averaged. For this reason, almost all surfaces, or rather large, macroscopic areas on them, may be considered homogeneous and isotropic. The specific form of the function Q, which depends on the properties of the liquid and the body surface, can be obtained by comparing the VMPL predictions with experimental data or the results of MD calculations.

The polarization vector components perpendicular and tangent to the surface have the form $s_\perp = (\mathbf{ns}) = s\cos\varphi$ and $\mathbf{s}_\parallel = \mathbf{s} - s_\perp\mathbf{n}$, respectively. Equation (99) contains two independent parameters: s^2 and $\cos\varphi$. Equivalent quantities $s_\parallel^2$ and $s_\perp$ may be used in their stead, i.e., $Q(s_\parallel^2, s_\perp)$ substituted

in (99). The body often bears uncompensated foreign charges or there are polar groups on its surface. The body surface is in the latter case a double layer, a capacitor, inside which molecules of liquid partially penetrate. In both cases, there is an electric field E_e^Γ in the surface layer whose thickness is of the order of the liquid molecule diameter, $d_{H_2O} \sim 0.3$ nm. For this reason, the layer energy changes if the sign of $s_\perp$ is reversed, i.e., generally speaking, $Q(s_\parallel^2, s_\perp) \neq Q(s_\parallel^2, -s_\perp)$.

If the polarization at the boundary is sufficiently small, $s \ll 1$, then, taking into account the arguments above, the surface contribution determined by Eqn (99) can be further simplified:

$$G_s = G_s^0 - P_0 d_{H_2O} \int_\Gamma \mathrm{d}f\, E_e^\Gamma s_\perp\,, \tag{100}$$

$$G_s^0 = -\frac{1}{2}\sqrt{C} P_0^2 \int_\Gamma \mathrm{d}f\,(\alpha_0 s_\parallel^2 + \beta_0 s_\perp^2)\,. \tag{101}$$

Here, G_s^0 is the contribution to the near-surface layer energy, which is determined by the presence/absence of hydrogen bonds between HBPL molecules and the surface and by the electrostatic interaction between the dipoles and the surface (see Section 5.2), α_0 and β_0 are dimensionless material constants that characterize the interaction between water molecules and a particular surface at a given temperature. The cross term in (101), which is proportional to the product $s_\parallel s_\perp$, is absent due to the indicated surface isotropy on the mesoscale intervals.

Equation (101) approximately determines the Gibbs energy of the surface layer of molecules in their most favorable state, compared with the unfavorable, metastable state whose energy is taken to be zero. So, the molecule loses two or three hydrogen bonds near a hydrophobic surface in the case of an unfavorable orientation and only one in the case of a favorable orientation [24, 25]. Thus, the parameter α_0 is mainly determined by hydrogen bonds. This observation may be used to evaluate α_0 for water. The energy of a single hydrogen bond is $E_H \sim 5$ kcal mol^{-1}. One molecule occupies the area $d_{H_2O}^2 \sim 0.1$ nm^2 on the surface. Therefore, we have for the interface with a vacuum at room temperature

$$\alpha_0 \sim \frac{2E_H}{\sqrt{C} P_0^2 d_{H_2O}^2} \sim 3-5\,. \tag{102}$$

As shown in Section 5.2, under the same conditions, $\beta_0 \sim \alpha_0$. In contrast to the term with α_0, the term β_0 in (101) has a purely electrostatic nature.

In the limiting case, when the surface is completely covered by polar groups, $E_e^\Gamma \sim P_0$, the ratio of the first term on the right-hand side of (100) to the last one is $\sim \beta_0\sqrt{C}/d_{H_2O} \sim 5 \gg 1$ (although exceptions are possible). For this reason, we use below expression (101) for the surface energy.

If the functions Q and $V(s^2)$ are known, then by minimizing the total free energy (98) with respect to the independent variable $\mathbf{s}(\mathbf{r})$ we arrive at the Euler equation in the volume of liquid, $\delta G/\delta\mathbf{s} = 0$, and at the same time the boundary conditions for the vector field $\mathbf{s}(\mathbf{r})$ on the surface. In particular, minimization of (98) with respect to $\mathbf{s}(\mathbf{r})$ yields, in addition to (40), the boundary condition

$$\left(\sqrt{C}\,\frac{\partial s_\alpha}{\partial n} + \sum_\beta Q_{\alpha\beta} s_\beta\right)_\Gamma = 0\,, \tag{103}$$

where

$$Q_{\alpha\beta} = \alpha_0 \delta_{\alpha\beta} + (\alpha_0 - \beta_0) n_\alpha n_\beta\,.$$

4.1.2 Flat uniform surface. Simplified form (101) of the energy of the HBPL layer adjacent to the body surface enables drawing important conclusions about possible types of surfaces with respect to their interaction with water.

We first study the case $E_e^\Gamma = 0$.

We consider a semi-infinite volume of water located in the region $z > 0$ and in contact with an infinite flat solid surface located at $z = 0$. In the absence of $\mathbf{E}_e$, the total field $\mathbf{E} = \mathbf{E}_p = (0, 0, -4\pi P_0 s_z)$. The polarization of water can be approximately found by minimizing free energy (98) using a test function of the form

$$\mathbf{s} = \left(s_x^{(1)}, 0, s_z^{(1)}\right) \exp\left(-\frac{z}{L_T}\right) + \left(s_x^{(2)}, 0, s_z^{(2)}\right) \exp\left(-\frac{z}{R_d}\right), \tag{104}$$

where $s_{x,z}^{(1,2)}$ are four variational parameters. The choice of exponential functions in this form is natural, since they are exact solutions of Eqn (40) for small polarization, $|\mathbf{s}| \ll 1$. The results of variational optimization with $V(s^2)$ from (30) for $B = 1$ are displayed in Fig. 9. Three completely different types of solutions are found, depending on the properties of the surface material, which are completely described in our model by two parameters, α_0 and β_0.

Region I on the (α_0, β_0) plane corresponds to sufficiently large values of β_0, when water molecules are polarized perpendicular to the interface, $|s_x^{(1,2)}| \approx 0$, which is a well-known sign of a hydrophilic surface. The calculation shows that the polarization in the liquid volume decays in this case exponentially at a short distance: $s_z^{(1)} = 0$, $|s_z| \sim \exp(-z/R_d)$.

Water molecules are polarized along the interface in region II, $|s_z^{(1,2)}|$, $|s_x^{(2)}| \approx 0$, and the polarization penetrates the liquid to a much greater distance: $|s_x^{(1)}| \sim \exp(-z/L_T)$. This, of course, is exactly what is expected from a hydrophobic surface [24–27]. The stability of such a state with respect to thermal fluctuations is proved in Section 4.2.3. It should be noted that the liquid/vacuum interface is a special case of hydrophobic contact, since the molecules lose on it at least one hydrogen bond.

Finally, region III corresponds to the absence of polarization in the mean-field approximation under consideration.

The boundaries between the regions of different polarization states, which are displayed in the diagram shown in Fig. 9, can be found in an analytical form. To do so, we use a simpler form of the test function instead of (104):

$$\mathbf{s} = \left[s_0^{\mathrm{II}} \exp\left(-\frac{z}{L_T}\right), 0, s_0^{\mathrm{I}} \exp\left(-\frac{z}{R_d}\right)\right].$$

Minimization of the free energy G by varying parameters s_0^{II} and s_0^{I} shows that the interface is hydrophilic, as in region I, if $\beta_0 > \nu = \sqrt{4\pi + A}$ at $\alpha_0 < \mu = \sqrt{A}$ and if $\beta_0 > \nu + (\alpha_0 - \mu)\sqrt{\mu/\nu} \equiv \beta(\alpha_0)$ at $\alpha_0 > \mu$. A hydrophobic-type body surface, as in region II, corresponds in the figure to the part of the plane $\alpha_0 > \mu$ at $\beta_0 < \beta(\alpha_0)$, i.e., the part located below the OB line and to the right of the OC line. The free energy as a function of polarization has two local minima: $G^{\mathrm{I}} = -S_\Gamma P_0^2 \sqrt{C}\nu(\beta_0 - \nu)^2/(4B)$ in region I and $G^{\mathrm{II}} = -S_\Gamma P_0^2 \sqrt{C}\mu(\alpha_0 - \mu)^2/(4B)$ in region II. Here, S_Γ is

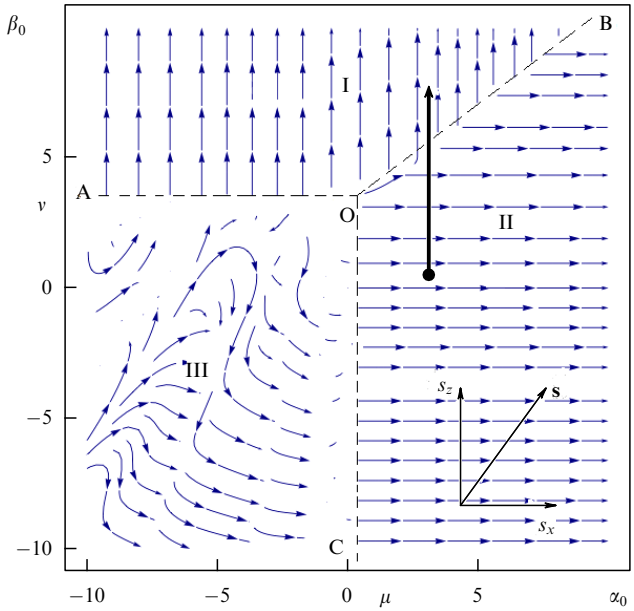

Figure 9. Polarization of water molecules at the HBPL/body interface obtained from variational solution (104). The lines with arrows indicate the direction of polarization (s_x, s_z) on the surface; the z axis is perpendicular to the surface, and the x axis is parallel to it. Regions I and II describe hydrophilic and amphiphilic surfaces, respectively. A nonzero random polarization emerges in region III due to thermal fluctuations, but its time average value is at any point zero. An instantaneous image of the polarization obtained by means of computer calculation at a certain nonzero temperature is displayed. The oblique dashed straight line OB shows the line of the first-order phase transition, amphiphilicity ⇆ hydrophilicity, that separates regions I and II. The meaning of the transition shown by a solid arrow is explained in the text.

the surface area. Corresponding polarization values are

$$s_0^{\mathrm{I}} = \sqrt{\frac{\nu(\beta_0 - \nu)}{B}}, \qquad s_0^{\mathrm{II}} = \sqrt{\frac{\mu(\alpha_0 - \mu)}{B}}.$$

Test functions more accurate than those presented above may be employed. The previous functions contained exponentials $\exp(-z/L_T)$ and $\exp(-z/R_{\mathrm{d}})$ with fixed characteristic spatial scales L_T and R_{d}. To clarify the calculation, these scales may also be chosen to be an additional variable parameter. All the presented results vary in this case insignificantly, within the limits of the VMPL error. For example, new scales turn out to be close to L_T and R_{d} if the parameters α_0 and β_0 increase to values at which polarization becomes significant, $s \sim 1$.

The equilibrium condition $G^{\mathrm{I}} = G^{\mathrm{II}}$ is satisfied on the OB line defined by the equation $\beta_0 = \beta(\alpha_0)$, which is displayed in Fig. 9. The inequalities $G^{\mathrm{II}} < G^{\mathrm{I}}$ and $G^{\mathrm{II}} > G^{\mathrm{I}}$ hold in 'hydrophobic' and 'hydrophilic' regions II and I, respectively. Thus, a first-order phase transition occurs on the OB line. Since $G \propto S_\Gamma$, this transition is sharp for large surfaces and occurs immediately upon crossing the OB. This circumstance explains, for example, experiment [206], in which a change in the contact angle of water was observed after the hydrophobic hexane was removed from the surface of TiO_2 metal oxide by ultraviolet radiation, and the contact angle changed abruptly as the radiation dose increased. Therefore, chemically adsorbed ions O_2^-, O^- [207] and dipole hydroxyl groups [208] that emerge on the surface as hexane is removed change the wetting properties of the surface, increasing β_0 to a value sufficient to cross the boundary of regions I and II, as shown by the arrow in Fig. 9.

Thus, the polarization vector $\mathbf{s}$ of the surface layer in the VMPL, i.e., its time-averaged value at any point on the surface, can be zero (the 'neutral surface' belonging to region III) and directed perpendicular (the hydrophilic surface belonging to region I) or parallel (the hydrophobic surface of region II) to the surface. There are no cases where the angle φ between this vector and the normal falls in the interval $(0, \pi/2)$ on a large surface (we consider here, of course, homogeneous surfaces, $\alpha_0(\mathbf{r}) = \mathrm{const}$, $\beta_0(\mathbf{r}) = \mathrm{const}$). The absolute value of the polarization vector on the surface in cases I and II can take any value within the range $0 < s < 1$. Such a surface could be called in case II partially hydrophobic, keeping the name hydrophobic for the surface with $s \approx 1$. A more common name, which we use below, is the amphiphilic surface. In the general case, the polarization of the liquid has for such a surface the form $\mathbf{s} = \mathbf{s}_{\parallel} \exp(-z/L_T)$, where $\mathbf{s}_{\parallel} = [s_x(x, y), s_y(x, y), 0]$ is a purely 2D polarization vector.

The wetting properties of surfaces are usually characterized by only one parameter — the wetting angle. Such a description is incomplete, in agreement with the conclusions obtained in MD calculations (see, e.g., [209]). As shown in this section, a full and fairly accurate description is ensured in reality using two parameters, α_0 and β_0 (for a more accurate description, a third parameter should be added, namely, E_{e}^{Γ}), which are temperature-dependent. Each surface at a certain temperature has a corresponding point on the (α_0, β_0) plane. If temperature or any other external parameter changes, this point describes a certain path in this plane.

We briefly discuss the case $E_{\mathrm{e}}^{\Gamma} \neq 0$. Repeating the calculation presented above, we conclude that now, similar to $E_{\mathrm{e}}^{\Gamma} \neq 0$, a liquid at the interface with large homogeneous surfaces may only have three types of polarization, I, II, and III, and they cannot exist concurrently. This implies that the diagram displayed in Fig. 9 remains qualitatively valid, but the boundaries OA, OB, and OC that separate different wettability types become curvilinear. If E_{e}^{Γ} changes, they move; therefore, an alternative explanation of experiments [206] is also possible. Due to the removal of hexane, water comes into contact with the polar surface of TiO_2. An increasing field E_{e}^{Γ} emerges in this case, which causes the motion of the OB line of the amphiphilicity ⇆ hydrophilicity phase transition. The point on the diagram marked by a black dot remains as a result stationary, while the line itself moves and passes through this point, which leads to a change in the wettability of the surface.

4.1.3 Curved homogeneous surface. So far, we have only considered flat surfaces. It is of interest to consider how the curvature of an immersed body surface affects the polarization of a liquid it creates.

We consider a body in the form of a cylinder of radius R_0 and height $H_0 \gg R_0$. As in Section 4.1.2, we select the test function in the form of a solution to linearized equation (40): $\mathbf{s} = a\hat{\boldsymbol{\varphi}} K_1(r/L_T) + b\hat{\mathbf{r}} K_1(r/R_{\mathrm{d}}) + c\hat{\mathbf{z}} K_0(r/L_T)$. Here, a, b, and c are the variational parameters, $\hat{\boldsymbol{\varphi}}$, $\hat{\mathbf{r}}$, and $\hat{\mathbf{z}}$ are the unit basis vectors of the cylindrical coordinate system, and K_n are the MacDonald functions. A calculation similar to that performed for a flat surface shows that the diagram in Fig. 9 remains qualitatively true for a curved surface. The polarization directed along $\hat{\boldsymbol{\varphi}}$, which we call the φ polarization, is force-free, i.e., the density of polarization charges is zero for

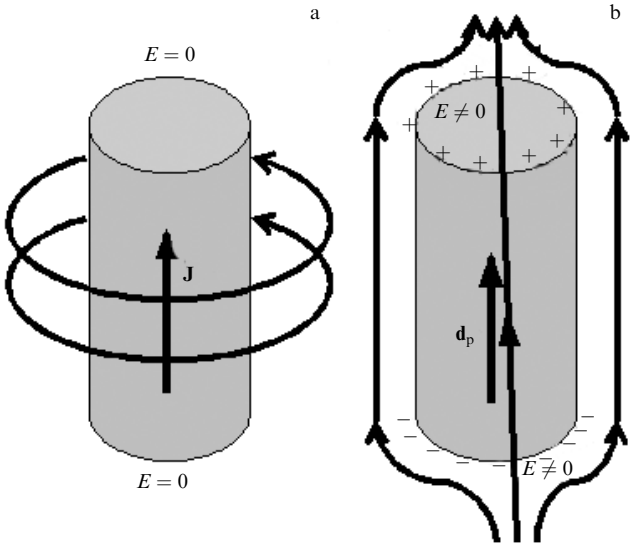

Figure 10. Polarization of liquid near a cylindrical hydrophobic surface: (a) force-free and (b) force-based configurations. Plus and minus signs indicate the areas of concentration of polarization charges whose absolute values are the same, and signs opposite. The meaning of the vectors **J** and $\mathbf{d}_\mathrm{p}$ is explained in Section 5.

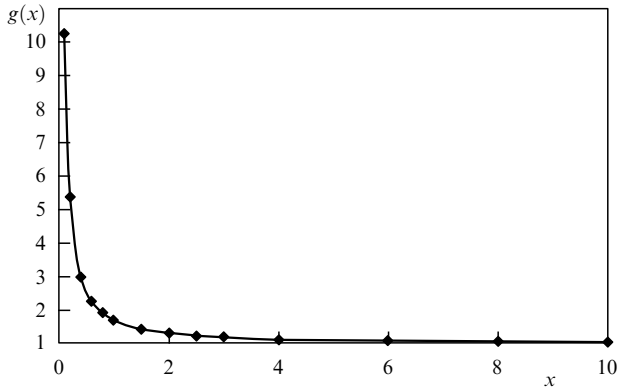

Figure 11. Function $g(x)$ that presents the dependence of the critical parameters of the spontaneous emergence of polarization on the surface of a cylinder immersed in HBPL.

this polarization (Fig. 10a). There are polarization charges of equal magnitude and opposite in sign at the ends of the z polarized cylinder (Fig. 10b). It is shown below that the energy of the electric field created by these charges is insignificant for typical biological bodies, $\sim 50-100$ K $\ll T$; therefore, the z polarization for such bodies can approximately be considered force-free as well. On the contrary, r polarization is a force-based polarization.

It is shown in Section 4.1.2 that polarization vanishes for a flat surface in case I if the parameter β_0 diminishes to $\beta^\mathrm{cr} = \nu$, and, in case II, to $\alpha^\mathrm{cr} = \mu$. The critical parameters for which the φ polarization, r polarization, and z polarization vanish in the case of a curved cylindrical surface are as follows: $\alpha_\varphi^\mathrm{cr} = \mu g(x_0)$, $\beta_r^\mathrm{cr} = \nu g(R_0/R_\mathrm{d})$, and $\alpha_z^\mathrm{cr} = \mu p(x_0)$. Here, $x_0 = R_0/L_T$, $g(x) = -K_1'(x)/K_1(x)$, $p(x) = -K_0'(x)/K_0(x)$. The function $g(x)$ is plotted in Fig. 11, while the plot of the function $p(x)$ looks very similar and differs only slightly from it. Figure 11 shows that, as surface curvature increases, polarization decreases and finally vanishes. We can clarify this conclusion using the φ polarization as an example. Since $s \ll 1$ at $\alpha_0 \approx \alpha_\varphi^\mathrm{cr}$, we obtain from (30), (47), and (101) the expression for the free energy in the Landau form: $G/S_\Gamma \propto -\Delta\alpha_\varphi a^2 + C_0 a^4$, where $\Delta\alpha_\varphi = \alpha_0 - \mu g(x_0)$ and $C_0 \propto B$ is a positive number. It can be seen that the polarization exists at $\alpha_0 > \alpha_\varphi^\mathrm{cr}$ and vanishes at $\alpha_0 < \alpha_\varphi^\mathrm{cr}$, a situation which, according to (102) and Fig. 11, occurs at $R_0 \lesssim 0.15$ nm. The diameter of this cylinder is approximately equal to the size of the water molecule.

In the case of φ polarization, the formulas for the polarization and the free energy, which are determined by the entropy contribution and deformation of hydrogen bonds, have the following form:

$$s(r) = s_0 \frac{K_1(r/L_T)}{K_1(x_0)}\,, \qquad G_\varphi^\mathrm{II} = -\pi P_0^2 C H_0 \frac{x_0^2 K_1^4(x_0)\Delta\alpha_\varphi^2}{8BJ_\varphi}\,,$$
$$s_0^2 = \frac{x_0 K_1^4(x_0)\mu\Delta\alpha_\varphi}{4BJ_\varphi}\,, \qquad J_\varphi = \int_{x_0}^{\infty} \mathrm{d}x\, x K_1^4(x)\,. \tag{105}$$

Similar formulas for z polarization may be obtained from Eqn (105) by making replacements $K_1 \to K_0$ and $\Delta\alpha_\varphi \to \Delta\alpha_z = \alpha_0 - \nu p(x_0)$. It may be concluded then that for typical biological bodies $G_\varphi^\mathrm{II} < G_z^\mathrm{II}$, and the difference $G_\varphi^\mathrm{II} - G_z^\mathrm{II}$ weakly depends on the cylinder radius R_0:

$$G_\varphi^\mathrm{II} - G_z^\mathrm{II} \approx -\frac{3\pi P_0^2 C H_0 \Delta\alpha_\varphi}{4B} \sim 0.5\, H_0\ [\mathrm{eV}] \gg T\,, \tag{106}$$

where H_0 is measured in nanometers. This result may be easily obtained in the limiting case $R_0 \gg L_T$. Result (106) is confirmed at $R_0 \lesssim L_T$ by a numerical calculation. The φ polarization is seen to be much more advantageous in terms of energy than the z polarization. For this reason, in the absence of charges and polar groups on the body, z polarized bodies should be rare in nature.

4.2 Ferroelectric phase transition on the interfaces between polar liquid with hydrogen bonds and amphiphilic bodies

It should be recalled that amphiphilic surfaces are type II. The HBPL polarization vector near this surface is parallel to it, and its absolute value lies in the $0 < s \lesssim 1$ range.

4.2.1 Free energy of the near-surface layer. Setting $\mathbf{E}_\mathrm{e} = 0$, we accurately calculate the free energy of the liquid adjacent to the amphiphilic surface assuming the latter to be flat and infinite. For the polarization that vanishes at infinity, the next to last term in (47) can be represented in this case after integration by parts as

$$-\frac{1}{2}\int \mathrm{d}^3 r\, \mathbf{P}(\mathbf{r})\mathbf{E}_\mathrm{p}(\mathbf{r}) = \frac{1}{2}\int \mathrm{d}^3 r\, \rho_\mathrm{p}\varphi_\mathrm{p}$$
$$= \frac{1}{2}\int \mathrm{d}^3 r\, \mathrm{d}^3 r'\, \frac{\rho_\mathrm{p}(\mathbf{r})\rho_\mathrm{p}(\mathbf{r}')}{|\mathbf{r}-\mathbf{r}'|}\,. \tag{107}$$

Below we mainly consider the scales

$$R = |\mathbf{r}-\mathbf{r}'| \gg L_T\,; \tag{108}$$

therefore, in consideration of the results of Section 4.1.2, we transform (107) after integrating by the coordinates z and z' into the following form:

$$\approx \frac{1}{2}L_T^2 \int \mathrm{d}f\, \mathrm{d}f'\, \frac{\rho_\mathrm{p}(\mathbf{r})\rho_\mathrm{p}(\mathbf{r}')}{|\mathbf{r}-\mathbf{r}'|} = \frac{1}{2}D\int \mathrm{d}f\, \mathrm{d}f'\, \frac{(\nabla\mathbf{s})_\mathbf{r}(\nabla\mathbf{s})_{\mathbf{r}'}}{|\mathbf{r}-\mathbf{r}'|}\,.$$

Here and below, $D = L_T^2 P_0^2$, $\mathbf{r} = (x, y)$, and $\mathbf{r}' = \mathbf{r} = (x', y')$ are two-dimensional vectors lying in the plane of the surface.

We obtain for the free energy

$$G[\mathbf{s}(\mathbf{r})] = \frac{1}{2} M \sum_{\alpha,\beta=x,y} \int \mathrm{d}f \frac{\partial s_\alpha}{\partial x_\beta} \frac{\partial s_\alpha}{\partial x_\beta} + \frac{1}{2} D \int \mathrm{d}f\, \mathrm{d}f' \frac{(\nabla \mathbf{s})_{\mathbf{r}} (\nabla \mathbf{s})_{\mathbf{r}'}}{|\mathbf{r} - \mathbf{r}'|} + R_0 \int \mathrm{d}f\, (s^2 - s_0^2)^2 , \tag{109}$$

where the parameters $M = P_0^2 C L_T/2$, $R_0 = P_0^2 B L_T/4$, and $s_0^2 = \mu(\alpha_0 - \mu)/B$ are introduced. The last term takes into account the results of Section 4.1.2.

4.2.2 Case $D = 0$. Topological Berezinskii–Kosterlitz–Thouless phase transition on an amphiphilic surface. We quote the information pertaining to the case $D = 0$ from [210–213], which is necessary for the further investigation of the phenomena described by free energy (109).

Equation (109) shows that $G[\mathbf{s}(\mathbf{r})] = \min$ for the ferroelectric state of the layer: $\mathbf{s}(\mathbf{r}) = \text{const}$, where $s = |\mathbf{s}(\mathbf{r})| = s_0$. If $D = 0$, this state is unstable with respect to long-wave thermal fluctuations with $s \approx s_0$, in the study of which we can put $\mathbf{s}(\mathbf{r}) = s_0 \mathbf{S}(\mathbf{r})$, where $\mathbf{S}(\mathbf{r}) = (\cos\theta, \sin\theta)$, $\theta = \theta(\mathbf{r})$. We arrive then at the classical XY model [214]:

$$G[\theta(\mathbf{r})] = \frac{I}{2} \int \mathrm{d}f\, (\nabla\theta)^2 = \frac{I}{2} \sum_{\mathbf{k}} k^2 |\theta_{\mathbf{k}}|^2 = I \sum_{\mathbf{k}\,(k_y>0)} k^2 \left[(\theta'_{\mathbf{k}})^2 + (\theta''_{\mathbf{k}})^2\right] , \tag{110}$$

where $I = M s_0^2$, $\theta_{\mathbf{k}} = \int \mathrm{d}f\, \theta(\mathbf{r}) \exp(-\mathrm{i}\mathbf{k}\mathbf{r})/\sqrt{S_T}$, $\theta'_{\mathbf{k}} = \operatorname{Re}\theta_{\mathbf{k}}$, and $\theta''_{\mathbf{k}} = \operatorname{Im}\theta_{\mathbf{k}}$.

It follows from (110) that the distribution of the angle θ over Fourier components has the form

$$\mathrm{d}W \propto \prod_{\mathbf{k}\,(k_y>0)} \mathrm{d}\theta'_{\mathbf{k}}\, \mathrm{d}\theta''_{\mathbf{k}} \exp\left\{-\frac{I k^2}{T}\left[(\theta'_{\mathbf{k}})^2 + (\theta''_{\mathbf{k}})^2\right]\right\};$$

therefore, $\langle \theta_{\mathbf{k}} \theta_{\mathbf{k}'} \rangle = \langle |\theta_{\mathbf{k}}|^2 \rangle \delta_{\mathbf{k}',-\mathbf{k}}$, where $\langle |\theta_{\mathbf{k}}|^2 \rangle = 2\langle (\theta'_{\mathbf{k}})^2 \rangle = T/(I k^2)$. Hence, we obtain for the correlation function of the angles at different points

$$\langle \mathbf{S}(\mathbf{r}) \mathbf{S}(\mathbf{r}') \rangle = \langle \cos\Delta\theta \rangle = \exp\left[-\frac{1}{2}\langle (\Delta\theta)^2 \rangle\right] = \left(\frac{R}{L_T}\right)^{-T/(2\pi I)} . \tag{111}$$

Here, $\Delta\theta = \theta(\mathbf{r}) - \theta(\mathbf{r}')$, $\mathbf{R} = \mathbf{r} - \mathbf{r}'$, and the following relation is taken into account:

$$\langle (\Delta\theta)^2 \rangle = \frac{2T}{S_T} \sum_{\mathbf{k}} \frac{1 - \cos(\mathbf{k}\mathbf{R})}{I k^2} = \frac{T}{\pi I} \int_0^{k_{\max}} \frac{\mathrm{d}k}{k} \left(1 - J_0(kR)\right) \approx \frac{T}{\pi I} \ln\left(\frac{R}{L_T}\right) , \tag{112}$$

which is valid at $R \gg L_T$. It is also taken into account that $\Delta\theta$ is a random Gaussian variable. In addition, our description of the layer is only valid under condition (108), which corresponds to $k_{\max} \ll 1/L_T$; therefore, $k_{\max} \sim 1/L_T$ was chosen as the upper integration limit.

Equation (111) shows that, similar to the theory of superfluidity of a 2D Bose gas [215, 216], for $D = 0$, the correlations of our order parameter $\langle \mathbf{s}(\mathbf{r}) \mathbf{s}(\mathbf{r}') \rangle \approx s_0^2 \langle \mathbf{S}(\mathbf{r}) \mathbf{S}(\mathbf{r}') \rangle$ at low temperatures decrease slowly, according to a power law, as R increases. Therefore, there is no long-range order at any temperature; however, a short range order does exist. In the case of a Bose gas, this indicates the existence of a collective effect — two-dimensional superfluidity.

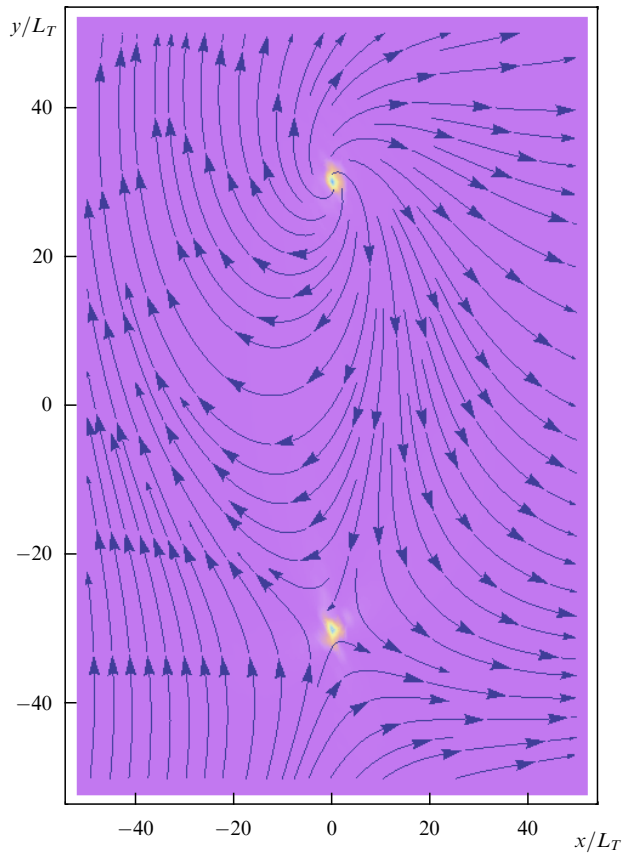

Figure 12. Polarization and distribution of total energy density at $T = 0$; a vortex and an antivortex are located at the points $(0, \pm 30)$. Light areas correspond to regions of high energy density, in which the centers of the vortices are located. The polarization is uniform at infinity: $\mathbf{s} = \text{const}$, $|\mathbf{s}| = 1$. The angle between the axis of the pair and the polarization at infinity is $\pi/4$. The calculation was performed at $D \neq 0$ (see Section 4.2.3).

As temperature increases, vortex–antivortex pairs emerge. The typical polarization pattern created by such a pair on an infinite flat surface, which is obtained by calculations, is shown in Fig. 12. If the upper vortex is compassed in the positive direction, i.e., counterclockwise, the polarization vector rotates by an angle of 2π, so the upper vortex has a topological charge $q = 1$. Consequently, the lower vortex charge is $q = -1$. The topological charge inside an arbitrary closed two-dimensional contour C is determined in general by the formula $Q = (2\pi)^{-1} \int_{\mathrm{C}} \mathrm{d}\theta$, where contour C is compassed in a positive direction.

A vortex–antivortex pair on the surface of a protein-like body looks as shown in Fig. 13.

We now calculate the pair energy $u(R)$ on a flat surface if the distance between the vortex cores is R. We consider that the cores of the vortex and antivortex are located at the points with coordinates $\mathbf{r}_1 = (-R/2, 0)$ and $\mathbf{r}_2 = (R/2, 0)$, respectively. By minimizing energy (110), we obtain the Laplace equation $\Delta\theta = 0$. Its solution, which is valid everywhere except for the regions inside the vortex cores, where the approximate formula (110) itself is no longer valid, has the

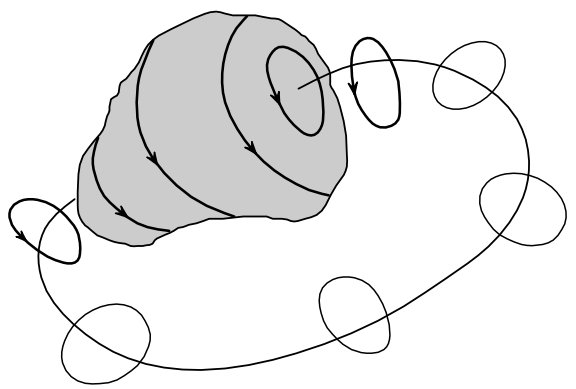

Figure 13. Excited state of a liquid with a single vortex–antivortex pair captured by the surface of a hydrophobic body immersed in the liquid.

form $\theta(\mathbf{r}) = \varphi_1 - \varphi_2$. Here, $\varphi_{1,2}$ are the angles between the vectors $\mathbf{r} - \mathbf{r}_{1,2}$ and the x axis, respectively. We obtain from here and from Eqn (110)

$$u(R) = \frac{1}{2} IR^2 \int \frac{\mathrm{d}x\,\mathrm{d}y}{\left[(x+R/2)^2 + y^2\right]\left[(x-R/2)^2 + y^2\right]} \approx 2\pi I \ln\left(\frac{R}{L_T}\right). \quad (113)$$

Following [210–213], we include into consideration the pairs and transform energy (110) into the form

$$G \approx \frac{I}{2}\int \mathrm{d}f\,(\nabla\psi)^2 - 2\pi I \sum_{1 \leqslant i < j \leqslant 2N_\mathrm{p}} q_i q_j \ln\left(\frac{r_{ij}}{L_T}\right). \quad (114)$$

Here, ψ is the fluctuation part of the angle θ that drives the vanishing of correlations as R increases at low temperatures (see (111)), $r_{ij} = |\mathbf{r}_i - \mathbf{r}_j|$, $i, j = 1, 2, \ldots, 2N_\mathrm{p}$ are the numbers of the vortices, q_i are their topological charges, and N_p is the number of pairs. The entire surface is topologically neutral: $\sum_i q_i = 0$; otherwise, the Gibbs energy of the liquid would be proportional to the logarithm of the surface area, i.e., infinite.

In the case of a Bose gas at low temperatures, the paired vortices remain in a bound state due to the logarithmic attraction between the vortex pair components. The number of pairs is small, so their presence does not destroy the short-range order in spin directions considered above. The same is true in our case. This is indicated by the power-law dependence of the correlation on R (111) due to thermal fluctuations generated by the first term in (114). This term does not contain singularities, and it is this feature that was used to derive Eqn (111). If $T > T_\mathrm{BKT}$, where

$$T_\mathrm{BKT} = \frac{\pi I}{2}, \quad (115)$$

the existence of unpaired rather than paired vortices becomes thermodynamically more advantageous. The pairs dissociate and a 'plasma' is formed that consists of free N_p vortices and N_p antivortices [210–213]. Indeed, consider a single vortex or anti-vortex on a surface with a characteristic size L. In this case, we have $\theta = \pm\varphi$, where φ is the azimuthal angle (see notations in Section 2.8); therefore, $(\nabla\theta)^2 = 1/r^2$, and the internal energy of the liquid is $U = (I/2)\int \mathrm{d}f/r^2$. The integral diverges for large r, so we get with logarithmic accuracy $U \approx \pi I \ln(L/L_T)$. The number of ways to place the vortex on the surface is $\Gamma \sim S_\Gamma/L_T^2 \sim L^2/L_T^2$, so the entropy and Helmholtz energy have the form $S = \ln(L^2/L_T^2)$, and $F = U - TS = (\pi I - 2T)\ln(L/L_T)$, respectively. It can be seen that the formation of a single vortex is thermodynamically advantageous for $T > \pi I/2$, from which Eqn (115) follows. In the 'plasma' of pairs of vortices and anti-vortices that emerges at $T > T_\mathrm{BKT}$ as a result of dissociation, the power-law dependence on R (111) is replaced by an exponential one. A topological Berezinskii–Kosterlitz–Thouless (BKT) second-order phase transition occurs. In the case of a two-dimensional Bose gas, the BKT transition destroys its superfluidity.

It is instructive to derive result (115) using a method that will be needed later on to analyze a more complicated case $D \neq 0$.

Of interest to us is the behavior of the system at

$$T \approx T_\mathrm{BKT}, \quad (116)$$

when the size of a typical pair is large, i.e., the condition $R \gg L_T$ is satisfied. We can ignore in this case the first term in (114) that describes thermal fluctuations, owing to which we can represent the energy of the system in the form

$$G = -\frac{1}{2}\sum_{i,j}^{2N_\mathrm{p}} q_i q_j u(r_{ij}) = \frac{1}{2}\sum_i q_i \Phi(\mathbf{r}_i). \quad (117)$$

A 'topological potential' was introduced in (117), as is done in classical electrostatics,

$$\Phi(\mathbf{r}) = -\sum_j q_j u(\mathbf{r} - \mathbf{r}_j) = -\int u(\mathbf{R})\rho_\mathrm{TP}(\mathbf{r}')\,\mathrm{d}^2\mathbf{r}'. \quad (118)$$

Here, $\mathbf{R} = \mathbf{r} - \mathbf{r}'$, $\rho_\mathrm{TP}(\mathbf{r}) = \sum_j q_j \delta^{(2)}(\mathbf{r} - \mathbf{r}_j)$ is the density of the topological charges of the vortices. Substituting formula (113) into (118), we obtain

$$G = -\pi I \sum_{i \neq j} q_i q_j \ln\left(\frac{r_{ij}}{L_T}\right) = \frac{1}{2}\sum_i q_i \Phi(\mathbf{r}_i). \quad (119)$$

The potential $\Phi(\mathbf{r})$ in (118) satisfies the Poisson equation, $\hat{L}_\mathbf{r}\Phi(\mathbf{r}) = -4\pi^2 I \rho_\mathrm{TP}(\mathbf{r})$, where the notation $\hat{L}_\mathbf{r} = \Delta_\mathbf{r}$ is introduced, and the relation $\Delta_\mathbf{r} \ln(|\mathbf{r} - \mathbf{r}'|/L_T) = 2\pi\delta^{(2)}(\mathbf{r} - \mathbf{r}')$ is used.

We keep exploiting the analogy with electrostatics. Since, according to (117), the energy of the charge q in the external potential Φ is equal to $G = q\Phi$, the force that acts on the charge has the form $\mathbf{F} = q\mathbf{E}$, where an analogue of the electric field vector — the 'topological' field $\mathbf{E} = -\nabla\Phi$ — is introduced. The pair energy in this field is $q_+\Phi(\mathbf{r}_+) + q_-\Phi(\mathbf{r}_-) \approx -\mathbf{d}\mathbf{E}$. The topological dipole moment of the pair $\mathbf{d} = q_+\mathbf{r}_+ + q_-\mathbf{r}_- = \mathbf{r}$, where $\mathbf{r} = \mathbf{r}_+ - \mathbf{r}_-$, is introduced here.

Let us put the test charge Q at the coordinate origin. The equation for the potential $\Phi_Q(\mathbf{r})$ of a pointlike charge Q has the form

$$\hat{L}_\mathbf{r}\Phi_Q(\mathbf{r}) = -4\pi^2 I Q \delta^{(2)}(\mathbf{r}) - 4\pi^2 I \rho_\mathrm{TP}(\mathbf{r}). \quad (120)$$

We assign the numbers $a = 1, 2, \ldots, N_\mathrm{p}$ to the pairs and separate the summation over pairs and over charges in pairs

in the expression for $\rho_{\rm TP}(\mathbf{r})$:

$$\rho_{\rm TP}(\mathbf{r}) = \sum_j q_j \delta^{(2)}(\mathbf{r}-\mathbf{r}_j) = \sum_a \left[\delta^{(2)}(\mathbf{r}-\mathbf{r}_{a+}) - \delta^{(2)}(\mathbf{r}-\mathbf{r}_{a-})\right].$$

The coordinate of the ath pair is $\boldsymbol{\rho}_a = (\mathbf{r}_+ + \mathbf{r}_-)/2$, so $\mathbf{r}_{a\pm} = \boldsymbol{\rho}_a \pm \mathbf{r}_a/2$. Linear expansion in the small vector $\mathbf{r}_a$ yields the standard result: $\rho_{\rm TP}(\mathbf{r}) = -\nabla\mathbf{P}$, where $\mathbf{P}(\mathbf{r}) = \sum_a \mathbf{d}_a \delta^{(2)}(\mathbf{r}-\boldsymbol{\rho}_a) = n_{\rm p}\langle\mathbf{d}\rangle$ is the polarization vector of the gas of vortex–antivortex pairs, $n_{\rm p}$ is the surface density of the pairs, and the symbol $\langle\ldots\rangle$ means averaging over the microscopic section of the surface that contains a large number of pairs, as well as averaging over the statistical ensemble. It should be noted that, after such averaging, the topological charge inside the contour C,

$$Q_{\rm TP} = \int_{\rm C} {\rm d}f\, \rho_{\rm TP}(\mathbf{r}),$$

is, generally speaking, a fractional number.

The general form of the expression for polarization in the weak field approximation is as follows:

$$\mathbf{P}(\mathbf{r}) = \int {\rm d}f'\psi(|\mathbf{r}-\mathbf{r}'|)\mathbf{E}(\mathbf{r}') = -\int {\rm d}f'\psi(|\mathbf{r}-\mathbf{r}'|)\nabla\Phi(\mathbf{r}'). \quad (121)$$

We get for a slowly changing field $\mathbf{P}(\mathbf{r}) \approx \chi\mathbf{E}(\mathbf{r}) = -\chi\nabla\Phi(\mathbf{r})$, where $\chi = \int {\rm d}f\,\psi(\mathbf{r})$ is the susceptibility of the HBPL surface layer,

$$\rho_{\rm TP}(\mathbf{r}) = \chi\Delta_{\mathbf{r}}\Phi_Q(\mathbf{r}). \quad (122)$$

We transform Eqn (120) with Eqn (122) taken into account

$$\Delta_{\mathbf{r}}\Phi_Q(\mathbf{r}) = -\frac{4\pi^2 IQ}{1+4\pi^2 I\chi}\,\delta^{(2)}(\mathbf{r}).$$

This formula shows that the phase transition occurs under the condition

$$\chi = \infty, \quad (123)$$

the physical meaning of which is that pairs start dissociating, and free charges completely screen the test charge field.

There is only a small number of large-sized pairs in a state close to dissociation at temperatures slightly lower than $T_{\rm BKT}$. Most of the pairs have small dimensions. We divide for this reason the vortex pairs into two classes: small size pairs (small pairs, SPs) and large size pairs close to dissociation (large pairs, LPs). The SP cloud screens the LP field due to which the potential energy of the LP changes.

First, we calculate the polarizability $\alpha_{\rm p}$ of a single SP. The SP energy in the external field $\mathbf{E}$ is equal to $V(\mathbf{r}) = u(r) - \mathbf{r}\mathbf{E}$, where the pair energy is given by Eqn (113). The average SP dipole moment in the weak field approximation is

$$\langle\mathbf{d}\rangle = \frac{\int {\rm d}^2 r\, \mathbf{r}\exp(-V/T)}{\int {\rm d}^2 r\, \exp(-V/T)} \approx \alpha_{\rm p}\mathbf{E}.$$

Here, $\alpha_{\rm p} = I_3/(2TI_1)$ is SP polarizability. We introduced integrals of the form

$$I_n = \int {\rm d}^2 r\, r^{n-1}\exp\left(-\frac{u}{T}\right) = 2\pi\int_0^\infty {\rm d}r\, r^n\left(\frac{r}{L_T}\right)^{-\beta}, \quad (124)$$

where parameter $\beta = 2\pi I/T$. The susceptibility being sought is given by the formula $\chi = \alpha_{\rm p} n_{\rm p}$.

The density $n_{\rm p}$ at a temperature close to that of the transition may be calculated using the following arguments. The pairs at $T \approx T_{\rm BKT}$ only start dissociating, and the fraction of LPs is not large. The size of a typical pair is small, and interaction between the vortices remains unscreened and, therefore, the energy is approximately equal to $u(r)$. The statistical sum of a gas consisting of $N_{\rm p}$ pairs on the surface with area S_Γ has the form $z = z_1^{N_{\rm p}}/N_{\rm p}! \approx (z_1 e/N_{\rm p})^{N_{\rm p}}$. Here, $z_1 = \int {\rm d}^2 r_+\, {\rm d}^2 r_-\, \exp[-u(r)/T] = \int {\rm d}^2\rho\, {\rm d}^2 r\, \exp[-u(r)/T]$, where $\boldsymbol{\rho} = (\mathbf{r}_+ + \mathbf{r}_-)/2$. To avoid the Gibbs paradox, the $1/N_{\rm p}!$ factor is introduced in a standard way. Minimizing the free energy of the pair cloud $F_{\rm p}(N_{\rm p}) = -T\ln z$, we find $N_{\rm p} = z_1$, i.e., $n_{\rm p} = N_{\rm p}/S_\Gamma = I_1$, so

$$\chi = \frac{I_3}{2T}. \quad (125)$$

Thus, we obtain for the case $D = 0$ considered in this section

$$\chi = \frac{I_3}{2T} \propto \int_0^\infty {\rm d}r\, r^{3-\beta}. \quad (126)$$

The integrand in Eqn (126) is not valid for small r. However, there is no singularity for such r, since this region corresponds to the confluence of the vortex cores, in which all quantities remain finite. The integral converges for large r if $3-\beta < -1$, which corresponds to $T < T_{\rm BKT}$, and diverges if $T > T_{\rm BKT}$, which corresponds to the dissociation of pairs at such temperatures. The expression for the root-mean-square size of pairs, which is proportional to I_3, as it should be, also diverges.

4.2.3 Case $D \neq 0$. Specific features of the BKT transition in a two-dimensional dipole gas. Ordering phenomena in two-dimensional spin systems with dipole–dipole forces acting between particles were explored in detail in [217–229]. These studies showed that such interactions between the magnetic moments of atoms lead to the stability of long-range ferromagnetic order with respect to thermal fluctuations. This implies in our case that the HBPL layer adjacent to the amphiphilic surface at low temperatures in the ferroelectric state is $\mathbf{s}(\mathbf{r}) = {\rm const}$ [217, 218], where $s = s_0$, or has, like a piece of nonmagnetized soft iron, a domain structure that consists of polarized domain islands (see [219, 220, 222, 230], in which 2D spin systems were studied).

We now prove the stability of the ferroelectric state of the HBPL surface layer. To this end, we consider the case where the HBPL layer is polarized along the x axis that belongs to the plane of the surface, as shown in Fig. 14. Let the dipoles deviate at small angles $\theta(\mathbf{r})$, so that $\mathbf{s}(\mathbf{r}) \approx s_0(1,\theta)$. We obtain from (109) instead of (110)

$$G[\theta(\mathbf{r})] = \frac{I}{2}\int {\rm d}f\,(\nabla\theta)^2 + \frac{1}{2}Ds_0^2\int {\rm d}f\,{\rm d}f'\,\frac{(\theta_y)_{\mathbf{r}}(\theta_y)_{\mathbf{r}'}}{|\mathbf{r}-\mathbf{r}'|} = \frac{1}{2}\sum_{\mathbf{k}} g(\mathbf{k})|\theta_{\mathbf{k}}|^2, \quad (127)$$

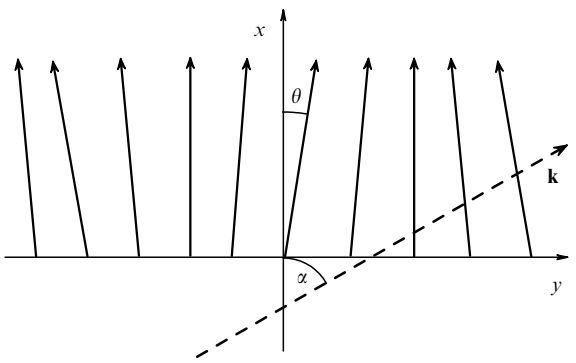

Figure 14. Propagation of a ferroelectric wave with the wave vector **k** in a near-surface layer of water (top view of the near-surface layer).

where $\theta_y \equiv \partial\theta/\partial y$, $g(\mathbf{k}) = Ik^2 + 2\pi D s_0^2 k \sin^2\alpha$, and α is the angle between the vector **k** and the y axis. It follows that the average polarization-vector deviation angle squared is

$$\langle\theta^2\rangle = \frac{1}{S_\Gamma}\sum_{\mathbf{k}}\langle|\theta_{\mathbf{k}}|^2\rangle = \frac{T}{4\pi^2}\int_{k\lesssim 1/L_T}\frac{\mathrm{d}^2k}{Ik^2 + 2\pi D s_0^2 k\sin^2\alpha}\,. \tag{128}$$

The integral in (128) diverges at $D = 0$, i.e., the uniform polarization is in this case unstable with respect to thermal fluctuations, as shown in Section 4.2.2. It should be noted that due to (108) $k \lesssim 1/L_T$. Therefore, $2\pi D s_0^2 k/(Ik^2) \gtrsim 4\pi/A \approx \varepsilon_0 \approx 88 \gg 1$, which simplifies the calculation of the integral. We obtain as a result the estimate

$$\langle\theta^2\rangle \sim \frac{T}{\pi^{3/2}P_0^2 L_T^2\sqrt{C}} \sim 2.5\times 10^{-3} \ll 1\,,$$

which indicates the stability of the ferroelectric state at low temperatures.

Thus, the ferroelectric ordering does not disagree with the Peierls–Mermin theorem [215, 216] regarding the absence of a long-range order in 2D systems. It is due to a new phenomenon: the long-range dipole–dipole interaction between molecules in a near-surface layer, which is described by the term with coefficient D in (109). This is another manifestation of long-range action characteristic of HBPL.

Equation (128) also shows that the long-range dipole–dipole interaction and the short-range interaction associated with the formation of hydrogen bonds are equally important for stabilizing ferroelectric ordering in the film, in full agreement with [227, 228]. The long-range order does not exist if any of these terms is missing: the integral diverges if $D = 0$ (no dipole–dipole interaction) or if $I = 0$ (no hydrogen bonds). This conclusion is consistent with Earnshaw's theorem on the instability of a classical dipole system, which is stabilized in our case by hydrogen bonds. It also implies that short-range intermolecular forces determine in the 2D case the structure of dipole ordering at large distances. The same observations have been made in studies [231–234] that explored classical two-dimensional systems of magnetic dipoles located at the nodes of lattices of various types. The ground state of a 2D lattice system of magnetic moments was shown to be ferromagnetic or antiferromagnetic, depending on the lattice type.

Attempts to elucidate the nature of the phase transition in a two-dimensional dipole gas have to date mainly relied on renormalization group methods [218, 220, 227, 235] and MD calculations [221, 223–225, 236, 237]. It was shown in [218, 223, 227] and in Section 4.2 that the thermal excitations predominant for short-range, contact interactions, i.e., at $D = 0$, are the polarization states $\mathbf{s}(\mathbf{r})$ that correspond to the gas of vortex–antivortex pairs. This property is also valid at $D \neq 0$. According to [227], the energy of interaction between the vortex and the antivortex linearly increases when $D \neq 0$ as the distance R between their cores grows. As stated in [227], it is for this reason that the nature of the phase transition that occurs as temperature increases is fundamentally different from the BKT transition. The physical mechanism of the transition considered in [227] is not discussed in that study, since it cannot be established within the renormalization group procedure.

We critically analyze in this section a statement in [227] about the different natures between the BKT transition and the phase transition in the HBPL film adjacent to the amphiphilic surface using to this end a combination of numerical calculations and a simple analytical model. We show that, similar to what occurs in plasma, a key role is played by the screening of attraction inside large pairs close to dissociation, which is due to the presence of small vortex pairs. This screening qualitatively changes the character of the dependence of the interaction energy between the vortex and the antivortex on the distance R between their cores: this dependence remains linear at small distances $R \lesssim L_T r_0$, where $r_0 \sim 5$ (see below), and becomes logarithmic at $R \gtrsim L_T r_0$. Therefore, the phase transition occurs following the standard BKT mechanism associated with the dissociation of pairs.

This conclusion is consistent with the results of Monte Carlo calculations in the Heisenberg anisotropic XY model containing long-range dipole–dipole interactions [237, 238]. Of course, numerical calculations per se cannot establish the physical mechanism of the phase transition. This can only be done on the basis of the analytical calculations presented in this section. In particular, the dependence of the second-order transition temperature on the dipole–dipole coupling constant D is established below. The agreement of this dependence with calculations [237, 238] is an additional confirmation of the conclusion made here regarding the BKT mechanism of the transition. We show that the only manifestation of the influence of the dipole–dipole interaction on the character of the BKT transition is a small increase in the transition temperature compared to the value that follows from (115).

We make calculations for the case $D \neq 0$ applying the method developed in Section 4.2.2. We first introduce dimensionless variables $\tilde{G} = G/I$, $\tilde{\mathbf{r}} = \mathbf{r}/L_T$ and dimensionless parameters $\Lambda_0 = R_0 L_T^2 s_0^4/I = B s_0^2/(2A)$,

$$\Lambda = \frac{D s_0^2 L_T}{I} = \frac{2}{A}\,, \tag{129}$$

and replace the polarization vector with the vector $\tilde{\mathbf{s}} = \mathbf{s}/s_0$. We omit for notational simplicity the tilde symbol above all these quantities.

The free energy reduced to the dimensionless form is expressed as follows:

$$G[\mathbf{s}(\mathbf{r})] = G_0 + G_{\mathrm{dd}}\,, \tag{130}$$

$$G_0 = \frac{1}{2}\int_\Gamma \mathrm{d}f\left[\sum_{\alpha,\beta=x,y}\frac{\partial s_\alpha}{\partial x_\beta}\frac{\partial s_\alpha}{\partial x_\beta} + \Lambda_0(s^2-1)^2\right], \tag{131}$$

$$G_{\mathrm{dd}} = \Lambda\int_\Gamma \mathrm{d}f\,\mathrm{d}f'\,\frac{(\nabla\mathbf{s})_{\mathbf{r}}(\nabla\mathbf{s})_{\mathbf{r}'}}{|\mathbf{r}-\mathbf{r}'|}\,. \tag{132}$$

Owing to the last term in (131), the state of the dipole gas is stable with respect to Earnshaw's instability, i.e., the collapse caused by dipole–dipole forces (132).

It should be noted that model (130) may be widely used, for example, for such 2D systems as magnets [236], ferroelectrics [239], quantum gases [240], and water molecules on the surface of proteins in biology [25].

Of interest to us is the behavior of the system at $T \approx T_{\mathrm{BKT}}$, when the size of a typical pair is large, as in Section 4.2.2, i.e., the condition $R \gg 1$ holds. We have for large vortex pairs $\nabla \mathbf{s} \sim 1/R$ and, consequently, $G_0 \sim \ln R$, $G_{\mathrm{dd}} \sim R$. Thus, the pair energy grows linearly as the distance R between the vortex and the antivortex increases, implying that the force of their attraction is constant [226, 227]. This behavior is very different from that observed in the model considered in Section 4.2.2 with only contact interactions, i.e., at $D = 0$, where the force that operates between the vortex and the antivortex decreases with an increase in the pair size R in inverse proportion to this size. This observation, as well as the results of [31, 227], enable representing the energy of the system in the form (117), (118), where now

$$u(r) \approx 2\pi \ln(1 + \alpha r) + K_0 r \tag{133}$$

and $\alpha \sim 1$. It was taken into account in (133) that, as $r \to 0$, the vortices in the pairs annihilate, which corresponds to the condition $u(0) = 0$. The logarithmic contribution to $u(r)$, which arises due to the presence of the G_0 term, describes interaction between vortices in the limit $\Lambda \to 0$ [213]; $K_0 \equiv K_0(\Lambda)$ is the tension coefficient of the effective 'string' connecting the vortex-antivortex pair that depends on the interaction 'strength' Λ (we note, however, that the term 'string' used here is conventional, since there is no string, i.e., no polarization bunch near the axis connecting the vortices is formed).

We note in this regard that the transition from Eqns (130)–(132) to the gas model of vortex-antivortex pairs is described by effective interaction (117), whose parameters at $D \neq 0$ must be selected from a comparison with the results of numerical calculations. The procedure for choosing the values of the parameters α and K_0 included in (133) is explained below. Moreover, formula (117) itself is approximate and also subject to verification.

We briefly describe the essence of subsequent calculations carried out in this section. Numerical calculations showed that all quantities of significance for establishing the nature of the phase transition depend on the parameter Λ_0 in (131) very weakly. This is due to the existence in our problem of a small parameter $1/\ln \varepsilon_0$, where ε_0 is static dielectric constant (44). The calculations were performed for this reason for $\Lambda_0 = 1$. It should be noted that, according to (129), the parameter Λ is rather large: $\Lambda \sim 10$. It turns out that, as Λ increases, the main physical quantities become saturated to reach asymptotic constants as early as at $\Lambda \sim 1$; therefore, there is no need for laborious calculations with such large Λ.

Equation (117) with $u(r)$ from (133) is, in studying the case $D \neq 0$, a basis for a phenomenological model that describes the properties of the HBPL layer adjacent to the amphiphilic surface. To verify Eqn (117), namely the additivity property of the HBPL layer energy with respect to vortices and antivortices, which follows from this equation, a series of *ab initio* computer calculations was performed in the molecular dynamics using the Langevin equation [241]. A mesh with nodes $i = 1, 2, \ldots, N_{\mathrm{g}}$ was introduced on the plane (x, y). A discrete representation of Hamiltonian (131) and (132) on this mesh was used to calculate the Langevin dynamics of the system at a fixed temperature for long time intervals, which made it possible to find statistical average values of the systems with the required accuracy.

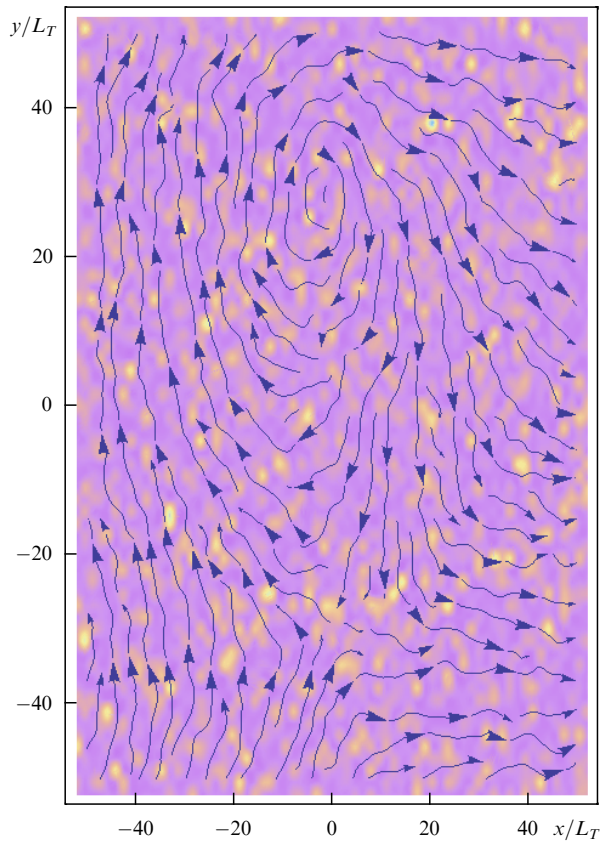

Figure 15. Polarization of the HBPL layer adjacent to the amphiphilic surface at a temperature close to T_{BKT}, which is calculated using the molecular dynamics method. A large number of vortex–antivortex pairs that emerge due thermal fluctuations are simultaneously present in this case. Their mutual influence creates a screening, as a result of which the linear nature of the interaction inside each pair is replaced with a logarithmic one. Owing to this, a BKT transition occurs.

To calculate the thermodynamically equilibrium polarization states taking fluctuations into account, the Langevin equations for polarization vectors at the mesh nodes were numerically solved:

$$\frac{\mathrm{d}\mathbf{s}_i}{\mathrm{d}t} = -\gamma \frac{\partial}{\partial \mathbf{s}_i}(G_0 + G_{\mathrm{dd}}) + \boldsymbol{\zeta}_i(t)\,. \tag{134}$$

The constant γ determines the model time of the liquid layer relaxation to the equilibrium state. The term $\zeta_{\alpha i}$ with $\alpha = (x, y)$ that describes random Gaussian noise satisfies the conditions $\langle \boldsymbol{\zeta}_i(t) \rangle = 0$ and $\langle \zeta_{\alpha i}(t) \zeta_{\beta j}(t') \rangle = 2T\gamma \delta_{\alpha\beta} \delta_{ij} \delta(t - t')$. The second-order Runge–Kutta algorithm was used to solve Eqns (134). The equations were integrated numerically with a sufficiently small time step, the optimal value of which was found to be $\Delta t = 0.005$. To determine the term (132) that describes the dipole–dipole interaction, we used the fast Fourier transform procedures in the NumPy package [242], which enabled calculation of this term in $O(N_{\mathrm{g}} \ln N_{\mathrm{g}})$ steps. Examples of typical polarization patterns of a two-dimensional gas of dipole molecules at zero and nonzero temperatures, which were obtained in this way, are displayed in Figs 12 and 15.

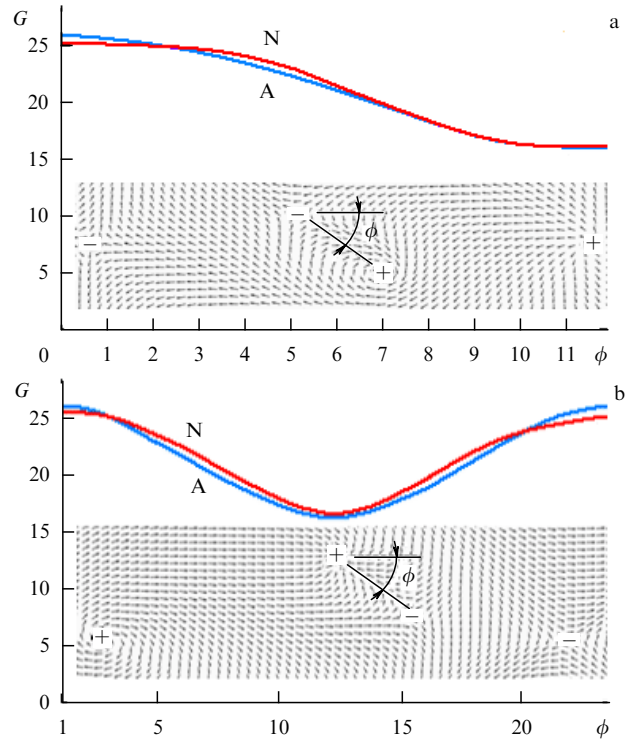

Figure 16. Free energy of a uniformly polarized 2D spin system with a small vortex pair located in the center of the configuration that describes the large vortex–antivortex pair (a) and a small pair slightly shifted with respect to the configuration center (b) as a function of the angle (in units $\pi/12$) between the small-pair axis and the x axis. The curves labeled N correspond to numerical calculations that use the Langevin equation, and those labeled A, to analytical approximation (135). Free energy is measured in units I (see the definition of dimensionless units used in this section before Eqn (129)).

An algorithm designed to find the state of the system was used to verify the assumptions based on which formula (117) was derived. First, we considered the zero temperature case, $T = 0$, for which vortex additivity rule (117) was verified. We applied to this end the imaginary relaxation time method that can be used to find local minima of the free energy functional in the configuration space of 2D vectors $\mathbf{s}_i = (s_{xi}, s_{yi})$ at the nodes $i = 1, 2, \ldots, N_g$ of a dense square mesh.

Following [243], we chose as the initial state, from which the solution of (134) started, the approximation $\mathbf{s}^{(0)}(\mathbf{r}) = (s_x^{(0)}(x, y), s_y^{(0)}(x, y))$ such that

$$s_x^{(0)} + \mathrm{i}s_y^{(0)} = \frac{2W}{1 + |W|^2}\,, \tag{135}$$

where

$$W = \prod_{j=1}^{2N_p} (z - z_j)^{q_j}\,,$$

$z = x + \mathrm{i}y$, and $z_j = x_j + \mathrm{i}y_j$ is the complex coordinate of the jth vortex with the topological charge q_j. For a topologically neutral gas of pairs, $\sum_j q_j = 0$; therefore, $W \to 1$ at $z \to \infty$, which is consistent with the physical boundary condition $\mathbf{s} \to (1, 0)$ at $r \to \infty$ adopted in calculations. We observed at the first stage of the imaginary-time dynamics at $T = 0$ a deformation of the initial polarization configuration that included a transition to an almost stable vortex pair. At the next stage the vortex pair cores approached each other much more slowly and eventually annihilated. Any initial configuration containing pairs undergoes at $T = 0$ a transition to the ground state, $s_x = 1$, $s_y = 0$. To ensure the stability of the pair, vortex pinning was introduced by adding the term $G_{\text{pin}} = \sum_j G_j$, $G_j = \int \mathrm{d}f\, V_j(\mathbf{r})[\mathbf{s}(\mathbf{r}) - \mathbf{s}_0(\mathbf{r})]^2$ to the free energy, where $V_j(\mathbf{r}) = -V_0 \exp[-(\mathbf{r} - \mathbf{r}_j)^2/a^2]$, $a \sim 1$. Pair production was observed at $T > 0$ along with annihilation; therefore, the gas as a whole turned out to be at equilibrium.

To verify formula (117), numerous diverse configurations differing in the number of vortex pairs were studied. Total energy values (117) and (133) were numerically reproduced for each of the configurations with an accuracy of $\sim 5\%$ (examples of typical verified vortex configurations are presented in Fig. 16). The accuracy that we were able to achieve is naturally limited by the magnitude of the perturbation associated with the pinning potential. This accuracy turned out to be quite sufficient to prove the approximate expression (117) for the multi-vortex configuration energy.

Numerical calculations made it possible to determine the functional dependence $K_0(\Lambda)$. It turns out that the physical configuration corresponding to a single pair loses stability at $\Lambda \gtrsim \Lambda_{\text{cr}} = 0.4$: a new small-sized vortex–antivortex pair emerges in the center between the large pair of vortices. If Λ increases further, the initial vortices turn out to be immersed in the polarization cloud of small pairs, which reduces the effective topological charges of the initial vortices. According to Eqns (117), (118), and (133), a decrease in the topological charge is equivalent to a decrease in the constant K_0, which implies that, as Λ increases, the value of $K_0(\Lambda)$ stabilizes; therefore, $K_0(\Lambda) \approx K_0(\Lambda_{\text{cr}}) \equiv K_0(\infty) \approx 3.1$ for $\Lambda > \Lambda_{\text{cr}}$. Thus, a saturation effect takes place: $K_0(\Lambda) \to K_0(\infty) \approx 3.1$ at $\Lambda \to \infty$ (see the inset in Fig. 17). The spontaneous pair production also follows from formula (117): if $\Lambda > \Lambda_{\text{cr}}$, the energy of a large pair decreases due to the emergence of a new small pair in the center of the configuration.

The parameter α in formula (133) is selected based on the condition of its consistency with the conclusion made in the previous paragraph: if $\alpha = K_0(\infty)/(2\pi)$ is chosen, a new pair emerges at $\Lambda = \Lambda_{\text{cr}}$, as it should.

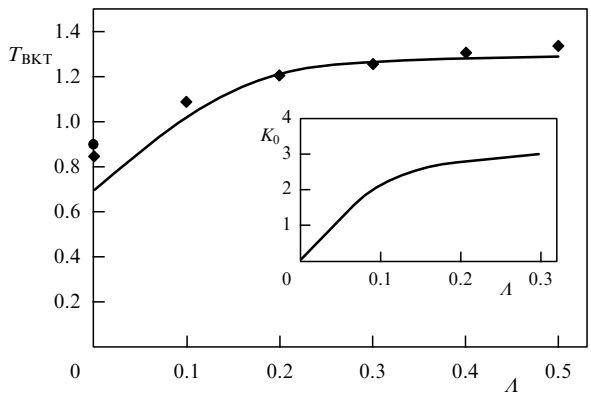

Figure 17. Transition temperature T_{BKT} as a function of the 'strength' of the dipole–dipole interaction Λ found from Eqn (139) (solid curve) and the numerical estimate T_{BKT} (diamonds) independent of the additive approximation (117), which is obtained ab initio from the MD calculation. The BKT result of [244, 245] that corresponds to $\Lambda = 0$ is indicated by a black dot. The inset shows the saturation effect of the pair tension coefficient K_0 as the dipole–dipole interaction strength Λ increases. The dependence $K_0 = K_0(\Lambda)$ is used to find the critical temperature from Eqn (138). Temperature is measured in units of I.

After formula (117) for energy has been verified in numerical calculations, it may be used to establish the nature of the phase transition and derive an analytical expression for the transition temperature. We apply to this end the method developed in Section 4.2.2. The potential $\Phi(\mathbf{r})$ satisfies by definition the Poisson equation, $\hat{L}_{\mathbf{r}}\Phi(\mathbf{r}) = \rho_{\mathrm{TP}}(\mathbf{r})$. The linear operator $\hat{L}_{\mathbf{r}}$ is defined here in such a way that $\hat{L}_{\mathbf{r}}u(\mathbf{r}-\mathbf{r}') = -\delta^{(2)}(\mathbf{r}-\mathbf{r}')$ or, in the Fourier representation, $L_{\mathbf{k}} = -1/u_{\mathbf{k}} = \{2\pi K_0 k^{-3} + 4\pi^2\alpha/[k^2(k+\alpha)]\}^{-1}$.

The equation for the potential $\Phi_Q(\mathbf{r})$ of a test point topological charge Q located at the coordinate origin has the form $\hat{L}_{\mathbf{r}}\Phi_Q(\mathbf{r}) = Q\delta^{(2)}(\mathbf{r}) + \rho_{\mathrm{TP}}(\mathbf{r})$. Repeating the operations performed in Section 4.2.2, we obtain the expression

$$\Phi_Q(\mathbf{r}) = Q\int\frac{\mathrm{d}^2k}{(2\pi)^2}\,\frac{\exp(\mathrm{i}\mathbf{k}\mathbf{r})}{L_{\mathbf{k}}+\chi k^2}\,, \tag{136}$$

where χ is the susceptibility of the near-surface HBPL layer defined in Section 4.2.2.

The main contribution to the integral comes at large distances, $r \gg r_0 = (2\pi K_0\chi)^{-1}$, from the region of small k, for which the term in the denominator proportional to k^3 can be disregarded. Thus, since $(\ln r)_{\mathbf{k}} = -2\pi/k^2$, the test charge potential behaves like a logarithm: $\Phi_Q(\mathbf{r}) = -(Q/2\pi\chi)\ln(r/C_1)$, $r \gg r_0$, where $C_1 \sim r_0$. In the inverse limit, i.e., at $r \ll r_0$, the potential is linear: $\Phi_Q(\mathbf{r}) \approx -QK_0 r$, $r \ll r_0$. Based on these properties, we use the following interpolation expression for the potential: $\Phi_Q(\mathbf{r}) \approx -(Q/2\pi\chi)\ln(1+r/r_0)$. This formula shows that the effective energy of a pair of size r is equal to $u(r) = U(r)$, where

$$U(r) = -\Phi_{Q=1}(r) = \frac{1}{2\pi\chi}\ln\left(1+\frac{r}{r_0}\right). \tag{137}$$

The scale r_0 is similar to the Debye screening radius of 2D interactions between topological charges. To demonstrate this fact, we consider for simplicity the case $\alpha = 0$. We obtain from (122) and (136) for the total charge located inside a circle of radius r centered on the test charge

$$Q_{\mathrm{t}}(r) = Q + \int_0^r 2\pi r'\,\mathrm{d}r'\rho_{\mathrm{TP}}(r')$$
$$= Q\int_0^\infty \mathrm{d}x\,\frac{x\exp(-x)}{\sqrt{x^2+(r/r_0)^2}} \approx \frac{Q}{\sqrt{1+(r/r_0)^2}}\,.$$

This formula shows that the test charge is *screened*, $Q_{\mathrm{t}} \approx 0$, at distances greater than r_0.

This conclusion is of importance for establishing the mechanism of the phase transition in the HBPL layer adjacent to the amphiphilic surface. The polarization of the small-pair gas results in the suppression of linear attraction between the vortices at large distances and its transformation into a logarithmic one. Thus, the phase transition associated with the dissociation of pairs has the same qualitative character as the BKT transition in the system with $D = 0$, i.e., with only contact interaction between molecules.

Comparing formula (137) with (113) and (115), we find the temperature of phase transition in the near-surface HBPL layer:

$$T_{\mathrm{BKT}} = \frac{1}{8\pi\chi}\,. \tag{138}$$

We obtain from this equation and from (124), (125), and (133) an implicit equation for T_{BKT}:

$$2\pi I_3 = 1\,,$$

or, in a more detailed form,

$$8\pi\int_0^\infty \mathrm{d}r\,\frac{r^3\exp(-K_0 r/T_{\mathrm{BKT}})}{(1+\alpha r)^{2\pi/T_{\mathrm{BKT}}}} = 1\,. \tag{139}$$

Formula (139) enables the results of model predictions for T_{BKT} to be compared with those of a numerical experiment, which is discussed below.

To avoid misunderstanding, we note that there is no disagreement between relations (123) and (138). Parameter χ in (138) is an intermediate quantity that arises in the process of calculations related to the case $D \neq 0$. The logarithmic dependence of the effective energy of interaction between large pairs (137) corresponds, according to Section 4.2.2, to the infinite value of physical susceptibility (123).

The weak field approximation, which requires $\langle\mathbf{d}\rangle \approx \alpha_{\mathrm{p}}\mathbf{E}$ and needs an additional substantiation, was used in the arguments presented here and in Section 4.2.2. To confirm that this approximation is realistic, we use Eqn (137) to find the average energy of interaction between the vortices at a temperature slightly less than T_{BKT}:

$$\langle U(r)\rangle = z_{\mathrm{p}}^{-1}\int_0^\infty \mathrm{d}r\,U(r)g_0(r) = T_{\mathrm{BKT}}\,\frac{1-4\tau}{-\tau(1-2\tau)}\,. \tag{140}$$

Here, $z_{\mathrm{p}} = \int_0^\infty \mathrm{d}r\,g_0(r)$, $g_0(r) = r\exp[-U(r)/T]$, and $\tau = (T - T_{\mathrm{BKT}})/T_{\mathrm{BKT}}$. It follows from (137), (138), and (140) that near the phase transition, at $|\tau| \ll 1$, the characteristic size of a pair close to dissociation is large, $r_{\mathrm{DP}} \sim r_0\exp[1/(4|\tau|)] \gg r_0$, and the topological 'electric' field is small, $\mathbf{E} = -\nabla U(r) \propto \exp[-1/(4|\tau|)]$. The smallness of the parameter $\exp[-1/(4|\tau|)] \ll 1$ underlies the above calculation. Indeed, the ratio of the characteristic topological 'electric' field ($\sim |\nabla U(r)|$) and the value of the field $\sim |\nabla u(r)|$ inside small-size pairs (see Section 4.2.2) is of the order of the specified small parameter. Thus, the weak-field approximation is applicable in the vicinity of the phase transition point.

The above analysis made it possible to establish the nature of the phase transition. This analysis was based on approximation (117), which, however, when verified, turned out to be quite accurate. Without resorting to the described approximation, we now provide a rigorous proof of the FPT existence in the surface liquid layer and compare its quantitative conclusions with the previous approximate calculation.

The Binder method was used for the numerical analysis of the critical behavior of the model, depending on the dipole–dipole interaction constant Λ [246]. The parameter $U_L = 1 - \langle\mathbf{s}^4\rangle/3/\langle\mathbf{s}^2\rangle^2$ ('Binder cumulant') was calculated as a function of temperature. Here, $\mathbf{s} = \mathbf{S}/N_{\mathrm{g}}$, $\mathbf{S} = \sum_{k=1}^{N_{\mathrm{g}}}\mathbf{s}_k$. According to one of the main theorems of statistical mechanics, statistical averaging $\langle\ldots\rangle$ over ensembles is equivalent to averaging over time in calculating molecular Langevin dynamics based on Eqn (134). The calculations used periodic boundary conditions and square meshes $L \times L$ with the number of independent nodes $N_{\mathrm{g}} = L^2$. According to [246], the point where the Binder cumulants for various sizes of the system L intersect determines the actual temperature of the phase transition, as shown in Fig. 18.

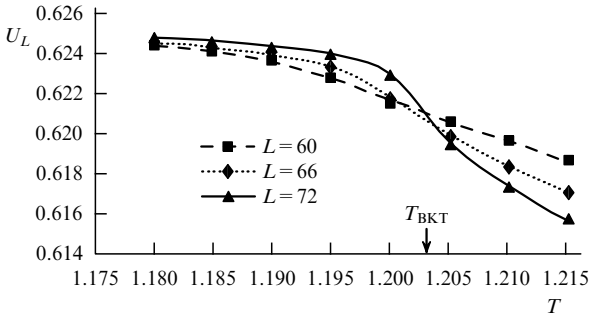

Figure 18. Explanation of the method applied to calculate the temperature of the ferroelectric phase transition T_{BKT} in molecular Langevin dynamics based on the Binder approach [246] and independent of approximations (117) and (118). The Binder parameter is calculated at $\Lambda = 0.2$. The calculation was carried out on a square surface divided into $L \times L$ identical cells. The values of L corresponding to each calculation are displayed. Temperature is measured in units of I.

In the absence of interaction, $K_0 = 0$ (or $\Lambda = 0$), and we find from Eqn (139) $T_{BKT} \approx 0.7$, a value that is fairly close to the results of Monte Carlo calculations: $T_{BKT} \approx 0.89$ [244] and $T_{BKT} \approx 0.86$ [245] obtained using square and triangular meshes, respectively. Our computer calculation yields in this limiting case

$$T_{BKT}(\Lambda = 0) = 0.85\,. \tag{141}$$

If Λ is large, which, as mentioned above, corresponds to typical HBPL, the transition temperature asymptotically approaches a constant value $T_{BKT}(\infty) \approx 1.4$. A similar result follows from Eqn (139): $T_{BKT}(\infty) \approx 1.3$. It should be noted that the arguments of [227, 228] based on the renormalization group analysis yield a significantly higher transition temperature: $T_c(\infty) = 2\pi$. This implies that in the renormalization group analysis it is rather difficult to take into account all the diagrams that are of significance for a description of screening. A similar conclusion follows from the results for the case $\Lambda = 0$. Indeed, presenting (115) in a dimensionless form, we get $T_{BKT} = \pi/2 \approx 1.57$. The renormalization group approach that takes into account the logarithmic interaction between pairs yields $T_{BKT} \approx 1.51$ [212]. Either value is very different, both from the above results obtained by the Monte Carlo method [244, 245] and from our result (141).

4.2.4 Interesting observation. An interesting conclusion may be drawn if the analytical approach developed in Sections 4.2.1–4.2.3 is applied to the formation of a quark–gluon plasma. We consider a gas of pairs of particles ('pi-mesons') with a linearly growing interaction energy $u(r) = \sigma r$ in three-dimensional space. If the 'pi-meson' size is sufficiently large, $r > a$, the formation of a new pair becomes energetically advantageous. Section 4.2.3 shows that this process is taken into account in our model: the number of particles is not specified in advance, but is found from the condition of minimum free energy. The mass of the newly formed pi-meson, $m \sim \sqrt{\hbar\sigma/c^3}$, and its size, $a \sim \sqrt{\hbar c/\sigma}$, are found from the energy balance $mc^2 \sim \sigma a$ and the uncertainty principle $a \sim \hbar/(mc)$. Carrying out an analytical calculation similar to that in Section 4.2.2, it may be concluded that, due to screening, we get instead of a linearly increasing interaction $u(r)$ an effective interaction of the form $U(r) = -[2\sigma/\kappa^2 r][1 - \exp(-\kappa r)]$ that contains a new size $1/\kappa = \sigma^2 a^3/(16\pi T^2)$ characterizing this screening. Thus, the polarization of the pion-nucleon gas leads to two effects: (1) a potential of quark ionization $I_0 = 2\sigma/\kappa$ emerges in the pi-meson that arises due to the emergence of correlations between nuclear matter particles; (2) the linear law of the interaction between colored charges is replaced at large distances between them ($r \gg 1/\kappa$) with the Coulomb law $U(r) = -(2\sigma/\kappa^2 r)$.

Similar to an ordinary plasma, there is no abrupt phase transition in this model to a state with free color charges. The dissociation degree of 'pions' is significant, $\sim \exp(-I_0/T) \sim 0.5$ at $T \sim mc^2 \sim 150$ MeV, which determines the characteristic temperature of quark–gluon plasma formation.

The arguments presented here are naturally not rigorous and, of course, may be a matter of a critical discussion.

4.3 Some results

The wettability properties of surfaces in contact with HBPL were quantitatively described above in the VMPL. The description of these properties in terms of the wetting angle was shown to be incomplete. A comprehensive description involves two parameters: α_0 and β_0 (in a more precise description, when polar groups are present on the surface, three parameters are required). Each surface at a certain temperature corresponds to a point on the (α_0, β_0) plane. The surfaces are divided into three types on the basis of wettability, these types occupying three nonoverlapping areas on the plane (α_0, β_0) (see Fig. 9).

The two-dimensional HBPL layer adjacent to the amphiphilic surface (region II in Fig. 9) is at low temperatures in the ferroelectric state. This state features a nonzero order parameter — the polarization vector, i.e., total dipole moment of molecules per unit surface area. As temperature increases in the layer, thermal fluctuations of the vortex-antivortex pair emerge, the interaction energy between which linearly grows as the distance between the vortices in the pairs increases. These excitations determine to a large extent the physical properties of the HBPL layer. As temperature grows, the surface density and sizes of pairs increase. The effect of screening of large pairs by a cloud of small pairs becomes significant. The linear dependence of the interaction energy of vortices in large pairs on the distance between them is replaced as a result with a logarithmic dependence. When a critical temperature is reached, whose value depends on the properties of the liquid and the surface, pairs are dissociated à la the BKT transition. The long-range order in the surface layer is destroyed as a result, and the layer becomes paraelectric. Thus, the BKT transition mechanism turns out to be universal and applicable to a much wider class of systems than was previously assumed.

Phenomenological relations (100) and (101) are presented in the most general form; therefore, they are applicable to any surface, including an amphiphilic one in the paraelectric state. The calculations presented in Sections 4.1 and 4.2 show that both the paraelectric state of the near-surface layer and the FPT according to the BKT scenario in this layer can exist. Consequently, region III in Fig. 9 directly corresponds to the indicated paraelectric state, while the BKT transition occurs on the OC line that separates regions II and III, when the parameters α_0 and β_0 change with temperature. On the other hand, when crossing the OA boundary, the polarization vector, which is an order parameter, changes in a continuous way. It clearly shows that the OA boundary must also

correspond to a second-order phase transition that occurs when the hydrophilic surface is heated. Molecular dipoles above the OA line are directed, on average, perpendicular to the surface. This automatically implies that the surface of the body maintains a large-scale continuous network of hydrogen bonds that breaks when heated, i.e., when the OA line is crossed. Most likely, it was this percolation transition that was observed in MD calculations in Refs [247–249] that studied the state of a hydrogen-bond network on weakly hydrophilic protein-like surfaces, which corresponds in VMPL to $s \ll 1$.

Fluctuation region III should actually have for these reasons a more complex nature than that presented in Sections 4.1 and 4.2. Two assumptions may be made here. The first is that fluctuation region III is subdivided in the case of a large surface into two subregions, which are separated by a boundary in the (α_0, β_0) plane: in one subregion, the fluctuating polarization vector is tangent to the surface, while in the other, it is perpendicular to it. According to the second assumption, both components of the fluctuating vector are simultaneously nonzero. This issue, which has not been studied yet, is an interesting problem. As for experiments [206], they only evidence that regions I and II exist.

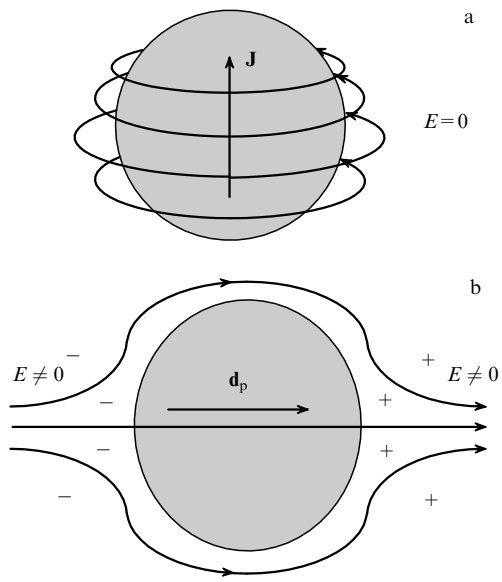

Figure 19. Polarization of liquid around a spherical hydrophobic body. (a) 'Force-free' and (b) 'force-based' polarization of liquid. In the former case, $\nabla \mathbf{s} = 0$, and the polarization charge of the liquid is zero. In the latter case, it is not zero. The meaning of the vectors $\mathbf{J}$ and $\mathbf{d}_\mathrm{p}$ is explained in the text.

5. Interaction between bodies immersed in polar liquid with hydrogen bonds

5.1 Key features of the interaction

We consider the case of a liquid that contains two systems of foreign charges. We have then $\rho_\mathrm{e}(\mathbf{r}) = \rho_1(\mathbf{r}) + \rho_2(\mathbf{r})$. The energy of interaction between them is given by the cross term in G_min in (50) taken at $\varepsilon_\infty = 1$ (calculations are carried out for a simplified form of free energy (47)):

$$G_\mathrm{int} = \int \mathrm{d}^3 r\, \mathrm{d}^3 r' \, \frac{\rho_1(\mathbf{r})\rho_2(\mathbf{r}')}{|\mathbf{r} - \mathbf{r}'|} \times \left[\frac{1}{\varepsilon_0} + \left(1 - \frac{1}{\varepsilon_0}\right) \exp\left(-\frac{|\mathbf{r} - \mathbf{r}'|}{R_\mathrm{d}}\right)\right]. \tag{142}$$

The interaction energy for a pair of point charges separated by distance R has the form that follows from Eqn (142),

$$G_\mathrm{int}(R) = \frac{1}{\varepsilon(R)} \frac{q_1 q_2}{R},$$

where we introduced a notation for the effective permittivity $\varepsilon(R)$ defined by the relation

$$\frac{1}{\varepsilon(R)} = \frac{1}{\varepsilon_0} + \left(1 - \frac{1}{\varepsilon_0}\right) \exp\left(-\frac{R}{R_\mathrm{d}}\right). \tag{143}$$

This dependence is consistent for the parameters $\varepsilon_0 \approx 88$ and those in Eqn (56) with MD calculations and with measurements [250–254]. It should be noted that, as can be seen from (43) and (44), Eqn (143) involves both spatial scales of the vector model, while the scale L_T is implicitly contained in ε_0.

The interaction between macroscopic bodies, however, is determined not only by the foreign charges (their definition is given at the end of Section 2.1.1) that are borne by these bodies. MD calculations show that uncharged bodies also polarize the liquid [24–27]. As shown in Section 4.1, this polarization arises spontaneously in the VMPL for amphiphilic surfaces if nonlinear terms $\sim s^4$ and of a higher order, which are absent in weak-field approximation (22), are taken into account in $V(s^2)$. The electric fields created by the polarization charges of the force configurations (Figs 10b and 19b) in linearized approximation (22) and (45) should be taken into account for this reason as additives to the external field $\mathbf{E}_\mathrm{e}$, as if the charges were located in vacuum rather than in liquid. This also follows from Eqn (7). Force-free polarizations can also be easily taken into account in the linearized VMPL equations. We conclude from the form of the polarization fields displayed in Figs 10 and 19, taking into account the next to last term in (47), that the addition to the HBPL free energy that comes from spontaneously emerging polarizations should be linear in the vectors $\mathbf{s}$ and $\operatorname{rot} \mathbf{s}$, and therefore it can be expressed as

$$G_\mathrm{int} = -P_0 \int \mathrm{d}^3 r \left\{\mathbf{E}_\mathrm{e}(\mathbf{r})\mathbf{s}(\mathbf{r}) + \mathbf{J}(\mathbf{r})\left[\nabla \times \mathbf{s}(\mathbf{r})\right]\right\}.$$

Integrating by parts, we obtain

$$G_\mathrm{int} = -P_0 \int \mathrm{d}^3 r\, \mathbf{E}^\mathrm{eff}(\mathbf{r})\mathbf{s}(\mathbf{r}).$$

Here,

$$\mathbf{E}^\mathrm{eff}(\mathbf{r}) = \mathbf{E}_\mathrm{e}(\mathbf{r}) + \left[\nabla \times \mathbf{J}(\mathbf{r})\right], \tag{144}$$

and an axial vector $\mathbf{J}(\mathbf{r})$ was introduced, which describes the force-free polarization of liquid by an immersed body with an amphiphilic surface (Figs 10a and 19a).

We assign number $a = 1, 2, \ldots, N_\mathrm{b}$ to the bodies. Their sizes are assumed to be sufficiently small, $\lesssim 2L_T \sim 3-4$ nm, which is most often true in applications to biology. We can consider then the bodies to be pointlike and set $\mathbf{J}(\mathbf{r}) = \sum_a \mathbf{J}^a \delta(\mathbf{r} - \mathbf{r}_a)$, where $\mathbf{r}_a$ is the radius vector of the ath body; $\mathbf{E}_\mathrm{e}(\mathbf{r}) = \sum_a \mathbf{E}_\mathrm{e}^a(\mathbf{r})$, where $\mathbf{E}_\mathrm{e}^a(\mathbf{r})$ is an electric field that would be created by the external and polarization charges of the ath particle located in the vacuum.

We calculate the polarization created by these bodies and the energy of their mutual interaction. We find to this end the minimum of initial formula (45) into which $\mathbf{E}^{\mathrm{eff}}(\mathbf{r})$ should be substituted instead of $\mathbf{E}_{\mathrm{e}}(\mathbf{r})$. We present the Fourier component of the polarization of the liquid in the form $\mathbf{s}_{\mathbf{k}} = \mathbf{f}_{\mathbf{k}} + \boldsymbol{\xi}_{\mathbf{k}}$, where $\mathbf{f}_{\mathbf{k}}$ is the average value of the polarization vector and $\boldsymbol{\xi}_{\mathbf{k}}$ is the fluctuation or deviation from this average. If we choose

$$f_{\mathbf{k}\alpha} = \frac{1}{P_0}\sum_{\beta}\left[F^{-1}(\mathbf{k})\right]_{\alpha\beta} E^{\mathrm{eff}}_{\mathbf{k}\beta} = \frac{1}{P_0}\left[\frac{1}{D}\,E_{\mathrm{e}\mathbf{k}\alpha} + \frac{\mathrm{i}}{d}\,(\mathbf{k}\times\mathbf{J}_{\mathbf{k}})_{\alpha}\right]$$
$$= \frac{1}{P_0\sqrt{V_1}}\sum_{a}\left[\frac{1}{D}\,E^{a}_{\mathrm{e}\mathbf{k}\alpha} + \frac{\mathrm{i}}{d}\,(\mathbf{k}\times\mathbf{J}^{a})_{\alpha}\right]\exp\left(-\mathrm{i}\mathbf{k}\mathbf{r}_a\right), \quad (145)$$

where $D = d + 4\pi$, $d = Ck^2 + A$, the terms linear in fluctuations drop out, and a nonnegative term quadratic in these quantities remains. We ignore the latter, given the conditions of the minimum free energy in the mean field approximation, to obtain

$$G = -\frac{1}{2}\sum_{\mathbf{k}}\frac{1}{d}\left(|\mathbf{E}^{\mathrm{eff}}_{\mathbf{k}}|^2 - \frac{4\pi|\hat{\mathbf{k}}\mathbf{E}^{\mathrm{eff}}_{\mathbf{k}}|^2}{D}\right)$$
$$= \sum_{\mathbf{k}}\left(\frac{|\mathbf{E}_{\mathrm{e}\mathbf{k}}|^2}{8\pi\varepsilon(k)} - \frac{1}{2d}\,|\mathbf{k}\times\mathbf{J}_{\mathbf{k}}|^2\right) = \sum_{a} G_a + \sum_{a<b} u_{ab}\,. \quad (146)$$

Here, $G_a = G^{\mathrm{e}}_a + G^{\mathrm{II}}_a$, G^{e}_a is the energy of the ath body in the liquid,

$$G^{\mathrm{e}}_a = \sum_{\mathbf{k}}\frac{|\mathbf{E}^{a}_{\mathrm{e}\mathbf{k}}|^2}{8\pi\varepsilon(k)}\,,$$

and G^{II}_a is the energy of the liquid in the case of its force-free polarization by this body (see Section 4.1), which yields in the point body approximation adopted here an expression that diverges at large k:

$$-\frac{1}{2V_1 d}\sum_{\mathbf{k}}|\mathbf{k}\times\mathbf{J}^{a}|^2\,.$$

It is clear that this divergence should be cut off for wave vectors of the order of the inverse body size.

Furthermore, u_{ab} in (146) is the sought interaction energy of the two bodies separated by the distance $\mathbf{R} = \mathbf{r}_a - \mathbf{r}_b$:

$$u_{ab}(\mathbf{R}) = u^{\mathrm{e}}_{ab} + u^{J}_{ab}\,, \qquad a \neq b\,, \quad (147)$$

where

$$u^{\mathrm{e}}_{ab} = \sum_{\mathbf{k}}\frac{1}{4\pi\varepsilon(k)}\,\mathbf{E}^{a}_{\mathrm{e}\mathbf{k}}\mathbf{E}^{b}_{\mathrm{e},-\mathbf{k}}\exp\left(-\mathrm{i}\mathbf{k}\mathbf{R}\right),$$

$$u^{J}_{ab} = -\sum_{\mathbf{k}}\frac{1}{V_1 d}(\mathbf{k}\times\mathbf{J}^{a})(\mathbf{k}\times\mathbf{J}^{b})\exp\left(-\mathrm{i}\mathbf{k}\mathbf{R}\right).$$

We conclude from (145) that the polarization may be represented in the coordinate representation as

$$\mathbf{s}(\mathbf{r}) = \sum_{a}\left[\mathbf{s}^{\mathrm{e}}_a(\mathbf{r}) + \mathbf{s}^{J}_a(\mathbf{r})\right],$$
$$\mathbf{s}^{\mathrm{e}}_a(\mathbf{r}) = \frac{1}{4\pi CP_0}\int\frac{\exp\left(-|\mathbf{r}-\mathbf{r}'|/R_{\mathrm{d}}\right)}{|\mathbf{r}-\mathbf{r}'|}\,\mathbf{E}^{a}_{\mathrm{e}}(\mathbf{r}')\,\mathrm{d}^3r'\,, \quad (148)$$
$$\mathbf{s}^{J}_a(\mathbf{r}) = \frac{1}{4\pi CP_0}\left[\mathbf{J}^{a}\times\nabla_{\mathbf{r}}\frac{\exp\left(-R_a/L_T\right)}{R_a}\right],$$

where $\mathbf{R}_a = \mathbf{r} - \mathbf{r}_a$. We introduce spherical coordinates (R_a, θ, φ) whose origin is on the particle and the z axis is directed along the vector $\mathbf{J}^a$. Only the azimuthal component of the vector $\mathbf{s}^{J}_a(\mathbf{r})$ is different from zero, which at $R_a \ll L_T$ is equal to $s^{a}_{\varphi} = -J^{a}\sin\theta/(4\pi CP_0R_a^2)$. According to Fig. 19a, we find from here for a spherical body of radius R_0 that $J = 4\pi CP_0R_0^2s_0$, where s_0 is the polarization value at the equator; this coincides rather accurately with the polarization for a cylindrical surface with radius R_0 (see Section 4.1).

We now take into account the polarization charges created by amphiphilic bodies in a liquid (Figs 10b and 19b). According to the discussion above, these charges are equivalent to foreign ones, i.e., their field can be included in the $\mathbf{E}^{a}_{\mathrm{e}}(\mathbf{r})$ field created by the foreign charges borne by the ath particle. The dipole moment created by polarization charges is represented by the following integral taken over the volume of liquid:

$$\mathbf{d}_{\mathrm{p}} = \int \mathrm{d}^3r\,\rho_{\mathrm{p}}(\mathbf{r})\mathbf{r} = \int \mathrm{d}^3r\,(-\nabla P_0\mathbf{s})\mathbf{r} = P_0\int \mathrm{d}^3r\,\mathbf{s}(\mathbf{r})\,. \quad (149)$$

Integration by parts was carried out here, and it was taken into account that the polarization at the amphiphilic body surface is directed along this surface.

To be specific, we consider a cylinder of height H_0 and radius R_0 such that

$$L_T \ll R_0 \ll H_0\,. \quad (150)$$

The main contribution to integral (149) comes from the large lateral surface, which, given the relation $R_0 \gg L_T$, may be considered flat (we thereby abandon here the approximation of point bodies). The polarization vector has the form

$$\mathbf{s} \approx s_0\exp\left(-\frac{\rho - R_0}{L_T}\right)\mathbf{I}\,.$$

Here, ρ is the distance from the observation point $\mathbf{r}$ to the cylinder axis and $\mathbf{I}$ is the unit vector directed along the cylinder axis from the negative polarization charge to the positive one. We obtain from here and Eqn (149) $\mathbf{d}_{\mathrm{p}} \approx q_{\mathrm{p}}H_0\mathbf{I}$, where q_{p} is the positive polarization charge

$$q_{\mathrm{p}} = 2\pi R_0L_TP_0s_0\,, \quad (151)$$

which is primarily concentrated at the edges of the upper cylinder end (consequently, the charge $-q_{\mathrm{p}}$ is located at the lower end edges). Indeed, the polarization vector, like the velocity of a liquid in a laminar flow, smoothly bends in this region around the front end, which is almost rectilinear at $R_0 \gg L_T$. Its value decreases in an approximately exponential way as the distance from the edge line increases at a characteristic length of $\sim L_T$, i.e., polarization is close here to force-free. The term containing the electric field may be disregarded in this case in Eqn (40). The polarization charge density is $\rho_{\mathrm{p}} = -P_0\nabla\mathbf{s} \sim P_0s_0/L_T$, and the charge itself is $q_{\mathrm{p}} \sim \rho_{\mathrm{p}}L_T^2 2\pi R_0 \sim 2\pi L_TR_0P_0s_0$, thus confirming result (151).

If $R_0 \ll L_T$, only one characteristic scale remains in the problem of finding q_{p}: R_0 itself; therefore, we can retain only the first term on the left-hand side of Eqn (40). Hence, $\nabla\mathbf{s} \sim s_0/R_0$, $\rho_{\mathrm{p}} \sim P_0s_0/R_0$, and $q_{\mathrm{p}} \sim C_0\rho_{\mathrm{p}}R_0^3 \sim C_0R_0^2P_0s_0$, where $C_0 \sim 2\pi$ is a constant, which is estimated from a comparison with the case $R_0 \gg L_T$ at the boundary of the region where these results are applicable, $R_0 \sim L_T$. The 'matching' of these two limiting cases yields an interpolative

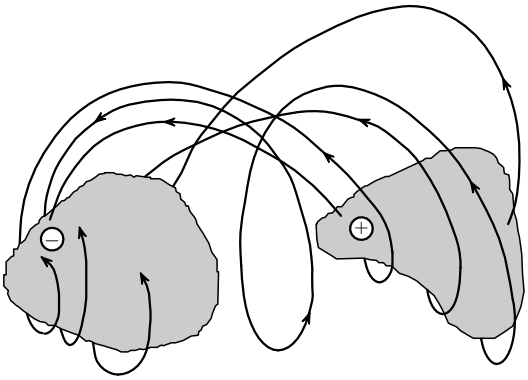

Figure 20. Polarization of a liquid near a pair of amphiphilic bodies with foreign charges on the surfaces.

expression for the case $R_\mathrm{d} \ll R_0 \ll H_0$ that is more general compared to (150):

$$q_\mathrm{p} = \frac{2\pi P_0 s_0 R_0^2 L_T}{\sqrt{R_0^2 + L_T^2}} \,.$$

We obtain in a similar way for a sphere of radius $R_0 \gg R_\mathrm{d}$

$$\mathbf{d}_\mathrm{p} \approx \frac{8\pi P_0 s_0 R_0^3 L_T}{3\sqrt{R_0^2 + L_T^2}}\,\mathbf{I}\,.$$

So, at values $R_0 = 0.5$ nm and $s_0 = 0.3$ typical of protein bodies these quantities are $d_\mathrm{p} = 10^{-17}$ (in the CGS units) and $q_\mathrm{p} \sim d_\mathrm{p}/(2R_0) \sim 0.3e$, respectively, where e is the elementary charge. The energy of the electric field G_a^e created by these charges is given by formula (142) divided by 2, in which $\rho_1(\mathbf{r}) = \rho_2(\mathbf{r}) = \rho_\mathrm{p}(\mathbf{r})$ should be put, yielding for such spheres an estimate $G_a^\mathrm{e} \sim 0.5 \times 10^{-14}$ erg $= 50$ K $\ll T$. Thus, the electrostatic energy of force-based polarizations can be ignored for the most common biological bodies.

The polarization of the liquid created by the ath body at a distance $R_a \gg \max(R_\mathrm{d}, H_\mathrm{max})$ from it (here, H_max means the largest dimension of the body) has the form

$$\mathbf{s}_a(\mathbf{r}) = \mathbf{s}_a^\mathrm{e}(\mathbf{r}) + \mathbf{s}_a^J(\mathbf{r}) \approx \frac{\varepsilon_0 - 1}{4\pi\varepsilon_0 P_0}\left[q_a \frac{\hat{\mathbf{R}}_a}{R_a^2} + \frac{3\hat{\mathbf{R}}_a(\mathbf{d}^a\hat{\mathbf{R}}_a) - \mathbf{d}^a}{R_a^3}\right] - \frac{\mathbf{J}^a \times \hat{\mathbf{R}}_a}{4\pi C P_0 R_a^2}\left(1 + \frac{R_a}{L_T}\right)\exp\left(-\frac{R_a}{L_T}\right). \qquad (152)$$

Here, $\hat{\mathbf{R}}_a = \mathbf{R}_a/R_a$, and $\mathbf{d}^a = \mathbf{d}_\mathrm{e}^a + \mathbf{d}_\mathrm{p}^a$ is the dipole moment of the ath body, which is the sum of the total dipole moment $\mathbf{d}_\mathrm{e}^a$ of the foreign charges and polar groups located on it, as well as the dipole moment of polarization charges $\mathbf{d}_\mathrm{p}^a$. An example of the polarization pattern of water created by two bodies is displayed in Fig. 20. Suchlike effects observed in MD calculations [28] are called the 'dipole bridge between biomolecules'. In addition, the vortex structures of the polarization vector were observed in the same calculations, which are associated with the last term in (152).

We now abandon the requirement $R \gg H_\mathrm{max}$. The solution is given in the case of force-based z polarization, as in Fig. 10b, by the formula $\mathbf{s}_a^\mathrm{e}(\mathbf{r})$ from (148), where $\mathbf{E}_\mathrm{e}^a$ is equal to the sum of the fields of foreign charges and the polar groups located on the body and two point polarization charges, q_p and $-q_\mathrm{p}$ (however, as shown in Section 4.1.3, bodies with z polarization almost never occur).

We now calculate the force-free φ-polarization for a thin ($R_0 \ll H_0$) cylinder at an arbitrary point. To do so, due to the additivity of the fields in approximation (22) considered here, it is sufficient to sum up the formula for $\mathbf{s}_a^J(\mathbf{r})$ from (148) over $\mathbf{r}_a$ along the cylinder axis, yielding

$$s_\varphi^J(\rho, z) = -\frac{s_0 L_T}{2K_1(R_0/L_T)}\frac{\partial}{\partial\rho}\int_{-H_0/2}^{H_0/2} \mathrm{d}z' \frac{\exp(-R_a/L_T)}{R_a}\,,$$

where $R_a = \sqrt{\rho^2 + (z - z')^2}$, $z = \mathbf{rI}$ and the radius vector $\mathbf{r}$ originates from the geometric center of the cylinder, and K_1 is the MacDonald function.

If the distance between the bodies is $R \gg \max(R_\mathrm{d}, H_\mathrm{max})$, we obtain for the energy of interaction between them, introducing the notation $\hat{\mathbf{R}} = \mathbf{R}/R$,

$$u_{ab}^\mathrm{e} \approx \frac{1}{\varepsilon_0}\bar{u}_{ab}^\mathrm{e}\,, \qquad (153)$$

$$\bar{u}_{ab}^\mathrm{e} = \frac{q_a q_b}{R} - q_a\frac{\mathbf{d}^b\hat{\mathbf{R}}}{R^2} + q_b\frac{\mathbf{d}^a\hat{\mathbf{R}}}{R^2} + \frac{\mathbf{d}^a\mathbf{d}^b - 3(\mathbf{d}^a\hat{\mathbf{R}})(\mathbf{d}^b\hat{\mathbf{R}})}{R^3}\,,$$

$$u_{ab}^J = \frac{1}{4\pi C}\,\bar{u}_{ab}^J\,, \qquad (154)$$

$$\bar{u}_{ab}^J = \left[\frac{\mathbf{J}^a\mathbf{J}^b}{L_T^2 R} + \frac{3(\mathbf{J}^a\hat{\mathbf{R}})(\mathbf{J}^b\hat{\mathbf{R}}) - \mathbf{J}^a\mathbf{J}^b}{R^3}\right]\exp\left(-\frac{R}{L_T}\right).$$

We conclude from Eqns (153) and (154) that the interaction between two amphiphilic bodies not bearing charges or polar groups is in the case of force-based polarization a long range one: $u(R) \propto 1/R^3$. This interaction in the case of force-free polarization extends to a distance $\sim L_T$: $u(R) \propto \exp(-R/L_T)$. The last formula is not a surprise since, as shown in Section 3.3, this dimension is an analog of the Debye radius in plasma physics. Equations (153) and (154) also show that, due to the emergence of the polarization of liquid created by neutral bodies, the interaction between these bodies becomes a long-range one; moreover, it proves to be rather strong and dependent on their orientation in space. This phenomenon may be a basis for a self-assembly mechanism in biological objects.

We discussed above interactions at distances that are larger than the dimensions of the bodies. A detailed analysis is needed for large bodies immersed in liquid. We consider as an example two thin parallel cylinders with the same radii R_0 and heights $H_0 \gg R_0$ located at a distance $R_0 \ll L \ll H_0$ from each other. The superposition principle $\mathbf{s}(\mathbf{r}) \approx \mathbf{s}_1(\mathbf{r}) + \mathbf{s}_2(\mathbf{r})$ holds at distances from both cylinders that exceed their radius. The vectors $\mathbf{s}_i(\mathbf{r}) = q_i s(r_i)\hat{\boldsymbol{\varphi}}_i$ describe the φ-polarizations created by each single cylinder (Fig. 10a). The dependence $s(r_i)$ is presented in (105); the 'topological charges' $q_{1,2} = \pm 1$ set the direction of polarization vector rotation around the axis of the corresponding cylinder, r_i are the distances from the observation point $\mathbf{r}$ to the axis of the corresponding cylinder, $\varphi_{1,2}$ are the azimuthal angles measured with respect to the axes of these cylinders (see Section 4.2), and $\hat{\boldsymbol{\varphi}}_i$ are the unit vectors directed along the gradients of these angles. A calculation using Eqn (47) yields a formula for the energy of interaction between the cylinders with φ-polarization:

$$u \approx 20\pi q_1 q_2 P_0^2 C H_0 s_0^2 \ln\left(\frac{L_T}{R_0}\right)\exp\left(-\frac{L}{L_T}\right)\frac{R_0^2}{L^2}\,.$$

Thus, if $q_1 q_2 > 0$, the cylinders repel each other, while if $q_1 q_2 < 0$, they attract each other.

We obtain in a similar way two parallel cylinders with z-polarization interacting according to the law

$$u \approx \frac{2\pi C P_0^2 \lambda H_0 K_0(L/L_T)}{\ln(L_T/R_0)} .$$

Here, $\lambda = 1$ and $\lambda = -1$ for parallel and antiparallel polarizations, respectively, and K_0 is the MacDonald function.

5.2 Estimation of the parameter in the expression for free energy that characterizes interaction of water molecules with the surface

We now estimate the parameter β_0 in formula (101) for the surface free energy.

Water molecules located on the surface of the body interact with this surface both by means of their hydrogen bonds, which determine the parameter α_0, and in an electrostatic way, due to the polarization of the body molecules by the electric field created by the static dipole moment $\mathbf{d}_0$. Given the geometry of the water molecule, we conclude that its typical distance to the surface is $h \sim d_{\mathrm{H_2O}}/2 \sim 0.15$ nm. It follows from (143) that the effective dielectric constant at such distances is $\varepsilon(R) \sim 1.5-2$. The relatively small dielectric constant is due to the smallness of h compared to the size of superdomains. The energy u of interaction between a point dipole and a body with a typical dielectric constant $\varepsilon_{\mathrm{b}} \sim 5-7$ may be calculated using the image method [1, 66]:

$$u = -\frac{\left[\varepsilon_{\mathrm{b}} - \varepsilon(R)\right] d_0^2}{\varepsilon(R)\left[\varepsilon_{\mathrm{b}} + \varepsilon(R)\right](2h)^3} \left(s_{\parallel}^2 + 3s_{\perp}^2\right) . \tag{155}$$

The term $s_{\parallel}^2$ here is of no interest, since the contribution from hydrogen bonds, comparable in magnitude to (155), and the alignment of dipoles along the surface due to these bonds are not taken into account [24–27]. It should simply be discarded for this reason. The number of water molecules per unit surface area is of the order of $n_0 d_{\mathrm{H_2O}}$. A comparison of the surface energy density $u n_0 d_{\mathrm{H_2O}}$ and (101) at room temperature yields the estimate $\beta_0 \sim 3$. According to Fig. 9, for hydrophilic bodies, $\beta_0 > \nu \approx 3.6$, which does not disagree with the estimate obtained above.

5.3 Interaction between two flat parallel surfaces

5.3.1 Measurement data and theoretical models. The forces that operate between hydrated objects of mesoscopic sizes play an important role in various chemical, physicochemical, and biological processes, nanoscale assembly mechanisms, etc. The interaction between particles in ionic solutions is described by the theory developed by Deryagin, Landau, Fairway, and Overbeek (DLFO) [255, 256]. We now consider the interaction between flat parallel surfaces separated by a layer of pure water with a thickness

$$0.3 \lesssim L \lesssim 3 \text{ nm} . \tag{156}$$

'Pure' water means here a water with a sufficiently low concentration n_{I} of dissolved ions ($n_{\mathrm{I}} \lesssim 0.02M$) (see below).

According to [257–259], there are at least three different modes of interaction between hydrophobic flat surfaces, which corresponds to long-range attraction. Electrostatic forces between oppositely charged sections on surfaces immersed in water prevail at large distances, $L \gtrsim 10$ nm. A significant contribution to the attraction is made at intermediate distances, $3 \lesssim L \lesssim 10$ nm, by the van der Waals interaction. It is characterized by a large value of the Hamaker constant, which is associated with proton jumps between neighboring water molecules. In addition, other interaction mechanisms that depend on the properties of the surfaces are also significant. Such interactions include [260–264]:

(1) steric effects: wave-like vibrations of the bilayer, protrusion-induced interaction that arises due to the emergence of mutually contacting protrusions on membrane surfaces;

(2) interaction between bilayers (in the case of electrolytes) [264];

(3) capillary forces that arise as a result of the spontaneous emergence of bridges consisting of submicroscopic bubbles.

These diverse mechanisms of interaction between bodies in a polar liquid, which are manifested at $L \gtrsim 3$ nm, and the ultra-long-range interaction associated with nonequilibrium (see Section 5.3.6) have no relation whatsoever to the range of distances between the flat surfaces under consideration (156). Numerous experiments show that all the mechanisms listed above are insignificant at such distances, and the interaction prevails whose character seems to be universal and only depends on the wettability of surfaces. Such interaction is referred to as the non-DLFO mechanism. An unambiguous explanation of its nature is lacking in the literature [257].

The goal of this section is to provide a theoretical analysis of region (156) on the basis of VMPL. We assume, following the results of Section 3.5, that the microscopic properties of a layer of the liquid sandwiched between surfaces are virtually the same as those of bulk water.

The so-called disjoint force, which is short-range but strong, operates between two hydrophilic surfaces S_Γ in pure water at distances of (156) between them. It is described by an empirical formula,

$$F = -\frac{\mathrm{d}G(L)}{\mathrm{d}L} = S_\Gamma p_{\mathrm{exp}} \exp\left(-\frac{L}{\lambda}\right) , \tag{157}$$

where $p_{\mathrm{exp}} \sim 5 \times (10^9 - 10^{10})$ din cm^{-2}, $\lambda \sim 0.2$ nm [257, 265–271], and $G(L)$ is the free Gibbs energy of the system. This repulsion, whose nature is electrostatic, is well explained in a number of phenomenological models [50, 51, 53, 257, 272].

Measurements [273–280] show that two hydrophobic surfaces attract each other with the force

$$F = -S_\Gamma p'_{\mathrm{exp}} \exp\left(-\frac{L}{\lambda'}\right) , \tag{158}$$

where the pre-exponential factor is about the same as in the case of hydrophilic surfaces, $p'_{\mathrm{exp}} \sim p_{\mathrm{exp}}$, but the quantity in the exponent is quite different: $\lambda' \sim 1.2$ nm.

5.3.2 Interaction between amphiphilic flat parallel surfaces. We consider two amphiphilic surfaces located at a distance L from each other. The polarization of liquid is in this case parallel to the surfaces, $\mathbf{s} = [s(z), 0, 0]$, and only depends on the coordinate z; therefore, there is no electric field: $\mathbf{E}_{\mathrm{p}} = \mathbf{E}_{\mathrm{e}} = 0$.

We assume first that there is a simplified linearized version of boundary condition (101). We obtain from this boundary condition and Eqns (47) and (98) a formula for the free energy

of the liquid:

$$G[s(z)] = -\frac{1}{2}\, S_\Gamma \sqrt{C} P_0^2 \alpha_0 (s_+^2 + s_-^2) + S_\Gamma P_0^2 \int_{-L/2}^{L/2} \mathrm{d}z \left[\frac{C}{2}\left(\frac{\mathrm{d}s}{\mathrm{d}z}\right)^2 + V(s^2)\right], \qquad (159)$$

where $s_\pm \equiv s(\pm L/2)$ is the water molecule polarization on the surfaces. The minimum free energy corresponds to $\delta G = 0$, which gives the boundary conditions

$$\left(\alpha_0 s - \sqrt{C} s'\right)_{z=L/2} = 0\,, \qquad \left(\alpha_0 s + \sqrt{C} s'\right)_{z=-L/2} = 0$$

and the Euler equation for polarization in the volume of liquid

$$-C s''(z) + 2V'(s^2) s = 0\,.$$

Taking this equation into account and integrating by parts in (159), we derive a formula for the equilibrium interaction energy:

$$G_{\min} = S_\Gamma P_0^2 \int_{-L/2}^{L/2} \mathrm{d}z \left[V(s^2) - s^2 V'(s^2)\right]. \qquad (160)$$

This equation shows that the interaction completely vanishes, $G = 0$, if the quadratic approximation for the equation of state $V(s^2) = As^2/2$ is used in the description of the liquid.

Therefore, the quadratic approximation is not applicable to the analysis of interaction between bodies. This is not a surprise, since, for the interaction between surfaces belonging to regions I and II (see Fig. 9) to occur, a spontaneous polarization of the near-surface liquid layers needs to emerge. As shown in Sections 4.1.2 and 4.1.3, this is not possible without nonlinearity. Thus, a nonzero interaction between surfaces only emerges if at least one more term is retained in Taylor's expansion $V(s^2)$ (30), yielding

$$G(L) \approx -S_\Gamma P_0^2 B \int_{-L/2}^{L/2} \mathrm{d}z\, s^4\,, \qquad (161)$$

which is expressed in its final form through elliptic integrals and looks rather cumbersome. It can be seen that this energy is determined by the constant B, i.e., the orientational entropy of liquid. We find from here for sufficiently large distances between surfaces, $\exp(-L/L_T) \ll 1$, the interaction force:

$$F(L) = -S_\Gamma 6 P_0^2 B s_0^4 \frac{L}{L_T} \exp\left(-\frac{L}{L_T}\right). \qquad (162)$$

Here, $s_0 = \sqrt{\sqrt{A}(\alpha_0 - \sqrt{A})/B}$ is the polarization of the liquid on an isolated surface (see Section 4.1.2) that corresponds to the limit $L \to \infty$. The main contribution to integral (161) comes at $L \gg L_T$ from the region where $s \ll 1$; therefore,

$$s \approx s_1(z) + s_2(z) = s_0 \exp\left(-\frac{z + L/2}{L_T}\right) + s_0 \exp\left(\frac{z - L/2}{L_T}\right),$$

and the contribution from the cross term $6 s_1^2 s_2^2$ in the formula for s^4 prevails.

Comparing (162) with (158), we obtain, under the assumption $s_0 \sim 1$, the above estimate $B \sim 0.15 - 1.5$. Thus, we can speak of a reasonable agreement between this VMPL prediction and experiments.

It should be noted that attractive force (162) is the result of the joint action described by the Oseen, entropy, and dipole–dipole contributions to free energy. These contributions are comparable in magnitude. This implies that the full interaction is a combined action of molecular forces naturally described by two characteristic distance scales: R_d and L_T. It was assumed in the calculation that the molecules of liquid on the surfaces are polarized in parallel and in the same direction with respect not only to the surfaces, but also to each other. The free energy of interaction between the plates is in this case negative, which corresponds to the ground state of the system. If the polarizations are oriented in the direction opposite to that of the surface polarization, this energy is positive, and therefore this state of the liquid between the surfaces is metastable. It should be noted that dependence (162) can become more complicated if second-order phase transitions described in Section 4 occur in near-surface hydrated water layers.

Formula (162) was derived under the assumption of weak polarization (22). We now consider the opposite case of a 'hard' boundary condition on an amphiphilic surface:

$$s|_\Gamma = s_0\,. \qquad (163)$$

The formula for the free energy of a liquid between two hydrophobic surfaces takes in this case the form

$$G = G_\mathrm{b} = S_\Gamma P_0^2 \int_{-L/2}^{L/2} \mathrm{d}z \left[\frac{C}{2}\left(\frac{\mathrm{d}s}{\mathrm{d}z}\right)^2 + V(s^2)\right], \qquad (164)$$

where the contribution from the bulk liquid alone is retained, while the contribution associated with the surface is ignored (99). The point is that condition (163) is by its nature fundamentally nonlinear: no matter what occurs in the volume, it always holds on surfaces. In other words, the surface energy does not change for any dependence $s(z)$ that satisfies condition (163): $G_\mathrm{s}[s(z)] = \mathrm{const}$. Indeed, since the free energy is minimal in equilibrium, condition (163) is obtained in the limiting case:

$$R_0 \to \infty\,, \qquad (165)$$

where parameter R_0 is defined in (109).

We consider an isolated flat surface immersed in a liquid and located at $z = 0$. To prove formula (164), we take G_s in the form of the last term in Eqn (109). We obtain from here and from Eqns (47) and (98) a formula for the energy of the liquid:

$$G = S_\Gamma P_0^2 \int_0^\infty \mathrm{d}z \left[\frac{C}{2}\left(\frac{\mathrm{d}s}{\mathrm{d}z}\right)^2 + \frac{A}{2}\, s^2\right] + G_\mathrm{s}\,,$$

where

$$G_\mathrm{s} = S_\Gamma R_0 \left[s^2(z=0) - s_0^2\right]^2. \qquad (166)$$

We find the lowest value G for the trial function

$$s(z) = s_1 \exp\left(-\frac{z}{L_T}\right).$$

It follows from here and Eqn (166), with Eqn (43) taken into account,

$$\frac{G(s_1)}{S_\Gamma} = R_0 (s_1^2 - s_0^2)^2 + \frac{1}{2}\, P_0^2 \sqrt{CA}\, s_1^2\,. \qquad (167)$$

Expression (167) has the smallest value at

$$s_1^2 = s_0^2 - \frac{P_0^2}{4R_0}\sqrt{CA}\,.$$

Using this value of parameter s_1 in (167) for the surface contribution to the free energy, we arrive at the expression

$$G_{\rm s} = S_\Gamma \frac{P_0^4 CA}{16R_0}\,.$$

In the limiting case (165), which corresponds to the 'rigid' boundary condition (163), $G_{\rm s} \to 0$, which had to be proved. The statement regarding the nonlinear character of condition (163) follows from the form of the dependence of (167) on s_1: this dependence contains terms with s_1^4.

Variation of Eqn (164) with respect to $s(z)$ yields the Euler equation, a solution of which for the polarization of liquid $s(z)$ is presented by an implicit equation,

$$z = \sqrt{\frac{C}{2}}\int_{s_C}^{s(z)} \frac{{\rm d}s'}{\sqrt{V(s'^2) - V_C}}\,.$$

Here, $V_C = V(s_C^2)$, and $s_C = s(0)$ is the polarization in the middle liquid layer, as shown in Fig. 21. The value of s_C may be found from the equation

$$L = \sqrt{2C}\int_{s_C}^{s_0} \frac{{\rm d}s}{\sqrt{V(s^2) - V_C}}\,. \qquad (168)$$

The interaction energy takes the form

$$G = S_\Gamma P_0^2\sqrt{2C}\int_{s_C}^{s_0} {\rm d}s\,\frac{2V(s^2) - V_C}{\sqrt{V(s^2) - V_C}} = S_\Gamma P_0^2\left[J(L) + V_C L\right],$$

$$J(L) = 2\sqrt{2C}\int_{s_C}^{s_0} {\rm d}s\,\sqrt{V(s^2) - V_C}\,.$$

Differentiating $J(L)$, we obtain with Eqn (168) taken into account

$$\frac{{\rm d}J}{{\rm d}L} = -L\,\frac{{\rm d}V_C}{{\rm d}L}\,, \qquad F(L) = -\frac{{\rm d}G}{{\rm d}L} = -S_\Gamma P_0^2 V_C\,.$$

If $\exp(-L/L_T) \ll 1$, the main, logarithmically large contribution to integral (168) comes from the spatial region wherein $s \ll 1$ and $V(s^2) \approx As^2/2$, yielding

$$L \approx 2L_T \ln\left(\frac{\beta s_0}{s_C}\right), \qquad \beta \sim 1\,,$$

$$V_C \approx \frac{1}{2}A\beta^2 s_0^2 \exp\left(-\frac{L}{L_T}\right),$$

$$F(L) \approx -\frac{1}{2}S_\Gamma P_0^2 A\beta^2 s_0^2 \exp\left(-\frac{L}{L_T}\right).$$

The pre-exponential factor in the last formula agrees with measurements [273–280]; the same is true for the exponential quantity. We used here a quadratic approximation for $V(s^2)$ (the first term in (30)). This does not imply, however, that the interaction between the surfaces may be obtained in the linear response theory, since the boundary condition $s|_\Gamma = s_0$ is essentially nonlinear. The point is that the quadratic approximation holds in the spatial region that makes the main contribution to the interaction strength being sought.

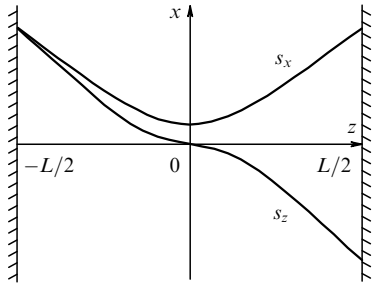

Figure 21. Nonzero components of water molecule polarization between two interacting flat surfaces. Plots of s_z and s_x are displayed for hydrophilic and hydrophobic surfaces, respectively.

5.3.3 Interaction between hydrophilic flat surfaces. The practical interest in this interaction is associated with biological membranes that primarily consist of a thin layer of amphipathic phospholipids which spontaneously orient themselves in such a way that their hydrophobic 'tail' regions prove to be hidden from the ambient polar liquid, while the hydrophilic polar groups make contact with water [281], as is shown in Fig. 22. Owing to the joint action of the effects described by the electric field $E_{\rm e}^\Gamma$ and the term with β_0 in Eqns (100) and (101), the molecular water dipoles are oriented in the direction perpendicular to the membrane planes.

Thus, we consider two membranes separated by a water-filled layer L in width. The polarization vector now has the form $\mathbf{s} = [0, 0, s(z)]$, and the corresponding boundary conditions are expressed as $s(-L/2) = s_0$ and $s(L/2) = -s_0$ (see Fig. 21).

Using the method described in [264], it is easy to consider the general case when free charges are present on membrane surfaces and in the volume, which leads to the formation of double layers. However, the contribution of these charges to the interaction between the surfaces is negligible at distances of (156) between the surfaces; therefore, even in this general case, we can put $\mathbf{E}_{\rm e} = 0$. Taking into account the relation $\mathbf{E}_{\rm p} = -4\pi\mathbf{P} = -4\pi P_0\mathbf{s}$, we obtain the following expression for free energy:

$$G\left[s(z)\right] = G_{\rm b} = S_\Gamma P_0^2\int_{-L/2}^{L/2} {\rm d}z\left[\frac{C}{2}\left(\frac{{\rm d}s}{{\rm d}z}\right)^2 + V(s^2) + 2\pi s^2\right],$$

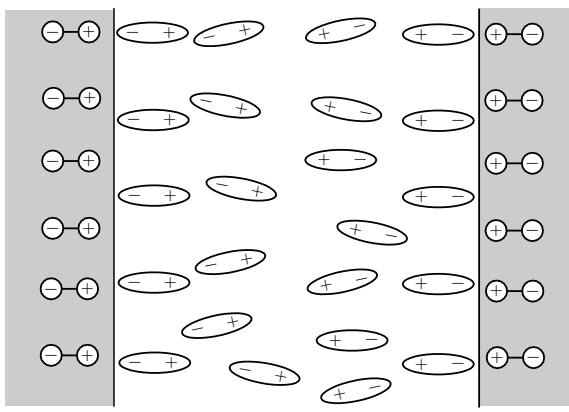

Figure 22. Typical polarization of water molecules between lipid membranes shown as shaded areas. Both the charges of the lipid polar groups and polarization of water molecules are schematically represented by corresponding charge symbols.

the minimization of which with respect to function $s(z)$ yields the equation for the polarization of water:

$$-C\,\frac{\mathrm{d}^2 s}{\mathrm{d}z^2} + \left(2V'(s^2) + 4\pi\right)s = 0\,.$$

The solution to this equation shown schematically in Fig. 21 can be obtained in the same way as in Section 5.3.2. The interaction strength is described by the dependence

$$F = S_\Gamma 2\pi P_0^2 s_0^2 \exp\left(-\frac{L}{R_\mathrm{d}}\right),$$

which was observed in [257, 265–271]. The corresponding pre-exponential factor $F/S_\Gamma = 2\pi P_0^2 s_0^2 \approx 3 s_0^2 \times 10^{10}$ dyn cm^{-2} is consistent with the data of these experiments. The force is positive, i.e., the membranes repel each other. Polarization charges emerge in the middle of the water layer (see Fig. 22), which is the physical reason for this repulsion. The force decreases exponentially at a characteristic distance $L \sim R_\mathrm{d} \sim \lambda$.

We note in conclusion that the approach proposed in this section is a natural generalization of the approaches proposed in [50, 51, 57–59, 282, 283].

5.3.4 Interaction between hydrophilic and hydrophobic surfaces. The interaction between hydrophilic and hydrophobic surfaces has been studied in a number of experiments [284–287]. Such systems are referred to as asymmetric.

We consider the case of charge-neutral surfaces. The hydrophilic and hydrophobic flat surfaces are located at $z = 0$ and $z = L$, respectively. Thus, the boundary conditions have the form

$$\begin{aligned} &s_z(0) = s_\mathrm{phi}\,, \qquad s_z(L) = 0\,,\\ &s_x(0) = 0\,, \qquad s_x(L) = s_\mathrm{pho}\,. \end{aligned} \tag{169}$$

Experiments were primarily focused on studying systems with weak polarization properties, such as mica. In this case, (see, e.g., [288]) $s_\mathrm{phi} \sim 0.1 \ll 1$ and $s_\mathrm{pho} \sim 0.1 \ll 1$; therefore, $s(z) \ll 1$ and $V(s^2) \approx As^2/2$. Similar to Sections 5.3.2 and 5.3.3, we obtain $\mathbf{E}_\mathrm{p} = -4\pi\mathbf{P} = -4\pi P_0[0, 0, s_z(z)]$ and

$$\begin{aligned} G(L) = {} & S_\Gamma P_0^2\left[-\frac{C}{2}\,s_\mathrm{phi}\left(\frac{\mathrm{d}s_z}{\mathrm{d}z}\right)_{z=0} + \frac{C}{2}\,s_\mathrm{pho}\left(\frac{\mathrm{d}s_x}{\mathrm{d}z}\right)_{z=L}\right]\\ & + S_\Gamma P_0^2 \int_{-L/2}^{L/2} \mathrm{d}z\,\left(V(s^2) - s^2 V'(s^2)\right). \end{aligned} \tag{170}$$

The Euler equations have the form $s_z''(z) - s_z/R_\mathrm{d}^2 = 0$, $s_x''(z) - s_x/L_T^2 = 0$. We obtain from here and Eqn (169) the polarization, energy, and interaction strength for flat surfaces, respectively:

$$s_z = s_\mathrm{phi}\,\frac{\sinh\left[(L-z)/R_\mathrm{d}\right]}{\sinh\left(L/R_\mathrm{d}\right)}\,, \quad s_x = s_\mathrm{pho}\,\frac{\sinh\left(z/L_T\right)}{\sinh\left(L/L_T\right)}\,,$$

$$G(L) = \frac{1}{2}\,S_\Gamma P_0^2 C\left[\frac{s_\mathrm{phi}^2}{R_\mathrm{d}}\coth\left(\frac{L}{R_\mathrm{d}}\right) + \frac{s_\mathrm{pho}^2}{L_T}\coth\left(\frac{L}{L_T}\right)\right],$$

$$F(L) = \frac{1}{2}\,S_\Gamma P_0^2\left[\frac{s_\mathrm{phi}^2}{\sinh^2\left(L/R_\mathrm{d}\right)} + \frac{s_\mathrm{pho}^2}{\sinh^2\left(L/L_T\right)}\right].$$

The force $F(L)$ at distances between the surface given by (156) describes repulsion in agreement with experiments. The inequality $L \gg R_\mathrm{d}$ was fulfilled in all experiments, owing to which the formula for the force may be simplified:

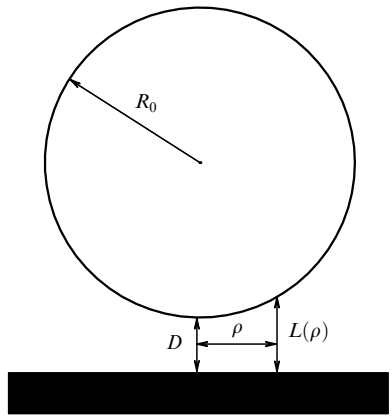

Figure 23. Geometry of interacting bodies in experiments where an atomic force microscope is used.

$$F \approx \frac{S_\Gamma P_0^2 s_\mathrm{pho}^2}{2\sinh^2\left(L/L_T\right)}\,. \tag{171}$$

To measure the force, an atomic force microscope is usually used, to the cantilevered tip of which a spherical colloidal particle with the diameter $R_0 \sim 10-15$ μm is attached. Thus, this device measures the force that acts between a flat surface and a sphere at distances $D \ll R_0$ between their boundaries. Equation (171) in this case yields

$$\begin{aligned} \frac{F}{R_0} &= \frac{P_0^2 s_\mathrm{pho}^2}{2}\int \frac{\mathrm{d}S}{\sinh^2\left[L(\rho)/L_T\right]}\\ &= \frac{P_0^2 s_\mathrm{pho}^2}{2}\int_0^\infty \frac{2\pi\rho\,\mathrm{d}\rho}{\sinh^2\left[L(\rho)/L_T\right]} = \frac{2\pi P_0^2 s_\mathrm{pho}^2 L_T}{\exp\left(2D/L_T\right) - 1}\,. \end{aligned} \tag{172}$$

The geometrical meaning of notations ρ, D, and $L(\rho) \approx D + \rho^2/(2R_0)$ is explained in Fig. 23. Formula (172), which is valid to a distance up to the molecular size, $D \gtrsim R_\mathrm{d}$, agrees with measurements [284–287]. It should be noted that, according to the same measurements, the force at $D \gtrsim 3$ nm strongly depends on experimental conditions, in particular, on the presence of air dissolved in water (see the discussion in Section 5.3.1).

5.3.5 Interaction between region-III surfaces. The force of interaction between such surfaces along with the average polarization of water molecules is zero in the mean field approximation: $\mathbf{s} = 0$, $G = 0$, $F = 0$. Hence, the energy of the liquid and this force are determined by thermal fluctuations. The resulting force is by definition a flow of momentum transferred between the surfaces through a liquid by means of dipole–dipole interactions between molecules. The force is in this case also a long-range interaction.

It is assumed in this section that the surface layer of the liquid in region III (see Fig. 9) is in the paraelectric state, and the fluctuating polarization vector is parallel to the surface. This condition is fulfilled at least near the OC line of the BKT transition. The liquid transforms into such a state as temperature increases in the process of motion from ferroelectric region II to paraelectric region III. The part of the

free energy of the 'liquid and two surfaces' system, which depends on the distance between the surfaces, leads to an interaction between these surfaces, similar to the way electromagnetic field fluctuations lead to the emergence of Casimir forces [289].

A regularization procedure similar to [290] was used in [49] to derive an expression for the interaction energy $G(L)$, which has the following form in the limiting cases of small and large distances:

$$G(L) \approx -S_\Gamma \frac{T}{2\pi L_T L} \exp\left(-\frac{L}{L_T}\right), \qquad L \gg L_T,$$

$$G(L) \approx -0.53 S_\Gamma \frac{T}{\pi L^2}, \qquad L \ll L_T.$$

It should be noted that in these limiting cases the energy is independent of the material constants α_0 and β_0. The corrections depending on the material of the surfaces are small and can be observed only at intermediate distances $L \sim L_T$. Thus, an attractive force emerges between interacting surfaces that belong to region III, which at $L \lesssim L_T$ is inversely proportional to the cube of the distance between them.

5.3.6 Example of interaction between bodies under nonequilibrium conditions. An enigmatic ultra-long interaction between hydrophilic surfaces and bodies immersed in a polar liquid was discovered in [291–298]. A plate made of a hydrophilic substance was immersed in water that contained colloidal particles about 1 μm in size. It was found that a zone several hundred micrometers wide is formed at the plate surface within a time of the order of 1 min, in which these particles are absent. Such a surface region was called the exclusion zone (EZ). Since the exclusion zone exhibits unusual properties, which distinguish it from bulk water (birefringence, absorption of electromagnetic waves with a wavelength near $\lambda = \lambda_0 = 270$ nm), it was assumed in Ref. [298] that water in the EZ is in a new, fourth state that differs from vapor, liquid, and ice by the presence in it of a long-range structure.

The most detailed exploration of this phenomenon was performed using as an example a hydrophilic ion-exchange membrane made of Nafion [299]. These membranes, which are widely used in fuel cells, are of great practical importance. Nafion is a hydrophobic polymer material (Teflon), to the polymer chains of which sulfo groups are attached, owing to which its surface has hydrophilic properties. It was also found that the formation of EZ is characteristic not of Nafion alone, but also of a wide range of hydrophilic surfaces, including surfaces of biological materials and metals (zinc, aluminum, tin, lead, and tungsten). It was also revealed that EZ is absent on the surfaces of noble metals, a circumstance that led the authors of [297] to the conclusion that electrochemical processes occurring on the surface play some role in the formation of EZ.

It is known [300–302] that a 'forest' of polymer chains sticking out from the Nafion surface is formed in water. Given all these circumstances, the authors of [303–305] proposed a model that satisfactorily explains the observations and does not involve the hypothesis regarding the fourth state of water. Studies of the luminescence that arises in the liquid enabled direct observation of the emergence of a polymer chain 'forest' in the EZ region. The existence of EZ was explained in early studies [303–305] by the direct ejection of colloidal particles by these chains. Birefringence is also easily explained in this model: as the chains emerge, the EZ region becomes anisotropic, which leads to birefringence.

The absorption of electromagnetic waves also finds an explanation in this model. Both the Nafion surface and the polymer chains sticking out from it acquire a negative charge as a result of electrolytic dissociation of sulfo groups. For this reason, the chains should form in equilibrium an approximately periodic 2D structure with a certain period a. Thus, Nafion in water resembles a brush with periodically arranged bristles. If a wave is incident on this brush and the resonance condition $\lambda_0 \approx 2a$ is satisfied, a wave reflected from the bristles emerges (the authors of [303–305] pointed out the similarity of this phenomenon to a photonic crystal); therefore, the absorption observed in [293, 294] at a wavelength of $\lambda_0 = 270$ nm is in reality a scattering phenomenon. Based on this, the authors of [303–305] concluded that $a \approx \lambda_0/2 \approx 135$ nm. It should be noted that the quoted wavelength refers to vacuum. Taking into account the refractive index of water $n_0 = 1.33$, we get $a \approx \lambda_0/(2n_0) \approx 100$ nm.

This explanation may be detailed in a mathematical approach. The wave propagates through a medium with a periodically changing refractive index $n(x) = n_0 + \delta n(x)$. We consider for estimates the one-dimensional Kronig–Penney model:

$$\delta n(x) = -\alpha \sum_{s=-\infty}^{+\infty} \delta(x - sa). \tag{173}$$

It is reasonable to assume that, due to the large lattice period a, the parameter α is sufficiently small compared to the polymer-chain thickness, so that the relation below holds:

$$k|\alpha| \ll 1, \tag{174}$$

where $k = n_0\omega/c = n_0 2\pi/\lambda$ is the wave vector in the medium. The conclusions that follow do not depend on the sign of α, so, to be specific, we assume that $\alpha > 0$. A monochromatic wave incident on a medium with a periodically changing refractive index that depends on its frequency ω corresponds to either the allowed band or the bandgap. In the former case, it enters the medium, being partially reflected, while in the latter case, it is reflected (completely, if the medium is semi-infinite) as is assumed in [303–305]. The widths (in terms of frequency ω) of the bandgaps are small under condition (174), while absorption was observed in a rather wide band near the wavelength $\lambda_0 = 270$ nm. Therefore, the first case, where the wave propagation along the 'brush' is characterized by quasi-momentum $q = n_{\text{eff}} 2\pi/\lambda$, seems to be more plausible. The last relation is a definition of the observed value of the refractive index n_{eff}. It should be noted that, as the frequency approaches the bandgaps, the reflection intensifies; therefore, the maximal absorption should be observed right there.

We now make an attempt to qualitatively explain in model (173) the increase in n_{eff} observed in [303–305] near the Nafion surface.

The dependence of frequency on quasi-momentum, i.e., the dispersion relation $\omega = \omega(q)$, is found from the equation [306]

$$\cos(qa) = \cos(ka) + k\alpha \sin(ka). \tag{175}$$

The lowest bandgap, which corresponds to the above resonance condition considered in [303–305], has under condition (174) the width $\Delta\omega \approx 4\pi\alpha c/(an_0)^2$. The wave dispersion law near the bottom of the upper allowed frequency band and the top of the lower one is, respectively,

$$\omega(q) \approx \frac{2\pi c}{\lambda_0} + \Delta\omega + \frac{c^2}{\Delta\omega n_0^2}\left(q - \frac{\pi}{a}\right)^2 ,$$

$$\omega(q) \approx \frac{2\pi c}{\lambda_0} - \frac{c^2}{\Delta\omega n_0^2}\left(q - \frac{\pi}{a}\right)^2 .$$

On approaching the surface, the thickness of bristles increases if only because of their rather wide length distribution, coalescence, etc. This corresponds to an increase in the parameter α and the band gap width $\Delta\omega$. If the wave frequency ω falls in the upper allowed band, then

$$n_{\text{eff}}\,\frac{2\pi}{\lambda_0} \approx \frac{\pi}{a} - \frac{n_0}{c}\sqrt{\Delta\omega\left(\omega - \frac{2\pi c}{\lambda_0} - \Delta\omega\right)} .$$

As $\Delta\omega$ increases, n_{eff} grows due to the factor in parentheses under the square root sign, which may explain the observations. If the frequency falls in the lower band, the dependence of n_{eff} on α is much slower. Thus, the first of these assumptions is preferable. Additional estimates are required here that would take into account the degree of wave nonmonochromaticity, estimated values of the coefficient α, etc.

Another mechanism for the emergence of EZ was established as a result of studies [291–298, 303–305, 307–310]: it is electrophoresis that explains this phenomenon in the case of metals [297] and surfaces coated with a hydrophilic monolayer [291]. The force acting on colloidal particles is generated by a quasi-neutral flow of ions formed on the surface and on polymer chains. This mechanism works in the case of Nafion concurrently with the aforementioned expulsion of colloidal particles by polymer brushes. It is supported by the results of study [295], which established that the EZ width substantially increases upon infrared irradiation of the Nafion surface. It can be assumed as an explanation that radiation accelerates electrochemical processes, which is a plausible option. This leads to an increase in the ion flow that enhances electrophoresis. Further research is required in this area.

In Ref. [307] the authors established the presence of HSO_3^- ions in EZ. It was found in [303] that the concentration of these ions decreases sharply at the EZ boundary, where the polymer chains abut against colloidal particles. The authors of [303] suggested that a brush slows down diffusion of ions simply because of a lack of space in the gaps between the polymer chains. This suggestion seems doubtful, since these gaps are large in comparison with the ion size. An alternative explanation for the slowdown of ion diffusion by EZ is plausible. The observed decrease in the concentration of ions is most likely due to their diffusion over the surface of chains alternating with penetration into the volume (so-called bulk mediated surface diffusion) [311, 312]. Adsorption onto the surface of chains apparently slows down diffusion. The observed ion diffusion coefficient has in this case the following form:

$$D_{\text{eff}} = D\,\frac{h}{h_{\text{por}}} . \qquad (176)$$

Here, $h = D\tau_{\text{a}}/b$ is the thickness of the water layer adjacent to the surfaces of the bristles, in which the nature of the ion diffusion significantly differs from that in the main volume of liquid between the bristles, $D \sim 10^{-5}\ \text{cm}^2\ \text{c}^{-1}$ is the coefficient of ion diffusion in bulk water, $b \sim 10^{-8}$ cm is the characteristic size of the jump-like change in the spatial position of the ion in water in the process of the elementary event of diffusion in the liquid volume, $h_{\text{por}} = a^2/(2\pi a_0)$ is the effective size of the porous space formed by the chains, and $a_0 \sim 0.5$ nm is the characteristic radius of the chain cross section that takes into account the ion size itself. The HSO_3^- ions may be adsorbed for some time τ_{a} on polymer chains with or without charge neutralization. Formula (176) is valid provided $h \lesssim h_{\text{por}}$, a condition which is obviously fulfilled in mesopores between chains.

The birefringence caused by a lattice of unbraided Nafion polymer chains is combined with the birefringence due to the optical reflection of the material at the water/Nafion surface interface [310]. However, this reflection alone cannot explain the observed increase in the refractive index in approaching the surface, which was found in [303].

Thus, the nature of the ultra-long interaction between hydrophilic surfaces and colloidal particles is gradually becoming clear, although many phenomena in this area are not understood yet. Moreover, sometimes new puzzles arise (see, e.g., [307]).

5.4 Discussion of the results

Based on the VMPL, we have calculated above the forces of interaction between macroscopic bodies immersed in a liquid. In particular, the strength of interaction between flat surfaces in water was determined for distances $L \lesssim 3$ nm between them. Measurements show that the nature of interaction is in this case universal and is only determined by the wetting properties of the surfaces and the dipole long-range action between HBPL molecules. The lower limit in (156) is due to the fact that dipole–dipole interaction between molecules is at such distances comparable to short-range forces. These latter forces are described in the considered phenomenological VMPL model by the Oseen term (25), which is similar to the so-called hydrophobic interaction explored in [67, 68]. Since the short-range forces vanish at distances of $\sim R_{\text{d}}$, small bodies with sizes $\lesssim R_{\text{d}}$ are characterized in the VMPL by hydration energy, which is proportional to their volume, in agreement with the conclusions of [67, 68]. This type of interaction has a negligible effect at large distances, such as (156), which are typical of biology.

If the surfaces are hydrophilic, molecules of liquid are polarized perpendicular to them, and interaction at mesoscopic distances $L \lesssim 3$ nm between the surfaces is repulsive, strong, short-range, and exponentially decreasing at the characteristic distance $\lambda = R_{\text{d}} \sim 0.2-0.3$ nm. Numerous measurements show that this character of interaction between hydrophilic surfaces of various natures is fairly universal. However, the last statement is only true in equilibrium cases, when the properties of the surface immersed in HBPL do not change with time. Section 5.3.6 presents a review of the studies of the surfaces where the equilibrium condition is not fulfilled. This results in the emergence of an interaction acting at ultra-long distances between the bodies immersed in the liquid, which is characterized by scale of less than 1 mm.

The interaction between hydrophobic surfaces, which is significantly more diverse, is explored to a much lesser extent.

While at $L \lesssim 3$ nm this interaction is quite universal, at $L \gtrsim 3$ nm it substantially depends on the method used to prepare the polar liquid composition, gaseous and solid impurities it contains, steric properties of surfaces, etc. It was shown that, in accordance with measurements, the interaction at $L \lesssim 3$ nm is attractive and relatively long-range (the interaction forces exponentially decrease over a mesoscopic characteristic length of $\lambda = L_T \sim 1.2-1.5$ nm). The polarization of water molecules is in this case parallel to the surfaces.

The forces operating between two hydrophobic or two hydrophilic surfaces are by their nature entropic or electrostatic.

Hydrophobic and hydrophilic surfaces at $L \lesssim 3$ nm repel each other. The calculated strength of their interaction is consistent with experimental results.

Regardless of the surface properties, the hydration forces are determined by nonlinear effects of liquid polarization in the volume or a similar nonlinearity of interaction between water and the immersed body. This implies that the interaction forces cannot be correctly calculated in the linear response approximation, which is used, for instance, in [52].

An intermediate mode of interaction between surfaces is predicted to exist if liquid polarization in the layers adjacent to them is in a chaotic, paraelectric state. The interaction is in this case much weaker and attractive. The attractive force between such surfaces decreases at $L \lesssim L_T$ according to a power law; namely, it is inversely proportional to the cube of the distance between them.

The presented model of hydration forces is applicable in the case of the complete absence or rather low concentration of free ions that emerge, for example, as a result of electrolytic dissociation of salts or surface polar groups. This limitation, of course, should be taken into account in comparing model predictions with measurements. The maximum value n_{I} at which the VMPL is still be applicable can be estimated using the condition $4\pi n_{\mathrm{I}} L_T^3/3 \sim 1$, which yields a limitation $n_{\mathrm{I}} \lesssim 0.02$ mol. For example, hydration forces were measured in [313] in a 1-molar-KCl solution. The ion concentration was in this case $n_{\mathrm{I}} = 1$ mol. The forces acting between the ions and water molecules in this experiment can destroy the molecular order and hydrophobic attraction in the form described here; therefore, our model in the presented form is not applicable to analyze this experiment.

6. Summary discussion

The dipole–dipole interaction between the molecules of polar liquids with hydrogen bonds features a long range and determines the main properties of the HBPL at scales larger than the distance between the nearest molecules. As in plasma, collective electric fields prevail at such distances. Short-range forces that ensure the stability of liquids are also of importance in an HBPL; a special role is played in this case by hydrogen bonds. We present the results obtained in the phenomenological vector model of polar liquids, in which the liquid is described by the order parameter — the polarization vector $\mathbf{s}(\mathbf{r})$, i.e., the average of unit vectors of the directions of dipole moments of molecules located near point $\mathbf{r}$. We have shown that the simplest, 'minimal' version of a VMPL already satisfactorily reproduces properties of a liquid at a spatial scale of $\gtrsim 0.3$ nm. The model contains two spatial scales: R_{d} and L_T. The domains of $\sim 2R_{\mathrm{d}} \sim 0.4-0.6$ nm in size, which weakly depends on temperature T, consist of molecules with strongly correlated dipole moments. Water is at room temperature in a paraelectric state. Superdomains of $\sim 2L_T \sim 2.4-3$ nm in size each contain ~ 100 molecules and consist of domains weakly correlated with respect to dipole moments.

A large value of the static dielectric constant of water ε_0 is associated with reorientation of superdomains in an external electric field. The electric field of external charges decreases in HBPLs by a factor of ε_0 at a characteristic size of $\sim L_T$. Thermal fluctuations in plasma are characterized by the Debye radius r_{D}, and, in the HBPL, by the parameter L_T. The parameter L_T is similar in this sense to r_{D}. The VMPL provides a relatively simple and at the same time detailed description of the interactions between macroscopic objects in the HBPL.

The existence of a ferroelectric phase transition (FPT) is predicted in supercooled liquid water at a temperature of $T_{\mathrm{c}} \sim -40\,^{\circ}\mathrm{C}$, which is confirmed in experiments with water-filled porous materials. Arguments are presented in favor of the existence of the FPT in bulk water. Long-range order in the molecular dipole directions spontaneously arises in water due to the long-range dipole interaction at $T < T_{\mathrm{c}}$. This order is destroyed by thermal fluctuations as temperature increases. The size L_T is the dipole correlation radius. It is infinite at the FPT point and decreases as temperature increases. In approaching the FPT, polarization vector fluctuations increase, which may be, if not the main, then at least one of the mechanisms underlying the so-called 'anomalous' properties of water.

The wettability properties of bodies are shown to be satisfactorily characterized by two or, in a more accurate description, three dimensionless parameters. Based on this property, surfaces are divided into three types: hydrophilic — type I, amphiphilic — type II (in the extreme case $s \to 1$ they are hydrophobic), and type III surface, near which $\mathbf{s} = 0$, $\langle \mathbf{s}^2 \rangle \neq 0$. At sufficiently low temperatures, states I and II feature a long-range order in the molecule dipole directions, which is due to the long range of dipole interaction. This order is destroyed as temperature increases due to the second-order phase transition, after which the surface layers of the liquid become state III paraelectric. The II $\to$ III conversion is shown to be a Berezinskii–Kosterlitz–Thouless topological phase transition. Experiments are discussed that evidence this idea. The calculated forces of interaction in water between two flat surfaces that belong to types I–I, II–II, and I–II are consistent with the measurements. An expression is given for the force of interaction between surfaces III–III, which can be verified in experiments. The approaches and the methods discussed in this review were used to estimate the solvation energy and protonation states of biomacromolecules and to calculate the dissociation constants of protein–ligand complexes. The use of VMPL in the calculations of systems that contain a large number of water molecules significantly reduces the computer time.

7. Conclusions

We reviewed the results of numerous studies carried out by various authors, which show that long-range forces and, as a result, collective effects generated by dipole–dipole interactions between molecules play a key role in polar liquids with hydrogen bonds. There is in this sense an analogy between HBPL and plasma, where particles interact according to the Coulomb law. Short-range forces in HBPLs are of no less

importance, as they ensure the stability of the liquid. A special role is played by hydrogen bonds, which determine, along with dipole–dipole interactions, the basic properties of such liquids and, in particular, water.

We now summarize the main manifestations of long-range action effects in HBPLs, meaning, to be more specific, water.

(1) The large value of the dielectric constant of water at zero frequency $\varepsilon(\omega = 0) = 88$ under normal conditions indicates that water is a paraelectric substance close on a temperature scale to ferroelectric. The character of the $\varepsilon(\omega)$ dependence indicates a two-scale structure with a different degree of correlation of molecule dipole moments.

(2) The smaller scale $R_{\mathrm{d}} \sim 0.2-0.3$ nm, which weakly depends on temperature, characterizes short-range forces. It is the radius of the domain within which thermal fluctuations are insignificant, and the directions of the molecule dipole moments are strongly correlated with each other.

(3) The larger scale L_T, which is generated by dipole–dipole interactions between molecules, substantially depends on temperature. Domains form clusters, superdomains, with a characteristic radius L_T, within which there is a balance between the onset of a correlation between domain dipole moments and the destruction of it by thermal fluctuations. Under normal conditions, the superdomains have characteristic size $\sim 2L_T \sim 3-4$ nm and contain ~ 100 molecules each.

(4) Due to the abovementioned correlation of dipoles, it is natural to describe the properties of water at spatial scales exceeding the size of the molecules using the polarization vector $\mathbf{s}(\mathbf{r})$ (1). The very existence of this order parameter is a direct consequence of the long-range nature of the dipole–dipole interaction. From this follows in a natural way the description of HBPL in a phenomenological vector model. The mathematical structure of the VMPL, which is definitively established in Section 2, is completely similar to that used in the phenomenological description of ferromagnetism (see [66, §§ 39, 43]). The VMPL equations are derived in a simplified approach by minimizing free energy (47). A more accurate description requires taking into account polarization of the electron shells of molecules, which leads to more general expression (39).

(5) The existence of the order parameter $\mathbf{s}(\mathbf{r})$ shows (see Section 3) that there is a molecular electric field $\mathbf{E}_{\mathrm{m}}$ in the vicinity of each molecule. The ordering effect of this field on molecular dipoles competes with thermal fluctuations that destroy the order, i.e., with the tendency of the liquid to increase orientational entropy.

(6) Parameter L_T characterizes large-scale correlations of molecular dipoles, the magnitude of thermal fluctuations of the polarization vector, and the distance at which the dipoles screen each other. The length L_T is in this sense analogous to the Debye radius r_{D} in plasma.

(7) As temperature decreases, the correlation radius L_T increases to infinity, which leads to a ferroelectric phase transition in bulk liquid water. Thus, the FPT is another manifestation of long-range action.

(8) The conclusion about the existence of the FPT in liquid water follows from both the mean-field approximation (39) (47) and calculations based on the ring-diagram method, which has no limitation associated with the mean field approximation.

(9) The singularity in the temperature dependence of the dielectric constant observed in experiments [33] is a direct indication of the existence of the FPT in bulk liquid water. These experiments failed to reach the FPT, although only a few degrees remained to achieve that temperature.

(10) An obstacle in experiments [33] was rapid bulk nucleation of the liquid, owing to which it becomes ice. Another possible reason is the emergence in water of a depolarizing field $\mathbf{E}_{\mathrm{p}}$, which prevents the FPT, as shown in Section 3. This phase transition occurs under sufficiently rapid decrease in temperature if a domain structure (see [66, § 44]) with a small or, in the limit, zero depolarizing field has enough time to be formed before nucleation occurs. If this requirement is not fulfilled, the FPT will be fundamentally unattainable in bulk liquid water at any cooling rate. The issue can be resolved by experiments similar to those carried out in [40].

(11) The FPT has been directly observed in experiments [16, 41, 42, 314] with water-filled porous materials MCM-41 and SBA-15 owing to lowering of the freezing temperature in small water samples. The pore size in these experiments was much larger than that of water molecules, which indicates the identity of microscopic properties of bulk liquid and the liquid investigated in pores (see Section 3.5).

(12) An assertion is known (see, e.g., [92]), that the orientation of water molecules in mesoscale and nanometer capillaries is 'imposed' by an external force, i.e., their interaction with pore walls, which leads to the FPT in the water contained in the pores. This is far from obvious, since a number of fairly realistic molecular dynamics calculations predict the existence of the FPT transition even in bulk water. In our opinion, pore walls contribute to the formation of a ferroelectric state for another reason (see Section 3.7). If the polarization vector is perpendicular to the pore walls, a depolarizing field $\mathbf{E}_{\mathrm{p}}$ emerges that prevents the phase transition. This field vanishes if the polarization vector is directed along the pore. In other words, the free energy of a liquid reaches its smallest value if its polarization vector is directed along the pore. The FPT occurs in this case, which was observed in experiments not only with mesopores [16, 41, 42, 314] but also with nanopores [92, 93].

(13) The existence of the FPT provides an explanation of the nature of fluctuations that destroy the correlation of domains on the $\gtrsim L_T$ scale. It follows from Eqns (31), (32), and (43) that the superdomain size L_T is determined by the distance to the FPT point on the temperature scale rather than by the absolute temperature itself. This observation clearly shows that these fluctuations are ordinary fluctuations of the order parameter. In the case under consideration, they are fluctuations of the polar liquid polarization vector $\mathbf{s}$ that occur near the second-order phase transition point. If parameter A decreases to zero, the dependence of free energy (57) on s becomes shallow, and the 'elasticity' that returns s to its equilibrium value vanishes. The thermal fluctuation amplitude increases as a result of such a 'weakening' of the polarization degree of freedom of the liquid.

It was hypothesized that the fluctuations in water are related to the proximity to the Widom line, which leads to the known unusual temperature dependences of its thermodynamic characteristics [103, 123, 128–139], i.e., to the emergence of water properties that are referred to as abnormal.

The Widom line arises in this approach due to the water being composed of clusters in which spatial packing of molecules is different. Their mutual transformation also leads to increased fluctuation in density, temperature, and other quantities. Based on a purely cluster model, it is hardly

possible to explain the observed λ singularity of the dielectric constant. In Section 3.7 we present evidence confirming that it is the weakening of the polarization degree of freedom that gives rise to the Widom line in water.

(14) The VMPL model provided a simple way to classify surfaces of the polar liquid interface with another medium and a quantitative content of such qualitative characteristics as hydrophobicity and hydrophilicity (see Section 4.1). The conclusion is drawn that the description of the wetting properties of a liquid using the contact angle is incomplete: at least two parameters, α_0 and β_0, should be used to this end, while the most complete description requires three parameters. It follows from the VMPL that the surfaces of bodies are classified into three types based on the wettability properties: hydrophilic — type I, amphiphilic — type II (in the extreme case $s \to 1$, hydrophobic), and type III surface, the liquid layer near which is not polarized. To the best of our knowledge, the last type has not yet been observed in experiments, but, apparently, manifested itself in MD calculations [247–249].

(15) As temperature decreases, the FPT may occur in the HBPL layer $\sim L_T$ thick adjacent to the amphiphilic surface, which is due to the long-range nature of dipole interaction between its molecules (see Section 4.2). This is a III $\to$ II transition. It is similar by its nature to the Berezinskii–Kosterlitz–Thouless phase transition. The key role is played here by the mutual screening of pairs of vortex-antivortex polarization configurations. The HBPL volume is in this case in a paraelectric state.

(16) The polarization of a liquid by the bodies immersed in it, which is also generated by the dipole–dipole interaction between molecules, leads to long-range interactions between the bodies (see Section 5). These interactions, which depend on the mutual orientation of the bodies, can play an important role in the self-assembly of micro-objects.

(17) The linearized version of vector model (22) and (45) reproduces such important effects observed in MD calculations as spontaneous polarization of a liquid in the vicinity of macroscopic bodies and the emergence of vortex-like polarization structures on the surface of a body immersed in a liquid. Force-free polarization configurations with $\nabla \mathbf{s} \approx 0$ and, as a result, with a small polarizing electric field prove to be energetically advantageous. This, in turn, leads to a strong long-range interaction between bodies immersed in a liquid.

(18) The existence of two scales, R_{d} and L_T, is confirmed by experiments in which the force of interaction between macroscopic objects at mesoscopic distances between their surfaces is measured.

Although the vector model of polar liquids under discussion is quite simple, it can nevertheless describe diverse properties of polar liquids. The computer resources necessary for calculations using the VMPL are comparable to those required for continuous solvation models applied in computational biophysics (see, e.g., [19, 20]). If a large number of water molecules are to be taken into account, the time of numerical calculations is significantly reduced due to the correct consideration of long-range effects. An example seems to be relevant in this relation. We plotted Fig. 9 by minimizing the free energy G in the VMPL using the variational principle. Only a few parameters were varied in this case. The development and debugging of the program took about 1 h. Calculation made using a PC lasted 1 min. As to Figs 12 and 15, they were obtained using the molecular dynamics method. Several days were needed to program and debug the code, this time primarily needed to remove the instabilities caused by the dipole long-range interaction between the molecules. The computer calculation per se of each figure lasted 1 day.

The development of fast solvation models is of the utmost importance for modeling biomolecules, designing drugs, etc. The quality of such models is the main limiting factor for accurate predictions of the binding capacity of protein–ligand complexes. The approaches and methods discussed above were used to estimate the solvation energy and biomacromolecule protonation states, and to calculate the dissociation constants of protein–ligand complexes [315–319].

It is of practical interest to develop a general model that would describe polarization properties of polar liquids that contain dissolved free ions. This goal may be achieved by combining the Deryagin–Landau–Fairway–Overbeek theory [121, 255, 256], the theory presented in [264], and the vector model of a polar liquid that we have developed.

The authors are grateful to G S Bordonskii, G D Koposov, A N Pershin, and L N Shestakov for the useful discussions.

References

1. Sivukhin D V *Obshchii Kurs Fiziki. Elektrichestvo* (General Course of Physics. Electricity) (Moscow: Nauka, 1977)
2. Earnshaw S *Trans. Camb. Phil. Soc.* **7** 97 (1842)
3. Jackson S M, Whitworth R W *J. Phys. Chem. B* **101** 6177 (1997)
4. Su X et al. *Phys. Rev. Lett.* **80** 1533 (1998)
5. Iedema M J et al. *J. Phys. Chem. B* **102** 9203 (1998)
6. Morishige K, Kawano K *J. Chem. Phys.* **110** 4867 (1999)
7. Debenedetti P G *J. Phys. Condens. Matter* **15** R1669 (2003)
8. Singer S J et al. *Phys. Rev. Lett.* **94** 135701 (2005)
9. Sarkisov G N *Phys. Usp.* **49** 809 (2006); *Usp. Fiz. Nauk* **176** 833 (2006)
10. Jähnert S et al. *Phys. Chem. Chem. Phys.* **10** 6039 (2008)
11. Malenkov G *J. Phys. Condens. Matter.* **21** 283101 (2009)
12. Cramer C J, Truhlar D G *Chem. Rev.* **99** 2161 (1999)
13. Rapaport D C *The Art of Molecular Dynamics Simulation* (Cambridge: Cambridge Univ. Press, 2004); Translated into Russian: *Iskusstvo Molekulyarnoi Dinamiki* (Izhevsk: Inst. Komp'yut. Issled., 2012)
14. Swenson J, Teixeira J *J. Chem. Phys.* **132** 014508 (2010)
15. Bordonskiy G S, Orlov A O *Kondens. Sredy Mezhfazn. Granitsy* **13** (1) 5 (2011)
16. Bordonskiy G S, Orlov A O *Phys. Solid State* **56** 1626 (2014); *Fiz. Tverd. Tela* **56** 1575 (2014)
17. Cerveny S et al. *Chem. Rev.* **116** 7608 (2016)
18. Born M *Z. Phys.* **1** 45 (1920)
19. Schaefer M, Karplus M *J. Phys. Chem.* **100** 1578 (1996)
20. Feig M et al. *J. Comput. Chem.* **25** 265 (2004)
21. Weeks J D, Chandler D, Andersen H C *J. Chem. Phys.* **54** 5237 (1971)
22. Huang D M, Chandler D *Proc. Natl. Acad. Sci. USA* **97** 8324 (2000)
23. ten Wolde P R, Sun S X, Chandler D *Phys. Rev. E* **65** 11201 (2001)
24. Kohlmeyer A, Hartnig C, Spohr E *J. Mol. Liq.* **78** 233 (1998)
25. LeBard D N, Matyushov D V *J. Phys. Chem. B* **114** 9246 (2010)
26. Lee C-Y, McCammon J A, Rossky P J *J. Chem. Phys.* **80** 4448 (1984)
27. Pohorille A et al. *J. Chem. Phys.* **87** 6070 (1987)
28. Higo J et al. *Proc. Natl. Acad. Sci. USA* **98** 5961 (2001)
29. Fedichev P O, Men'shikov L I, cond-mat/0601129
30. Men'shikov L I, Fedichev P O *Russ. J. Phys. Chem. A* **85** 906 (2011); *Zh. Fiz. Khim.* **85** 996 (2011)
31. Men'shikov L I, Fedichev P O *J. Struct. Chem.* **50** 97 (2009); *Zh. Strukt. Khim.* **50** 103 (2009)
32. Fedichev P O, Menshikov L I, arXiv:0808.0991
33. Hodge I M, Angell C A *J. Chem. Phys.* **68** 1363 (1978)
34. Stillinger F H, Hasted J B, Warshel A *Philos. Trans. R. Soc. Lond. B* **278** 97 (1977)
35. Angell C A, Shuppert J, Tucker J C *J. Phys. Chem.* **77** 3092 (1973)
36. Speedy R J, Angell C A *J. Chem. Phys.* **65** 851 (1976)

37. Ter Minassian L, Pruzan P, Soulard A *J. Chem. Phys.* **75** 3064 (1981)
38. Angell C A, Sichina W J, Oguni M *J. Phys. Chem.* **86** 998 (1982)
39. Huang C et al. *J. Chem. Phys.* **133** 134504 (2010)
40. Sellberg J A et al. *Nature* **510** 381 (2014)
41. Fedichev P O et al. *JETP Lett.* **94** 401 (2011); *Pis'ma Zh. Eksp. Teor. Fiz.* **94** 433 (2011)
42. Bordonskiy G S et al., arXiv:1204.6401
43. Petrov O V, Furó I *Prog. Nucl. Magn. Reson. Spectrosc.* **54** 97 (2009)
44. Men'shikov L I, Fedichev P O *Russ. J. Phys. Chem. A* **83** 967 (2009); *Zh. Fiz. Khim.* **83** 1103 (2009)
45. Fedichev P O, Menshikov L I, arXiv:0908.0632
46. Fedichev P O, Men'shikov L I *Phys. Part. Nucl. Lett.* **9** 71 (2012); *Pis'ma Fiz. Elem. Chastits At. Yadra* **9** 112 (2012)
47. Fedichev P O, Menshikov L I *JETP Lett.* **97** 214 (2013); *Pis'ma Zh. Eksp. Teor. Fiz.* **97** 241 (2013)
48. Vasiliev A Yu et al. *New J. Phys.* **16** 3011 (2014)
49. Menshikov L I, Menshikov P L, Fedichev P O *JETP* **125** 1173 (2017); *Zh. Eksp. Teor. Fiz.* **152** 1374 (2017)
50. Marčelja S, Radić N *Chem. Phys. Lett.* **42** 129 (1976)
51. Belaya M L, Feigel'man M V, Levadny V G *Chem. Phys. Lett.* **126** 361 (1986)
52. Eriksson J C, Ljunggren S, Claesson P M *J. Chem. Soc. Faraday Trans. 2* **85** 163 (1989)
53. Leikin S, Kornyshev A A *J. Chem. Phys.* **92** 6890 (1990)
54. Frodl P, Dietrich S *Phys. Rev. A* **45** 7330 (1992)
55. Beglov D, Roux B *J. Chem. Phys.* **104** 8678 (1996)
56. Ramirez R et al. *Phys. Rev. E* **66** 031206 (2002)
57. Azuara C et al. *Biophys. J.* **95** 5587 (2008)
58. Gong H, Freed K F *Phys. Rev. Lett.* **102** 057603 (2009)
59. Koehl P, Orland H, Delarue M *Phys. Rev. Lett.* **102** 087801 (2009)
60. Ivanitskii G R, Deev A A, Khizhnyak E P *Phys. Usp.* **57** 37 (2014); *Usp. Fiz. Nauk* **184** 43 (2014)
61. Terletskii Ya P, Rybakov Yu P *Elektrodinamika* (Electrodynamics) (Moscow: Vysshaya Shkola, 1990)
62. Klein L, Swift C *IEEE Trans. Antennas Propag.* **25** 104 (1977)
63. Kaatze U, Feldman Y *Meas. Sci. Technol.* **17** R17 (2006)
64. Ravdel' A A, Ponomareva A M (Eds) *Kratkii Spravochnik Fiziko-khimicheskikh Velichin* (Reference Data on Physicochemical Variables) (Leningrad: Khimiya, 1983)
65. Radzig A A, Smirnov B M *Reference Data on Atoms, Molecules, and Ions* (Springer Series in Chemical Physics, Vol. 31) (Berlin: Springer-Verlag, 1985); Translated from Russian: *Spravochnik po Atomnoi i Molekulyarnoi Fizike* (Moscow: Atomizdat, 1980)
66. Landau L D, Lifshitz E M *Electrodynamics of Continuous Media* (Oxford: Pergamon Press, 1960); Translated from Russian: *Elektrodinamika Sploshnykh Sred* (Moscow: Fizmatlit, 2005)
67. Chandler D *Nature* **437** 640 (2005)
68. Chandler D *Phys. Rev. E* **48** 2898 (1993)
69. Landau L D, Lifshitz E M *Statistical Physics* Pt. 1 (London: Butterwoth-Heinemann, 2008); Translated from Russian: *Statisticheskaya Fizika* Pt. 1 (Moscow: Fizmatlit, 2002)
70. Pauling L *The Nature of the Chemical Bond and the Structure of Molecules and Crystals*; *an Introduction to Modern Structural Chemistry* (Ithaca, NY: Cornell Univ. Press, 1960)
71. Stogryn A *IEEE Trans. Microwave Theory Tech.* **19** 733 (1971)
72. Liebe H J, Hufford G A, Manabe T *Int. J. Infrared Millim. Waves* **12** 659 (1991)
73. Hasted J B, Ritson D M, Collie C H *J. Chem. Phys.* **16** 1 (1948)
74. Bernal J D, Fowler R H *J. Chem. Phys.* **1** 515 (1933)
75. Ginzburg V *Sov. Phys. Solid State* **2** 1824 (1960); *Fiz. Tverd. Tela* **2** 2031 (1960)
76. Vaks V G, Larkin A I, Pikin S A *Sov. Phys. JETP* **24** 240 (1967); *Zh. Eksp. Teor. Fiz.* **51** 361 (1967)
77. Patashinskii A Z, Pokrovskii V L, Shepherd P J *Fluctuation Theory of Phase Transitions* (Oxford: Pergamon Press, 1979); Translated from Russian: *Fluktuatsionnaya Teoriya Fazovykh Perekhodov* (Moscow: Nauka, 1982)
78. Despretz M C *J. Franklin Inst.* **24** 422 (1837)
79. Angell C A *Annu. Rev. Phys. Chem.* **34** 593 (1983)
80. Rasmussen D H, MacKenzie A P *J. Chem. Phys.* **59** 5003 (1973)
81. Angell C "Supercooled water", in *Water and Aqueous Solutions at Subzero Temperatures* (Water, A Comprehensive Treatise, Vol. 7, Ed. F Franks) (New York: Plenum Press, 1982)
82. Ginzburg V L, Sobyanin A A *Sov. Phys. Usp.* **19** 773 (1976); *Usp. Fiz. Nauk* **157** 153 (1976)
83. Gell-Mann M, Brueckner K A *Phys. Rev.* **106** 364 (1957)
84. Lifshitz E M, Pitaevskii L P *Statistical Physics* Pt. 2 (Oxford: Pergamon Press, 1980); Translated from Russian: *Statisticheskaya Fizika* Pt. 2 (Moscow: Nauka, 1978)
85. Schreiber A, Ketelsen I, Findenegg G H *Phys. Chem. Chem. Phys.* **3** 1185 (2001)
86. Parfenov V, Kirik S, in *Proc. of the 4th Staroverov Readings, Krasnoyarsk, 2009*, p. 319
87. Imry Y *Introduction to Mesoscopic Physics* (Oxford: Oxford Univ. Press, 2002); Translated into Russian: *Vvedenie v Mezoskopicheskuyu Fiziku* (Moscow: Fizmatlit, 2004)
88. *McGraw-Hill Dictionary of Chemistry* (New York: McGraw-Hill, 2003)
89. Fröhlich H *Theory of Dielectrics: Dielectric Constant and Dielectric Loss* (Oxford: Clarendon Press, 1949)
90. Johari G P et al. *J. Chem. Phys.* **130** 126102 (2009)
91. Webber B, Dore J *J. Phys. Condens. Matter.* **16** S5449 (2004)
92. Gorshunov B P et al. *Nature Commun.* **7** 12842 (2016)
93. Dressel M et al. *J. Infrared Millim. Terahertz Waves* **39** 799 (2018)
94. Stanley H E et al. *J. Non-Cryst. Solids* **357** 629 (2011)
95. Findenegg G H et al. *Chem. Phys. Chem.* **9** 2651 (2008)
96. Steytler D C, Dore J C *Mol. Phys.* **56** 1001 (1985)
97. Bellissent-Funel M-C, Lal J, Bosio L *J. Chem. Phys.* **98** 4246 (1993)
98. Takamuku T et al. *J. Phys. Chem. B* **101** 5730 (1997)
99. Mancinelli R, Bruni F, Ricci M A *J. Mol. Liq.* **159** 42 (2011)
100. Ricci M A, Bruni F, Giuliani A *Faraday Discuss.* **141** 347 (2009)
101. Bruni F, Ricci M A, Soper A K *J. Chem. Phys.* **109** 1478 (1998)
102. Awschalom D D, Warnock J *Phys. Rev. B* **35** 6779 (1987)
103. Brovchenko I, Oleinikova A *Chem. Phys. Chem.* **9** 2660 (2008)
104. Mancinelli R, Bruni F, Ricci M A *J. Phys. Chem. Lett.* **1** 1277 (2010)
105. Mazza M et al. *Comput. Phys. Commun.* **180** 497 (2009)
106. Giovambattista N, Rossky P J, Debenedetti P G *Phys. Rev. E* **73** 041604 (2006)
107. Gallo P, Rovere M, Chen S-H *Phys. Chem. Lett.* **1** 729 (2010)
108. Morishige K, Nobuoka K *J. Chem. Phys.* **107** 6965 (1997)
109. Castrillón S R-V et al. *J. Phys. Chem. B* **113** 7973 (2009)
110. Solveyra E G et al. *J. Phys. Chem. B* **115** 14196 (2011)
111. Liu L et al. *J. Phys. Condens. Matter* **16** S5403 (2004)
112. Faivre C, Bellet D, Dolino G *Eur. Phys. J. B* **7** 19 (1999)
113. Hillig W B *J. Cryst. Growth* **183** 463 (1998)
114. Shimoda M et al. *J. Low Temp. Phys.* **64** 285 (1986)
115. Eddington A S *The Nature of the Physical World*: *Gifford Lectures* (*1927*) (Cambridge: Cambridge Univ. Press, 2012)
116. Gelfand M P, Lipowsky R *Phys. Rev. B* **36** 8725 (1987)
117. Frenkel J *Kinetic Theory of Liquids* (Oxford: The Clarendon Press, 1946); Translated from Russian: Frenkel Ya I *Kineticheskaya Teoriya Zhidkostei* (Leningrad: Nauka, 1975)
118. Koposov G D, Bardyug D Yu *Tech. Phys. Lett.* **33** 622 (2007); *Pis'ma Zh. Tekh. Fiz.* **33** (14) 80 (2007)
119. Sastry S et al. *Phys. Rev. E* **53** 6144 (1996)
120. Rebelo L P N, Debenedetti P G, Sastry S *J. Chem. Phys.* **109** 626 (1998)
121. Deryagin V B *Sov. Phys. Usp.* **13** 305 (1970); *Usp. Fiz. Nauk* **100** 726 (1970)
122. Stillinger F H *Philos. Trans. R. Soc. Lond. B* **278** 97 (1977)
123. Poole P H et al. *Nature* **360** 324 (1992)
124. Poole P H *Phys. Rev. Lett.* **73** 1632 (1994)
125. Mishima O, Stanley H E *Nature* **396** 329 (1998)
126. Stanley H E et al. *Physica A* **306** 230 (2002)
127. Pettersson L G M, Nilsson A *J. Non-Cryst. Solids* **407** 399 (2015)
128. Xu L et al. *Proc. Natl. Acad. Sci. USA* **102** 16558 (2005)
129. Bertrand C E, Anisimov M A *J. Phys. Chem. B* **115** 14099 (2011)
130. Stanley H E et al. *Physica A* **205** 122 (1994)
131. Tanaka H *J. Chem. Phys.* **105** 5099 (1996)
132. Harrington S et al. *J. Chem. Phys.* **107** 7443 (1997)
133. Yamada M et al. *Phys. Rev. Lett.* **88** 195701 (2002)
134. Jedlovszky P, Vallauri R *J. Chem. Phys.* **122** 081101 (2005)
135. Paschek D *Phys. Rev. Lett.* **94** 217802 (2005)
136. Paschek D, Rüppert A, Geiger A *Chem. Phys. Chem.* **9** 2737 (2008)
137. Liu Y, Panagiotopoulos A Z, Debenedetti P G *J. Chem. Phys.* **131** 104508 (2009)

138. Abascal J L F, Vega C *J. Chem. Phys.* **133** 234502 (2010)
139. Kumar P, Stanley H E *J. Phys. Chem. B* **115** 14269 (2011)
140. Truskett T M et al. *J. Chem. Phys.* **111** 2647 (1999)
141. Truskett T M, Dill K A *J. Phys. Chem. B* **106** 11829 (2002)
142. Lee H K, Swendsen R H *Phys. Rev. B* **64** 214102 (2001)
143. Girardi M et al. *J. Chem. Phys.* **126** 064503 (2007)
144. Stokely K et al. *Proc. Natl. Acad. Sci. USA* **107** 1301 (2010)
145. Mishima O *Phys. Rev. Lett.* **85** 334 (2000)
146. Mallamace F et al. *Proc. Natl. Acad. Sci. USA* **104** 18387 (2007)
147. Mallamace F et al. *Proc. Natl. Acad. Sci. USA* **105** 12725 (2008)
148. Mishima O *J. Chem. Phys.* **133** 144503 (2010)
149. Kumar P et al. *Proc. Natl. Acad. Sci. USA* **104** 9575 (2007)
150. Kumar P, Franzese G, Stanley H E *Phys. Rev. Lett.* **100** 105701 (2008)
151. Chen S-H et al. *Proc. Natl. Acad. Sci. USA* **103** 12974 (2006)
152. Debenedetti P G, Stanley H E *Phys. Today* **56** (6) 40 (2003)
153. Angell C A *Annu. Rev. Phys. Chem.* **55** 559 (2004)
154. Buldyrev S V et al. *Proc. Natl. Acad. Sci. USA* **104** 20177 (2007)
155. Han S et al. *Nat. Phys.* **6** 685 (2010)
156. Kumar P, Han S, Stanley H E *J. Phys. Condens. Matter* **21** 504108 (2009)
157. Angell C A *Science* **319** 582 (2008)
158. Limmer D T, Chandler D *J. Chem. Phys.* **138** 214504 (2013)
159. Overduin S D, Patey G N *J. Chem. Phys.* **138** 184502 (2013)
160. Holten V, Anisimov M A *Sci. Rep.* **2** 713 (2012)
161. Speedy R J *J. Phys. Chem.* **86** 982 (1982)
162. Moore E B, Molinero V *Nature* **479** 506 (2011)
163. Poole P H et al. *Comput. Mater. Sci.* **4** 373 (1995)
164. Ponyatovskii E G, Sinitsyn V V, Pozdnyakova T A *JETP Lett.* **60** 360 (1994); *Pis'ma Zh. Eksp. Teor. Fiz.* **60** 352 (1994)
165. Ponyatovsky E, Sinitsyn V, Pozdnyakova T *J. Chem. Phys.* **109** 2413 (1998)
166. Ponyatovsky E G, Sinitsyn V V *Physica B* **265** 121 (1999)
167. Zanotti J-M, Bellissent-Funel M-C, Chen S-H *Europhys. Lett.* **71** 91 (2005)
168. Myneni S et al. *J. Phys. Condens. Matter* **14** L213 (2002)
169. Wernet Ph et al. *Science* **304** 995 (2004)
170. Tokushima T et al. *Chem. Phys. Lett.* **460** 387 (2008)
171. Huang C et al. *Proc. Natl. Acad. Sci. USA* **106** 15214 (2009)
172. English N J, Tse J S *Phys. Rev. Lett.* **106** 037801 (2011)
173. Blackman M, Lisgarten N D *Proc. R. Soc. Lond. A* **239** 93 (1957)
174. Finney J L et al. *Phys. Rev. Lett.* **88** 225503 (2002)
175. Zaretskii A V, Howe R, Whitworth R W *Philos. Mag. B* **63** 757 (1991)
176. Jackson S M, Whitworth R W *J. Chem. Phys.* **103** 7647 (1995)
177. Buch V, Sandler P, Sadlej J *J. Phys. Chem. B* **102** 8641 (1998)
178. Rick S W *J. Chem. Phys.* **122** 094504 (2005)
179. Bramwell S T *Nature* **397** 212 (1999)
180. Knight C et al. *Phys. Rev. E* **73** 056113 (2006)
181. Feistel R, Wagner W *J. Phys. Chem. Ref. Data* **35** 1021 (2006)
182. Fukazawa H et al. *Astrophys. J. Lett.* **652** L57 (2006)
183. Fukazawa H et al. *Nucl. Instrum. Meth. Phys. Res. A* **600** 279 (2009)
184. Pauling L *General Chemistry* (New York: Dover Publ., 1988); Translated into Russian: *Obshshaya Khimiya* (Moscow: Mir, 1974)
185. Volkenstein M *Molecular Biophysics* (New York: Academic Press, 1977); Translated from Russian: *Molekulyarnaya Biofizika* (Moscow: Nauka, 1975)
186. Prokhorov A M (Ed.-in-Chief) *Fizicheskaya Entsiklopediya* (Encyclopedia of Physics) (Moscow: Sovetskaya Entsiklopediya, 1988)
187. Krivoglaz M A, Smirnov A A *The Theory of Order-Disorder in Alloys* (New York: American Elsevier Publ. Co., 1964); Translated from Russian: *Teoriya Uporyadochivayushchikhsya Splavov* (Moscow: Fizmatgiz, 1958)
188. Aptekar' I L, Ponyatovsky E G *Fiz. Met. Metalloved.* **25** 777 (1968)
189. Ponyatovsky E G, Aptekar' I L *Fiz. Met. Metalloved.* **25** 1049 (1968)
190. Moore E B, Molinero V *J. Chem. Phys.* **132** 244504 (2010)
191. Onsager L *J. Am. Chem. Soc.* **58** 1486 (1936)
192. Tomasi J, Persico M *Chem. Rev.* **94** 2027 (1994)
193. Debye P J W *Polar Molecules* (New York: The Chemical Catalog Co., 1929)
194. Stillinger F H *Science* **209** 451 (1980)
195. Wei D, Patey G N *Phys. Rev. Lett.* **68** 2043 (1992)
196. Ponomareva I et al. *Phys. Rev. B* **72** 140102(R) (2005)
197. Weis J-J *J. Chem. Phys.* **123** 044503 (2005)
198. Weis J J, Levesque D, Zarragoicoechea G J *Phys. Rev. Lett.* **69** 913 (1992)
199. Groh B, Dietrich S *Phys. Rev. Lett.* **72** 2422 (1994)
200. Ballenegger V, Hansen J-P *Mol. Phys.* **102** 599 (2004)
201. Matyushov D V *Phys. Rev. E* **76** 011511 (2007)
202. Bartke J, Hentschke R *Phys. Rev. E* **75** 061503 (2007)
203. Pounds M A, Madden P A *J. Chem. Phys.* **126** 104506 (2007)
204. Sciortino F *Chem. Phys.* **258** 307 (2000)
205. Sokolov A P, Hurst J, Quitmann D *Phys. Rev. B* **51** 12865(R) (1995)
206. Zubkov T et al. *J. Phys. Chem. B* **109** 15454 (2005)
207. Morrison S R *The Chemical Physics of Surfaces* (Berlin: Springer, 2013)
208. Caputo G et al. *J. Phys. Chem. C* **112** 701 (2008)
209. Maccarini M *Biointerphases* **2** MR1 (2007)
210. Berezinskii V L *Sov. Phys. JETP* **32** 493 (1971); *Zh. Eksp. Teor. Fiz.* **59** 907 (1970)
211. Berezinskii V L *Sov. Phys. JETP* **34** 610 (1971); *Zh. Eksp. Teor. Fiz.* **61** 1144 (1971)
212. Kosterlitz J M, Thouless D J *J. Phys. C* **6** 12 (1973)
213. Kosterlitz J *J. Phys. C* **7** 1046 (1974)
214. Stanley H E *Introduction to Phase Transitions and Critical Phenomena* (Oxford: Clarendon Press, 1971); Translated into Russian: *Fazovye Perekhody i Kriticheskie Yavleniya* (Moscow: Mir, 1973)
215. Mermin N D, Wagner H *Phys. Rev. Lett.* **17** 1133 (1966)
216. Hohenberg P C *Phys. Rev.* **158** 383 (1967)
217. Maleev S V *Sov. Phys. JETP* **43** 1240 (1976); *Zh. Eksp. Teor. Fiz.* **70** 2374 (1976)
218. Pokrovskii V L, Feigel'man M V *Sov. Phys. JETP* **45** 291 (1977); *Zh. Eksp. Teor. Fiz.* **72** 557 (1977)
219. Kashuba A B, Pokrovsky V L *Phys. Rev. B* **48** 10335 (1993)
220. De'Bell K et al. *Phys. Rev. B* **55** 15108 (1997)
221. Weis J-J *J. Phys. Condens. Matter* **15** S1471 (2003)
222. Giuliani A, Lebowitz J L, Lieb E H *Phys. Rev. B* **76** 184426 (2007)
223. Tomita Y *J. Phys. Soc. Jpn.* **78** 014002 (2009)
224. Alonso J J *J. Magn. Magn. Mater.* **322** 1330 (2010)
225. Baek S K, Minnhagen P, Kim B J *Phys. Rev. B* **83** 184409 (2011)
226. Feigel'man M V *Sov. Phys. JETP* **49** 395 (1979); *Zh. Eksp. Teor. Fiz.* **76** 784 (1979)
227. Maier P G, Schwabl F *Condens. Matter Phys.* **8** 103 (2005)
228. Maier P G, Schwabl F *Phys. Rev. B* **70** 134430 (2004)
229. Fukui K, Todo S *J. Comput. Phys.* **228** 2629 (2009)
230. Kaplan B, Gehring G A *J. Magn. Magn. Mater.* **128** 111 (1993)
231. Brankov J G, Danchev D M *Physica A* **144** 128 (1987)
232. Zimmerman G O, Ibrahim A K, Wu F Y *Phys. Rev. B* **37** 2059 (1988)
233. Bedanov V M, Gadiyak G V, Lozovik Yu E *Phys. Lett. A* **109** 289 (1985)
234. Belobrov P I, Gekht R S, Ignatchenko V A *Sov. Phys. JETP* **57** 636 (1983); *Zh. Eksp. Teor. Fiz.* **84** 1097 (1983)
235. Fisher M E *Rev. Mod. Phys.* **46** 597 (1974)
236. Whitehead J P, De'Bell K *J. Phys. Condens. Matter* **6** L731 (1994)
237. Rapini M, Dias R A, Costa B V *Phys. Rev. B* **75** 014425 (2007)
238. Mól L A S, Costa B V, arXiv:1109.1840
239. Bune A V et al. *Nature* **391** 874 (1998)
240. Baranov M A et al. *Chem. Rev.* **112** 5012 (2012)
241. Schlick T *Molecular Modeling and Simulation: An Interdisciplinary Guide* (Interdisciplinary Applied Mathematics, Vol. 21) (New York: Springer, 2010)
242. Oliphant T A *Guide to NumPy* Vol. 1 (Spanish Fork, UT: Trelgol Publ., 2006)
243. Belavin A A, Polyakov A M *JETP Lett.* **22** 245 (1975); *Pis'ma Zh. Eksp. Teor. Fiz.* **22** 503 (1975)
244. Tobochnik J, Chester G V *Phys. Rev. B* **20** 3761 (1979)
245. Ferer M, Velgakis M J *Phys. Rev. B* **27** 314 (1983)
246. Binder K, Heermann D W *Monte Carlo Simulation in Statistical Physics: an Introduction* Vol. 80 (Heidelberg: Springer, 2010); Translated into Russian: *Modelirovanie Metodom Monte-Karlo v Statisticheskoi Fizike* (Moscow: Fizmatlit, 1995)
247. Oleinikova A et al. *J. Phys. Chem. B* **109** 1988 (2005)
248. Oleinikova A et al. *Phys. Rev. Lett.* **95** 247802 (2005)
249. Smolin N et al. *J. Phys. Chem. B* **109** 10995 (2005)
250. Bopp P A, Kornyshev A A, Sutmann G *J. Chem. Phys.* **109** 1939 (1998)

251. Omelyan I P *Mol. Phys.* **93** 123 (1998)
252. Teschke O, Ceotto G, de Souza E F *Phys. Rev. E* **64** 011605 (2001)
253. Schaaf C, Gekle S *Phys. Rev. E* **92** 032718 (2015)
254. Fumagalli L et al. *Science* **360** 1339 (2018)
255. Derjaguin B V, Landau L D *Acta Physicochim. URSS* **14** 633 (1941); *Zh. Eksp. Teor. Fiz.* **11** 802 (1941)
256. Derjaguin B V *Theory of Stability of Colloids and Thin Films* (New York: Consultants Bureau, 1989)
257. Israelachvili J N *Intermolecular and Surface Forces* (Burlington, MA: Academic Press, 2011); Translated into Russian: *Mezhmolekulyarnye i Poverkhnostnye Sily* (Moscow: Nauchnyi Mir, 2011)
258. Drost-Hansen W *Ind. Eng. Chem.* **61** (11) 10 (1969)
259. Hammer M U et al. *Faraday Discuss.* **146** 299 (2010)
260. Helfrich W, Servuss R-M *Nuovo Cimento D* **3** 137 (1984)
261. Helfrich W *Z. Naturwissenschaften A* **33** 305 (1978)
262. Israelachvili J, Wennerström H *Nature* **379** 219 (1996)
263. Leite F L et al. *Int. J. Mol. Sci.* **13** 12773 (2012)
264. Parsegian V A, Gingell D *Biophys. J.* **12** 1192 (1972)
265. LeNeveu D M, Rand R P, Parsegian V A *Nature* **259** 601 (1976)
266. van Olphen H *An Introduction to Clay Colloid Chemistry: for Clay Technologists, Geologists, and Soil Scientists* (New York: Wiley, 1977)
267. Pashley R M *J. Colloid Interface Sci.* **80** 153 (1981)
268. Pashley R M *J. Colloid Interface Sci.* **83** 531 (1981)
269. Rabinovich Ya I, Derjaguin B V, Churaev N V *Adv. Colloid Interface Sci.* **16** 63 (1982)
270. Peschel G et al. *Colloid Polymer Sci.* **260** 444 (1982)
271. Horn R G, Smith D T, Haller W *Chem. Phys. Lett.* **162** 404 (1989)
272. Kjellander R, Marčelja S *J. Chem. Phys.* **82** 2122 (1985)
273. Israelachvili J, Pashley R *Nature* **300** 341 (1982)
274. Pashley R M et al. *Science* **229** 1088 (1985)
275. Claesson P M, Christenson H K *J. Phys. Chem.* **92** 1650 (1988)
276. Pashley R *Chem. Scripta* **25** 22 (1985)
277. Claesson P M et al. *J. Colloid Interface Sci.* **114** 234 (1986)
278. Parker J L, Cho D L, Claesson P M *J. Phys. Chem.* **93** 6121 (1989)
279. Rabinovich Ya I, Derjaguin B V *Colloids Surf.* **30** 243 (1988)
280. Christenson H K et al. *J. Phys. Chem.* **94** 8004 (1990)
281. Lipowsky R, Sackmann E (Eds) *Structure and Dynamics of Membranes* (Amsterdam: Elsevier, 1995)
282. Zhao S et al. *J. Chem. Phys.* **134** 194102 (2011)
283. Beglov D, Roux B *J. Phys. Chem. B* **101** 7821 (1997)
284. Faghihnejad A, Zeng H *Langmuir* **29** 12443 (2013)
285. Kokkoli E, Zukoski C F *J. Colloid Interface Sci.* **230** 176 (2000)
286. Freitas A M, Sharma M M *J. Colloid Interface Sci.* **233** 73 (2001)
287. Lee J-H, Meredith J C *Langmuir* **27** 10000 (2011)
288. Van Oss C, Giese R F *Clays Clay Miner.* **43** 474 (1995)
289. Casimir H B *Proc. K. Netherlands Akad. Wet.* **51** 793 (1948)
290. Boyer T H *Ann. Physics* **56** 474 (1970)
291. Zheng J, Pollack G H *Phys. Rev. E* **68** 031408 (2003)
292. Zheng J, Pollack G H, in *Water and the Cell* (Eds G H Pollack, I L Cameron, D N Wheatley) (Dordrecht: Springer, 2006)
293. Zheng J et al. *Adv. Colloid Interface Sci.* **127** 19 (2006)
294. Chai B et al. *J. Phys. Chem. A* **112** 2242 (2008)
295. Chai B, Yoo H, Pollack G H *J. Phys. Chem. B* **113** 13953 (2009)
296. Chai B, Pollack G H *J. Phys. Chem. B* **114** 5371 (2010)
297. Chai B, Mahtani A G, Pollack G H *Contemp. Mater.* **3** (1) 1 (2012)
298. Pollack G H *The Fourth Phase of Water: Beyond Solid, Liquid, and Vapor* (Seattle, WA: Ebner and Sons, 2013)
299. Mauritz K A, Moore R B *Chem. Rev.* **104** 4535 (2004)
300. Gebel G *Polymer* **41** 5829 (2000)
301. Bass M et al. *J. Phys. Chem. B* **114** 3784 (2010)
302. Bass M et al. *Macromolecules* **44** 2893 (2011)
303. Bunkin N et al. *Water* **4** 129 (2013)
304. Bunkin N F et al. *J. Phys. Chem. B* **118** 3372 (2014)
305. Bunkin N F et al. *JETP* **119** 924 (2014); *Zh. Eksp. Teor. Fiz.* **146** 1051 (2014)
306. Galitski V, Karnakov B, Kogan V *Exploring Quantum Mechanics: a Collection of 700+ Solved Problems for Students, Lecturers, and Researchers* (Oxford: Oxford Univ. Press, 2013); Translated from Russian: *Zadachi po Kvantovoi Mekhanike* (Quantum Mechanical Problems) (Moscow: Nauka, 1992)
307. Gudkov S V et al. *Entropy* **16** 6166 (2014)
308. Bunkin N F et al. *J. Chem. Phys.* **148** 124901 (2018)
309. Bunkin N F et al. *J. Chem. Phys.* **149** 164901 (2018)
310. Spencer P D, Riches J D, Williams E D *Fluid Phase Equilib.* **466** 103 (2018)
311. Bychuk O V, O'Shaughnessy B *J. Phys. II France* **4** 1135 (1994)
312. Perepukhov A M et al. *Trudy Mosk. Fiz.-Tekh. Inst.* **7** 174 (2015)
313. Mastropietro D J, Ducker W A *Phys. Rev. Lett.* **108** 106101 (2012)
314. Bordonskiy G S, Orlov A O, arXiv:1303.4873
315. Zentner I et al. *Bioorg. Med. Chem. Lett.* **23** 1132 (2013)
316. Zentner I et al. *Chem. Med. Chem.* **8** 426 (2013)
317. Joce C et al. *Bioorg. Med. Chem. Lett.* **20** 5411 (2010)
318. Fedichev P et al. *PLoS Curr.* **3** RRN1253 (2011)
319. Timakhov R et al. *Acta Naturwissenschaften* **3** 47 (2011)